Real-time Analysis of Ring Closing Metathesis Reactions

by

Jie Liu
Bachelor of Science, St. Francis Xavier University, 2014
Bachelor of Chemical Engineering, Changzhou University, 2011

A Thesis Submitted in Partial Fulfillment
of the Requirements for the Degree of

MASTER OF SCIENCE

in the Department of Chemistry

Supervisory Committee

Real-time Analysis of Ring-Closing Metathesis Reactions

by

Jie Liu
Bachelor of Science, St. Francis University, 2014
Bachelor of Chemical Engineering, Changzhou University, 2011

Supervisory Committee

Dr. J. Scott McIndoe, Department of Chemistry
Supervisor

Dr. Alexandre Brolo, Department of Chemistry
Departmental Member

Abstract

Supervisory Committee
Dr. J. Scott McIndoe, Department of Chemistry
Supervisor
Dr. Alexandre Brolo, Department of Chemistry
Departmental Member

Ring closing metathesis (RCM) is a chemical transformation that converts a bis-alkene compound into a cycloalkene. It is catalyzed by transition metal complexes containing carbene ligands (that feature metal-carbon double bonds). The mechanism is well-understood, however, there are numerous details of the reaction that are less well understood, especially concerning catalyst activation and decomposition and formation of byproducts. This thesis takes a new approach to the study of RCM: analysis of the reaction using real-time mass spectrometric techniques.

Electrospray ionization (ESI) mass spectrometry was employed in this study, and the real-time aspect was enabled by using pressurized sample infusion (PSI). Observation of the reactants and products was enabled using charge-tagged bis-alkenes of the general formula $[Bu_2N\{(CH_2)_nCH=CH_2\}_2]^+$ $[PF_6]^-$. These were synthesized in two steps using a generally applicable methodology to generate a wide range of ring sizes of the product, from 5- to 15-membered rings. Examination of their behavior under carefully optimized RCM conditions using Grubbs' second-generation catalyst showed a wide variation in reaction rates and amount of byproducts, largely due to ring-strain effects (especially high for 5- and 9-membered rings). Byproducts always exhibited a 14 Da mass unit difference from starting materials or products, and Orbitrap MS analysis confirmed it was CH2. Isomerization was suspected to lead to byproducts. A pathway for byproducts via isomerization and cross metathesis was proposed. The source of actual isomerization catalyst was believed to be from the precatalyst itself as the evidence of precatalyst decomposition was observed. Finally, to prove our isomerization hypothesis, an authentic isomerization catalyst was deliberately added into a fast and clean reaction along with Grubbs' second-generation catalyst, and it produced the expected byproducts. Only small amounts of oligomeric intermediates were observed, probably because of the low concentrations used. $[ClPCy_3]^+$ was a new short-lived decomposition product stemming

from catalyst breakdown, along with already-known imidazolium and protonated phosphine decomposition products.

Overall, the thesis provides deep new insights into the nature of RCM reactions, in particular revealing the importance of isomerization in RCM reactions that are slow due to ring strain effects and in uncovering a new decomposition pathway for important RCM catalysts.

Table of Contents

List of Tables

Table of Schemes

List of Figures

List of abbreviations

ESI	Electrospray ionization
MS	Mass Spectrometry
EI	Electron ionization
RCM	Ring Closing Metathesis
Q	Quadrupole
MALDI	Matrix assisted laser desorption ionization
ToF	Time-of-Flight
RTICR	Fourier transform ion cyclotron resonance
MCP	Microchannel plate detector
AC	Alternating Current
DC	Direct current
m/z	Mass over Charge ratio
MS/MS	Tandem Mass Spectrometry
CID	Collision Induced Dissociation
FWHM	Full width of the peak at half maximum
ppm	Parts per million
PSI	Pressurized sample infusion
PEEK	Poly ether ether ketone
dba	Benzylideneacetone
Ar	Aromatic group
psi	Pounds per square inch

rf	Radio frequency
NMR	Nuclear magnetic resonance
NHC	*N*-Heterocyclic carbene
Bu	Butyl group
MBH	Morita-Baylis-Hillman
ROMP	Ring-opening metathesis polymerization
RT	Room temperature
Da	Daltons
CM	Cross metathesis
GuII	Grubbs' second generation catalyst
CDP	cyclodepolymerization
ADMET	Addition metathesis polymerization
SHOP	Shell higher olefin process

List of compounds

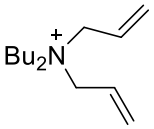

R5

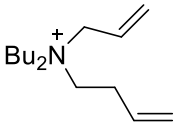

R6

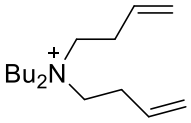

R7

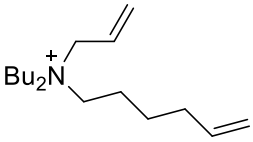

R8

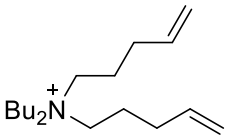

R9

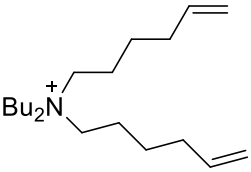

R11

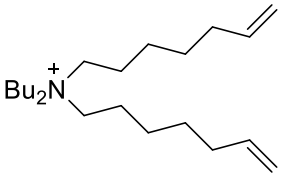

R13

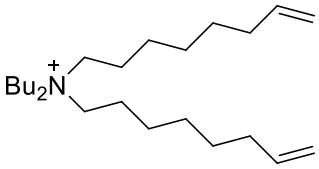

R15

Acknowledgments

Especially thanks to Dr. J. Scott McIndoe to have me in his group in beautiful Victoria, BC. I feel lucky and happy to study in McIndoe group.

Chapter 1: Introduction to Real-Time monitoring by ESI-MS

1.1 Introduction

Mass spectrometry is one of the most important analytical techniques used today for the determination of elements, especially in the trace and ultratrace range. It can do isotopic and structural analysis of organic and bioorganic compounds, due to its very high sensitivity, low detection limits and the possibility of analyzing very small sample volumes.

A mass spectrometry is an instrument for generating gas-phase ions, separating them according to their mass-to-charge ratio using electric fields, and counting the number of ions.

Mass spectrometry is more than 100 years old and a lot of different types of mass spectrometry have been developed for different cases (Figure 1.1 show some types of mass spectrometry), and new techniques are regularly introduced. The most sold instrument in world-wide is electron ionization mass spectrometry (EI-MS). EI-MS uses a metal filament applied with high voltage causes electrical current to produce heat, electrons in analyte molecular are pulled off to create ions when passing through the electric field. But fragmentation of analyte molecular occurs to such extent that unfragmented analyte molecular is rarely survived. The good view of this technique is to create “fingerprint” of a certain substance, which is legally reliable, but it is also limitation of this method – it requires a library. Electron ionization has been considered as “hard” ionization technique due to this high extent of fragmentation.[1] In contrast, electrospray ionization is considered as a “soft” ionization technique because fragmentation is rarely occurring and the molecular ion is easily passed into analyzer.[2]

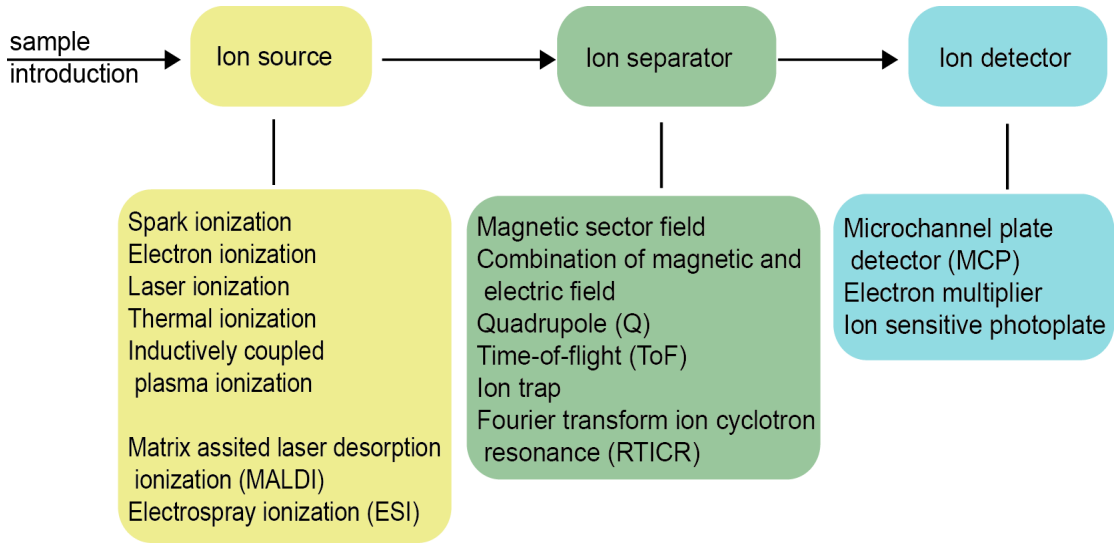

Figure III.1: Different types of ion source, ion separator and ion detector for mass spectrometer.

Additionally, EI-MS can only create cations (an electron capture version does exist but is not so efficient), which is not ideal because it is often beneficial to analyze both ion modes. Unlike EI, electrospray ionization (ESI) is suitable for the study of involatile organometallic compounds and catalyzed reactions that may including both cations and anions.[3] The first ESI experiment was carried in the late sixties[4] and was developed in the mid-1980s[5,6] by Fenn's group (Fenn was awarded the Nobel Prize[7] in 2003 for his work on ESI) and today it is commonly used as a "soft" ionization method for the investigation of large molecules such as proteins[8], and catalytic reactions, including olefin metathesis.[9]

The instrument used in this work includes an electrospray ionization source, combination of quadrupole and reflection time-of-flight analyzer, a hexapole collisioncell and a microchannel plate detector. The following part of this chapter will discuss all of these components.

1.2 Electrospray ionization

In an electrospray ionization source, a flow (at a flow rate of 5-20 µl/min) of solvent (usually polar) that contains analyte passes through a highly charged and heated capillary (3~5 kV, also acts as one electrode) into a chamber at atmospheric pressure. Due to very high voltage, a Taylor cone will form at the tip of capillary and spray fine droplets (Figure 1-2[10]). A heated gas flow (usually nitrogen gas, cheap and safe) is applied at the same direction as the spray to remove the solvent from the droplets. As the solvent vaporizes, droplets become smaller and smaller, until at a certain stage ion repulsion in droplets will be greater than solvent surface tension and ions will evaporate from the surface of the droplet.[11]

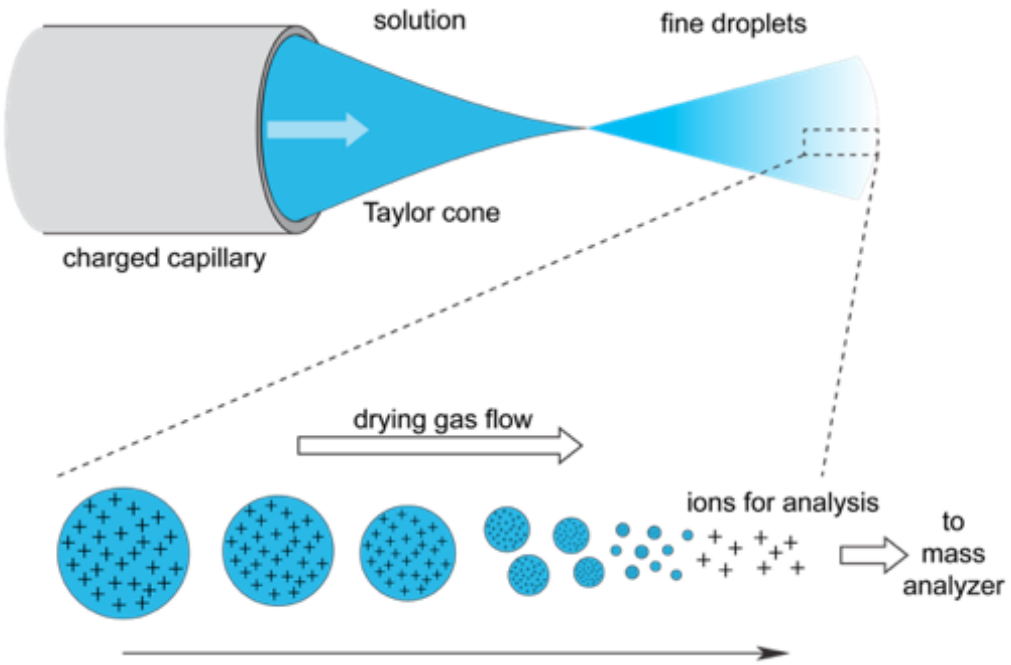

Figure III.2: Creation of fine highly charged droplets in strong electric field.

A portion of the spray is drawn into the mass spectrometer through the sample cone (the pressure at this stage is about 1 mbar), and then ions pass through the extraction cone to the analyzer (see Figure 1.3). The pressure at this stage is about 1.0×10^{-5} mbar.

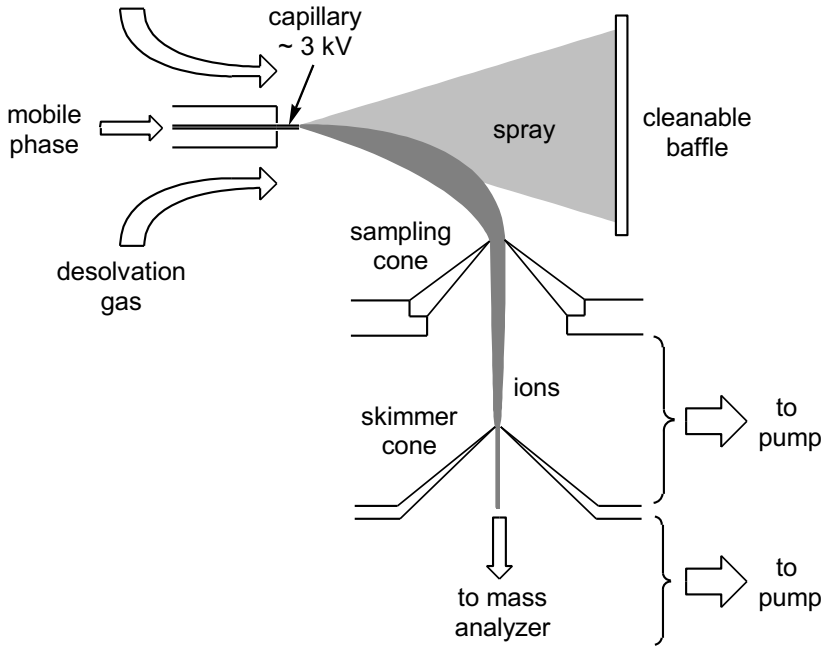

Figure III.3: An electrospray source at atmospheric pressure.

1.3 Quadrupole mass analyzer

The first analyzer that ions meet in our system is the quadrupole mass analyzer. Quadrupole mass analyzers were first introduced in 1953 by Paul and Steinwedel[12] and today they are one of the most popular mass analyzer used in mass spectrometry as they are compact, reliable, inexpensive and can be easily coupled with other analyzers. A quadrupole analyzer consists of four hyperbolic or cylindrical rod-shaped electrodes installed perfectly parallel to each other (see Figure 1.4). The voltage applied between each pair of electrodes are radio frequency (AC – alternating current) voltage and overlaid by

direct current (DC) voltage. A positive ion entering the quadrupole will be pulled towards to the negative charged rod, with appropriate DC and AC applied, the polarity of electric field will change before the ion reaches the rod, so the direction of the ion will change as well.

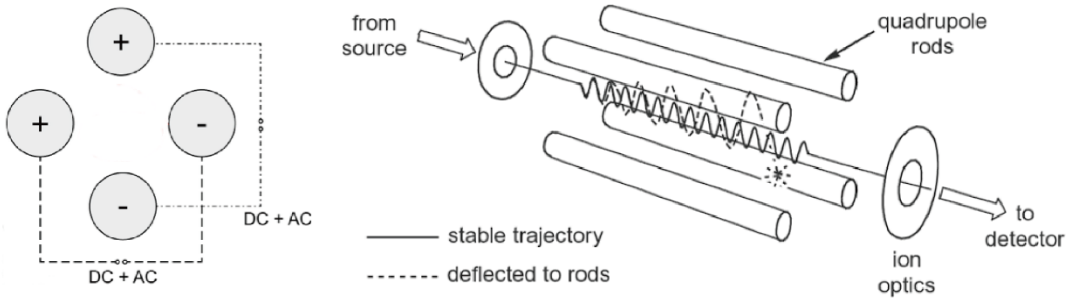

Figure III.4 Diagram of a quadrupole mass analyzer showing ion paths.

However, for ions with large mass, it will be influenced by DC more than AC, the AC could be not strong enough to change the direction and ions reach the rod to be discharged. For ions with low *m/z*, they are influenced by AC more than DC, and AC could be too strong for turning ions' direction, which makes small mass ions oscillate with greater and greater amplitude, and finally, ions reach the rod to be discharged. For a certain mass ion, it will oscillate with an appropriate amplitude and pass through the quadrupole safely. With the application of DC and AC, these four electrodes can create an electric field that allows only selected *m/z* ions pass through. The principle working behind this is described by the "Mathieu equation" (Equation 1):

$$\frac{d^2u}{d(\frac{\omega t}{2})^2} + (a_u - 2q_u \cos \omega t)u = 0 \qquad \text{Equation (1)}$$

where u stands for either x or y, ω as circular frequency. a_u and q_u depend on direct

current voltage U and radio frequency voltage V:

$$a_u = a_x = -a_y = \frac{8eU}{m\omega^2 r_0^2}$$

and

$$q_u = q_x = -q_y = \frac{4eV}{m\omega^2 r_0^2}$$

where m as the mass of ion and r_0 as field radius.

The trajectory of ions in the quadrupole can be described by a_x and q_x for x direction and a_y and q_y for y direction. Values of x and y can be obtained by solving these equations. However, the solution to Mathieu equation is complicated and are classified as "stable" or "unstable" depending on whether the amplitude of oscillation increases exponentially or not. A stability diagram is shown in Figure 1.5. The scanning of all ions extracted from source is carried out with U and V applied, and the U/V ratio will be kept constant while scanning. The slope U/V must be chosen to fit a line that passes as close to the top of the stable area peak as possible but still through stable area in order to obtain best resolution – as the line A demonstrated in Figure 1.5, m_3 is the only ion can pass through. In order to pass through more ions, the slope U/V ratio can be lowered (line B) both m_2 and m_3 are located in stable area and can pass through, but this also lowers resolution. A quadrupole can act not only as a mass filter, but also an ion guide when only radio frequency current is applied. As showed in Figure 1.5, if only V applied, the slope would be 0 and all ions in the stable area will pass through. In such application, quadrupoles, or hexapoles, or even octapoles are employed as ion guides as they are able to contain, direct and constrain ions into a narrow beam. This ability is important in mass spectrometers, because most of the ions are generated in atmospheric pressure and the ion

beam from the source is easily be dispersed by collision with the desolvation gas and residual solvent, or by gas in the collision cell.

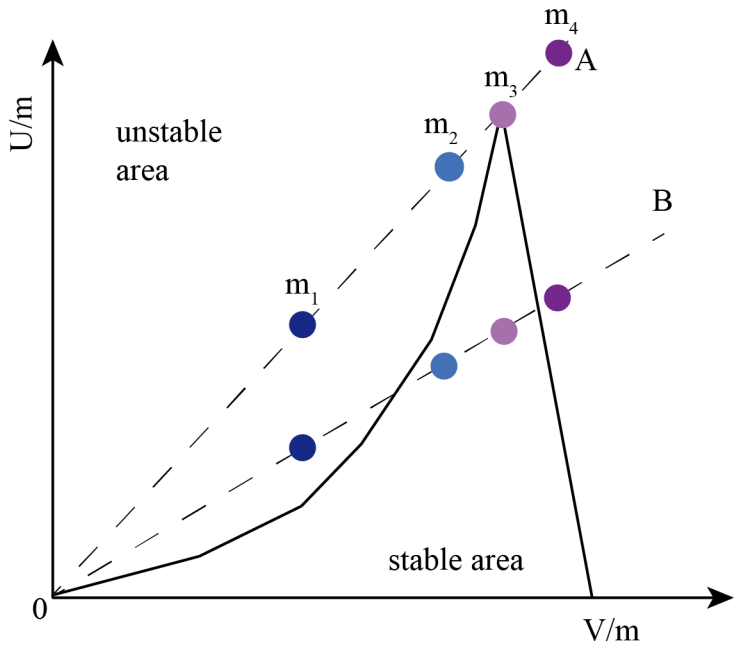

Figure III.5: Stability diagram based on Mathieu equation.

1.4 Time-of-flight analyzer

The second analyzer in the instrument employed in this work is a Time-of-Flight (ToF). The ToF analyzer was first introduced by Stephens in 1946[13] and the first instrument was built by Cameron and Eggers in 1948.[14] It was then further developed by Ionov and Mamyrin[15] and later by Wiley and McLaren[16] to improve the resolution, and formed the basis of ToF instrument today. Time-of-Flight analyzer is also very popular in mass spectrometry due to its high resolution and ability to collect an entire spectrum at once (i.e. it is not a scanning instrument).

A Time-of-Flight analyzer consists a pusher and a drift tube (see Figure 1.6). The pusher pulses the narrowed ion beam emerging from the quadrupole with different mass-to-charge ratio (*m/z*) into the drift tube at the same time at slit 1 of this tube, which makes all ions possess same kinetic energy.

The drift tube is under high vacuum and has no field applied, which means it can extract ions from source simultaneously. All extracted ions be accelerated with an acceleration voltage (V, the pusher) into a field free region with uniform energy. The flight time of ions are related to *m/z*. Ions with less *m/z* can travel faster and reach to detector earlier than ions with large *m/z*, so that ions can be separated according to their time of flight in the tube, and this can be converted to *m/z* mass spectrum. In Figure 1.6, ions from source have been accelerated by pusher to position 1 at time t_0 with same kinetic energy and move toward to the ion detector, and due to light mass ions (with less *m/z*) has highest velocity, it will reach the detector first at flight time t_l and be detected, medium ions (with medium *m/z*) reach at the flight time t_m after light ions, and the heaviest ions (with large *m/z*) reach last at the flight time t_h.

$$E_{kinetic} = \frac{1}{2}mv^2 \qquad \text{Equation (2)}$$

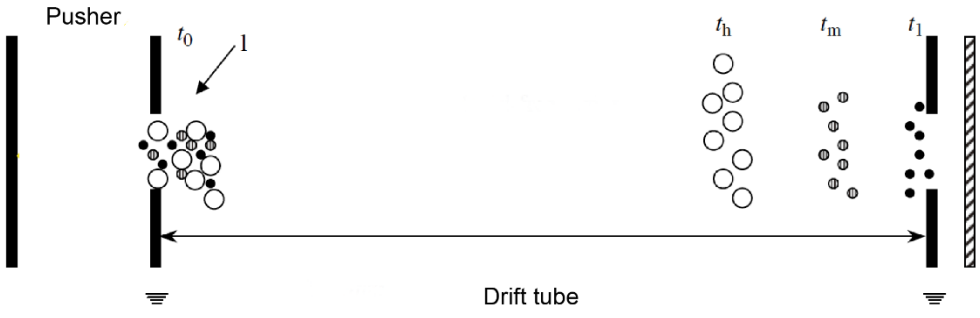

Figure III.6: Simplified diagram of ToF analyzer.

The velocity of each ion can be calculated by Equation 2, so the flight time can be calculated through equation $t = {}^{d}/_{v}$, where d is the length of drift tube. The resolution of time for different mass ions is proportional to the length of drift tube, which means the longer the drift tube is, the higher resolution can be obtained. Resolution is also inversely proportional to the velocity of ions, which related to the acceleration voltage applied on the pusher, so lower energy produced by pusher is preferred to obtain higher resolution

Higher resolution on ToF analyzer was wanted. A normal ToF can actually separate ions with significant different *m/z* very well, however, ions that enter time-of-flight analyzer have neither exact starting time nor exact kinetic energy, even for ions have same *m/z*, which will make the peak broad. To improve the resolution, Mamyrin introduced the first reflectron Time-of-Flight analyzer in 1973[17] which increased the resolution from a few hundred to several thousand. The reflectron-ToF consists of pusher, drift tube and ion reflector (Figure 1.7). As normal ToF, the pusher accelerates ions enter the field free drift tube, the ion reflector is located behind the tube possess uniformly electric field generated by parallel rings and acting as an ion mirror. Ions pass through drift tube will penetrate this electric field until they reach a kinetic energy of zero and then are accelerated in the opposite direction, pass through the tube again and reach the detector. During this trajectory, these ions that possess higher kinetic energy can penetrate the ion reflector deeper and travel farther compared to ions that possess lower kinetic energy. And, as a result, all ions with the same *m/z* will arrive at the detector at the same time, greatly increasing the resolution of the analyzer.

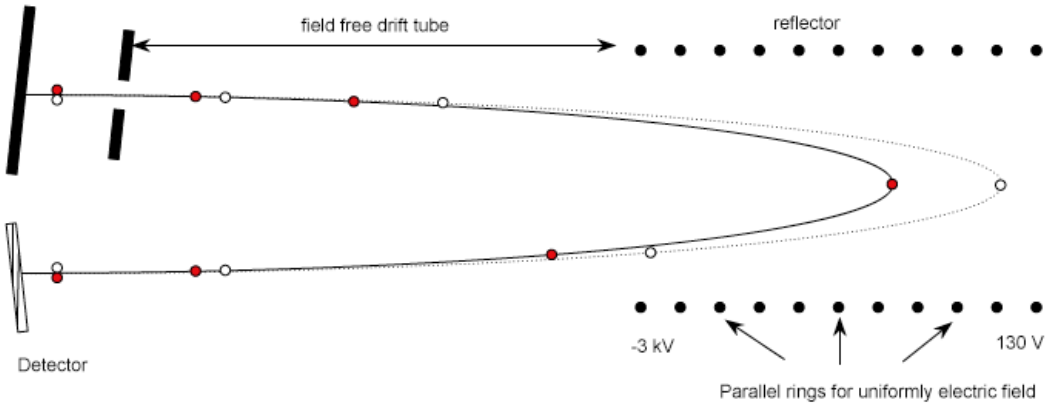

Figure III.7: Simplified diagram of a reflection ToF analyzer.

The advantages of ToF analyzers are their (theoretically) unlimited mass range, speed and relatively high resolution. However, in order to resolve very large ions, a long drift tube is required. Multiple reflectors can be used in some certain cases.[18]

1.5 Tandem Mass Spectrometry via Collision-Induced Dissociation

A tandem Mass Spectrometry (MS/MS) experiment would be desired for some particular interested ions. In the most common MS/MS experiment, a first mass analyzer would be used to isolate a selected precursor ion out from impurities and other unwanted ions, the precursor ion then undergoes activation to yield product ions and neutral fragments, and then, second mass analyzer analyzes the product ions. The most often applied method to achieve fragmentation is the use of collision gases (usually a noble gas) in a cell (quad- or hexapole) – Collision-Induced Dissociation (CID). When ions of interest are transferred into collision cell, they will collide with a stationary collision gas and part of the kinetic energy is converted into internal energy to bring ions to an excited vibrational state. At a certain stage, with enough internal energy, target ions are more in favor of direct bond

cleavage, and the possibility of product ions depends on the property of target ions so some structural information can be obtained.

According to Warhaftig diagram,[19] the ions generated by ion source can be classified into three categories. First category of ions can reach the detector before any fragmentation happened with a lifetime greater than 10^{-6} s, second category of ions fragment before leaving the source and only the fragments be detected with a lifetime less than 10^{-7} s, third category of ions have intermediate lifetime between 10^{-6} and 10^{-7} s, are stable enough to be selected by the first mass analyzer and containing enough excess energy to allow it fragment before reaching the detector. CID technique can be applied to the third category of ions to accelerate the fragmentation as well as the first category of ions to force fragmentation to happen. With a quadrupole time-of-flight (Q-ToF) MS instrument (Figure 1.8), our group is capable of conducting such an MS/MS experiment.

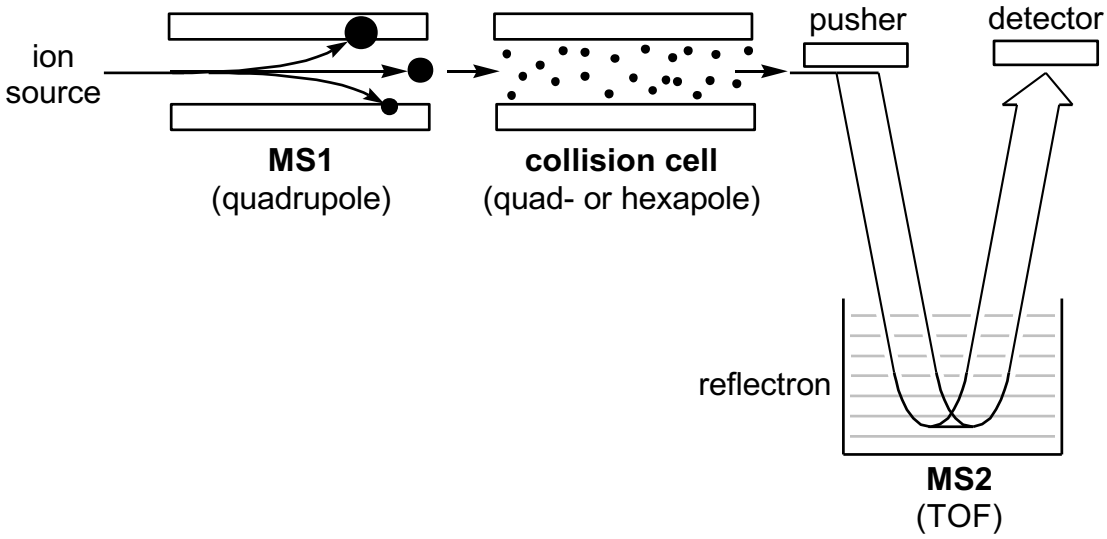

Figure III.8: A simplified diagram of Q-ToF instrument which was employed in this work.

For MS studies where all ions are expected to pass through and be detected regardless of mass, quadrapole (in Figure 1.8) as the first analyzer is set in RF-only mode (where only radio frequency current applied) to narrow and guide ion beams through the collision cell without any fragmentation, then be separated by the second analyzer ToF and reach the detector. For MS/MS studies, MS1 is used to select a precursor ion, which is fragmented in the collision cell, and the product ions spectrum collected using MS2. There are many scan modes available using MS/MS enabled instrument, such as "precursor ion scan mode" which focusing of the second spectrometer with a selected *m/z* ion while scanning the masses using first spectrometer, all of the precursor ions that produce ions with the selected mass through reactions for fragmentations will be recorded; and "neutral loss scan mode" which requires both spectrometer scanning at the same time but with a constant mass offset between them, thus detection occurs only if ions pass through first analyzer can produce fragment ion with the mass difference between two analyzers when it leaves collision cell. However, due to the limitation of ToF analyzer (not capable of isolating ions), a Q-ToF instrument can only run two scan modes for MS/MS experiment, one is "selected ion monitoring mode" which the first analyzer selected target ion and pass through collision cell without fragmentation and through second analyzer reach detector. The other mode is "product ion scan mode" which similar to the first mode but ions fragmented in collision cell and product ions be analyzed by ToF.

1.6 Microchannel Plate (MCP) – the detector

Finally, ions must be counted by a detector to give electric signal. A typical detector used for ToF is the multichannel electron multiplier. It was first introduced by Goodrich and

Wiley in 1962[20] and consisted of many electron multiplier tubes, with each tube capable of generating a detectable electronic signal when an ion enters the tube.[21,22] For a single channel, a hollow tube with semiconducting inner surface is applied with voltage of about 2 kV between the ends and it will give an uniform field along the axis. As the ion enters, the velocity of the ion causes collision on the inner surface and generates secondary electrons, the secondary electrons are carried along the tube by the axial field while their transverse velocity causes further impacts on the inner surface and generates more electrons. The amplified electrons are collected at the other end to give a detectable electric signal.[23] Microchannel plates were developed to reduce the electron multiplier tube to a few micrometers: 4 to 25 for channel diameter and 6 to 30 μm for hole spacing between each channel. It is important to notice that each channel can only count one ion at one time, and before it can count another same ion, it requires a little bit time to reset, if more than one ions with same *m/z* enter the same channel, it can only register as one while other ions can be registered as normal. In practical, if the concentration for one ion is too high, the detector saturates, and concentrations are no longer proportional to the counts.

1.7 Resolution and mass accuracy

Resolution of a mass spectrometer represents the ability of this instrument to separate ions with different *m/z*. An instrument with high resolution will be able to distinguish two peaks very close in mass and give sharp peaks in the spectrum. There are two common methods for resolution calculation, one more common definition follows Equation 3:

$$R = m/\Delta m \qquad \text{Equation (3)}$$

where m is the mass of the ion and Δm is the distance to next peak with 10% valley (easier to use full width at 5% maximum) as showed in Figure 1.9. However, this definition can't represent the actually resolution for Time-of-flight instrument because for MS instrument with ToF analyzer usually give sharp peaks but broad base, and by the definition will give unreasonably low value for the resolution. Another definition commonly used for ToF instrument uses full width of the peak at half maximum (FWHM) for Δm, and this definition is becoming the standard. As shown in the figure, Δm at 5% maximum is 0.208 and according to the first definition gives a resolution of 1000/0.208 = 4800, Δm at half maximum is 0.1 and the second definition gives a resolution of 1000/0.1 = 10 000. It is important to apply the same definition in each case when comparing resolution of mass spectrometers, and generally, in this thesis, all resolution discussed correspond to the FWHM definition unless otherwise mentioned.

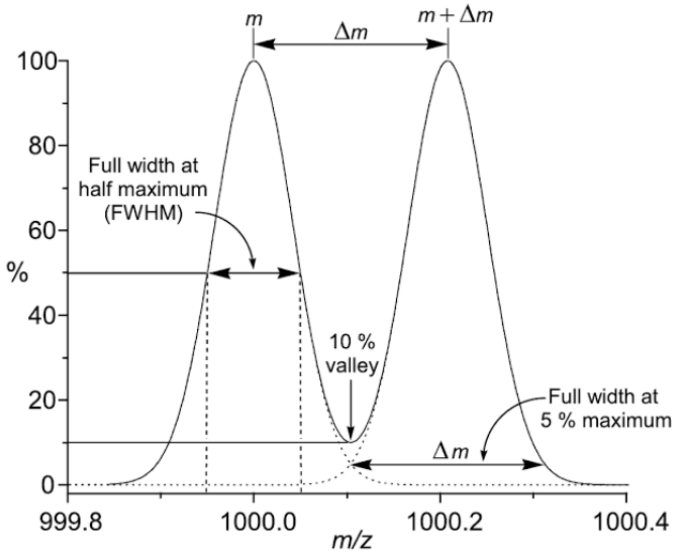

Figure III.9: Two definitions that give mass resolution.

High resolution resolution is not only desired to distinguish ions with very close mass, but also desired to provide accurate mass data. Mass accuracy is usually reported in parts per million (ppm) and the calculation follows Equation 4:

$$Mass\ accuracy\ (ppm) = 10^6 \times \frac{m_{calculated} - m_{observed}}{m_{observed}} \qquad \text{Equation (4)}$$

The requirement of high resolution for the determination of exact mass becomes obvious if compare peaks showed in Figure 1.10. The observed mass is picked at the maximum value of the peak, a well calibrated high resolution mass spectrometer can provide a mass accuracy of 5 ppm or better. As showed in Figure 1.10, peaks with low resolution are so broad it is hard to pick the maximum value within the limit. An instrument must have resolution at least 5000 to claim the ability to collect accurate mass data, however, resolution of >10 000 is desirable. The instrument used in this work with a Q-ToF analyzer has resolution of ~5000. Fortunately, our department is equipped with an mass spectrometer with an Orbitrap mass analyzer[24,25] that has resolution of up to 150 000 and mass accuracy 2-5 ppm.

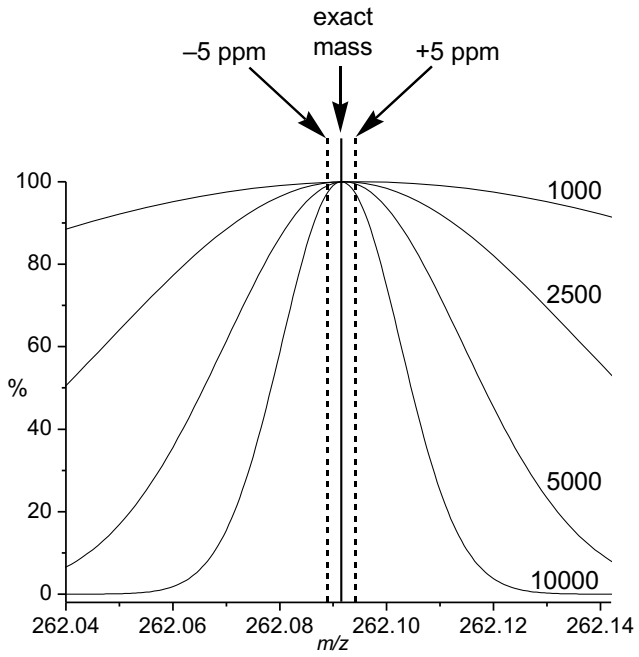

Figure III.10: Peaks with different resolution picked at maximum within 5 ppm range.

Accurate mass data can also be used to predicate the elemental composition of an ion. The elemental composition predication is reasonably reliable for organic compounds (simple elements, often just carbon, hydrogen, oxygen and nitrogen plus any other possibilities expected). However, it is only unambiguous with *m/z* < 500 because the number of possible combinations of elements increases exponentially with *m/z* when it greater than 500. An example showed in Table 1, matches for element formula increase significantly when *m/z* getting close to 1000 and this just for C, H, O, N.

Table III.1: Number of potential matches for only C, H, N, O.

m/z	200.2	300.3	400.4	500.5	600.6	700.7	900.9	1001.0
Matches within 5 ppm	1	2	2	2	3	4	50	139

1.8 Continuous reaction monitoring via PSI-ESI-MS

There are many different methods of introducing sample solutions to an ESI-MS, such as tandem HPLC. Our group avoids any kind of pump system for two main reasons: first, every pump has an appreciable internal volume; second, a pump system always involving multiple types of different materials that vary in their resistance to the wide range of solvents employed in chemical reactions. A simple set up called Pressurized Sample Infusion (PSI) [26,27] was employed in this work, which can deliver reaction mixture to ESI-MS with a precise flow rate enabling real-time monitoring of the reaction. The PSI method requires a Schlenk flask, a rubber septum, and a hose connected to a supply of pressurized and regulated inert gas (usually nitrogen gas, however, could be replaced by other gases such as hydrogen or oxygen if desired), it also requires a short length of PEEK (poly ether ether ketone) capillary tubing and a PEEK chromatography fitting that can connect PEEK tubing to the ESI source. The set up is shown in Figure 1.11. A slight overpressure (1-5 psi) of inert gas is applied to the reaction mixture in Schlenk flask, and the solution is continuously introduced into the mass spectrometer through the PEEK tubing.

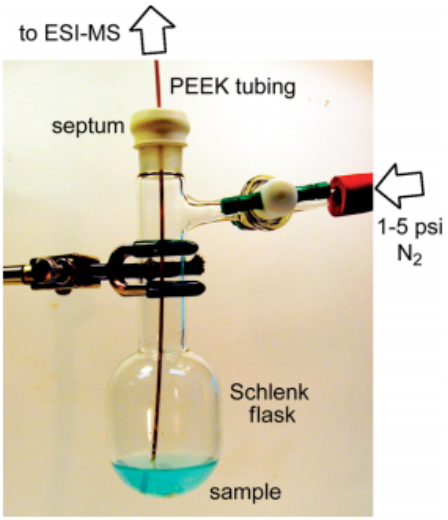

Figure III.11: Set up for PSI delivering system. Modified from reference [27].

By using an appropriate regulator capable of providing accurately delivering pressure in the recommended range (1-5 psi), PSI can introduce a continuous flow with a precise rate. The relation between pressure and flow rate can be predicated through the Hagen-Poiseuille equation:

$$P = \frac{128\mu LQ}{\pi d^4} \qquad \text{Equation (5)}$$

where P is the pressure (Pa), μ is the dynamic viscosity, L is the tube length, Q is the volumetric flow rate and d is the inner diameter of the tube.[28]

1.9 Preparation of ions

As discussed above, electrospray ionization is a "soft" ionization method that transfer ions from liquid phase to the gas phase. Direct monitoring of reaction solutions with (PSI-)ESI-MS is a useful protocol for the investigation of reaction mechanisms and the actual intermediates involved.[29,30] ESI-MS requires ions be prepared in solution before

delivered to the instrument, however, some important organic reactions been most often carried out using neutral reagents with metal catalyst, such as propene polymerization,[31] Stille reaction,[32] dephosphorylation,[33] but these neutrals are undetectable by MS. Ions from such reagents and their further intermediates and products must therefore be formed in some way and later transferred into gas phase to be detected. Several examples are discussed below to demonstrate applications of ESI-MS in catalytic science.

Inherently-charged systems

Reactions with inherently charged catalysts allow for straightforward analysis, as the reaction mixture can be simply injected into the mass spectrometer directly (at appropriate concentration).

One good example for this is the famous Heck reaction. Heck was awarded the 2010 Nobel Prize in Chemistry, which he shared with Ei-ichi Negishi, and Akira Suzuki, for the discovery and development of this reaction. The Heck reaction involves palladium-catalyzed cross couplings of an organo-halide with an alkene in the present of Pd(0) as the catalyst to yield product a substituted alkene with new C-C bond formation and byproduct HX (Scheme 1.1).

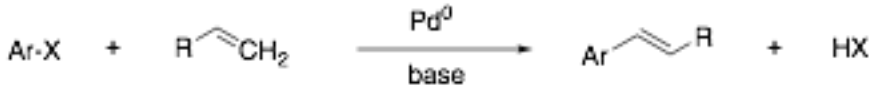

Scheme III.1: Overall reaction of Heck palladium-catalyzed cross coupling reaction. Ar is typically aromatic, X usually Br, and the base usually be week base.

These reactions are widely employed for pharmaceutical, agrochemical and fine chemical industries.[34,35] However, it is most often carried out by using neutral aryl-halide,

but one example that using arene diazonium salts as the arylating partner instead of the traditional neutral-halide was reported initially by Heck and further developed by Matsuda and co-workers,[36] and a generalized catalytic cycle shown in Scheme 1.2.

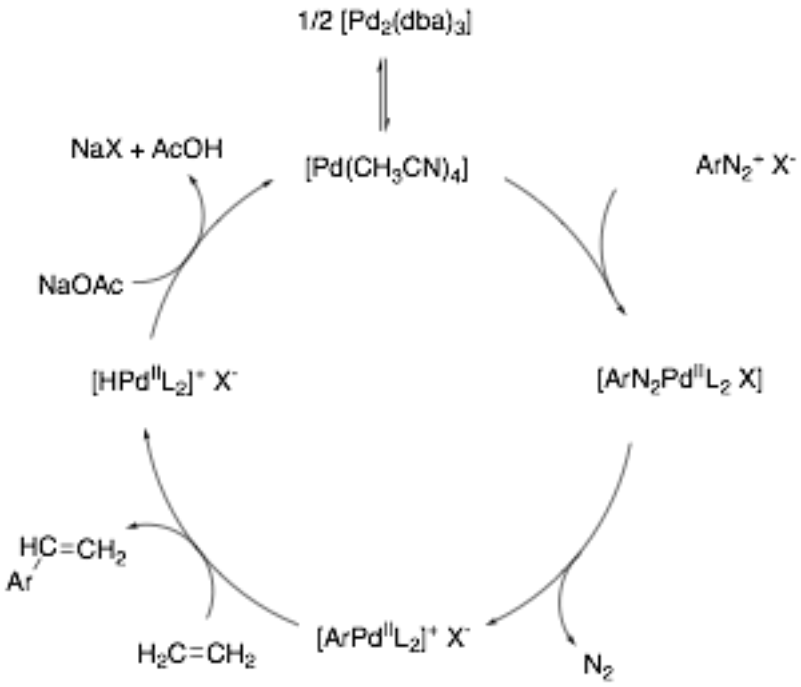

Scheme III.2: Generalized cyclic cycle for Heck reaction with arene diazonium salt used as the arylating partner. L could be both dibenzylideneacetone (dba) or acetonitrile. Modified from reference [38].

The active catalyst $Pd(NCCH_3)_4$ is from precursor $[Pd_2(dba)_3]$ where both dba and acetonitrile can coordinate to Pd(0), then the arene diazonium salt coordinates to Pd(0) and the nitrogen extruded to create charge at Pd(II). The alkene can then insert between Ar and Pd(II) and yield hte product through β-elimination. A week base such as NaOAc can reduce the palladium and regenerate Pd(0). Note that the point here is not to discuss the detailed mechanism of Heck reaction, but to show that arene diazonium salts are able to create charge on palladium which is involved in all intermediates and makes this whole reaction

suitable for ESI. And mass spectrum (Figure 1.12) clearly that showed several types of $[ArPd^{II}L_2]^+$ intermediates, the ligand could be two dba, two acetonitrile, dba + acetonitrile or even three acetonitrile. It would be very difficult to determine structure if using NMR technique because this example is phosphine free and this is where mass spectrometer has advantage.

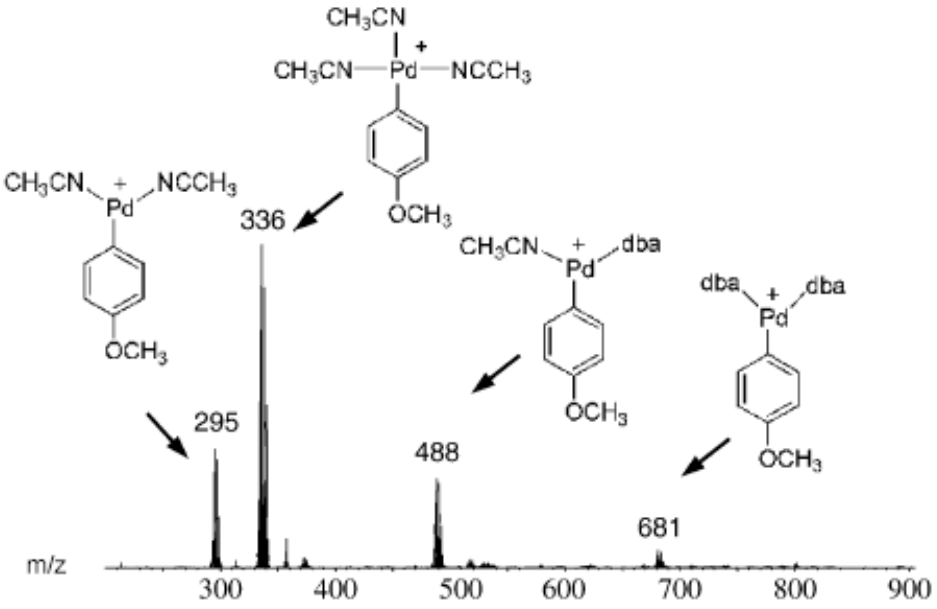

Figure III.12: Selected ESI(+)-MS spectrum of a solution of the arene dizonium salt and palladium catalyst in acetonitrile. Modified from reference [38].

Charged tag

Investigation of catalytic reactions that contain inherently-charged species is relatively straightforward, however, most of the important organometallic reactions that proceed through neutral intermediates while there are no reliable ionization mechanisms to make it MS detectable. To study these systems, charged or chargeable tags are required which append charge by covalently bonding to the reactant. By using the charged tag reagent, all

intermediates involving the charged tag would be detectable by MS, in principle. However, the charged tag reagents must not affect the catalysis in any significant way through steric or electronic effects.

An example for this is the study of charge tagged Morita-Baylis-Hillman (MBH) reaction monitored by ESI-MS. The MBH reaction involves new C-C bond formation between the α-position of alkene and and aldehyde with DABCO as the catalyst (Scheme 1.3).[37]

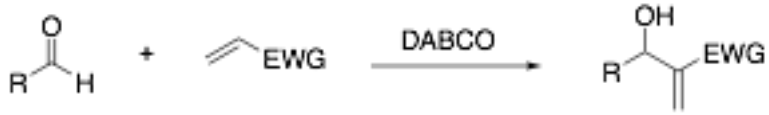

Scheme III.3: Overall reaction of MBH. R on aldehyde could be aryl, alkyl or heteroaryl.

The MBH reaction has been widely studied and have shown high synthetic utility because this reaction employed a organo-catalytic system without the use of heavy metal, reaction occurred under mild conditions, and all materials are commercially available with high atom economy.[38] However, all materials are neutral and there are no reliable ionization mechanisms for this reaction which makes it undetectable for MS, but with some charge tag used can make the system visible for MS. A generalized mechanism for the MBH reaction is showed in Scheme 1.4.

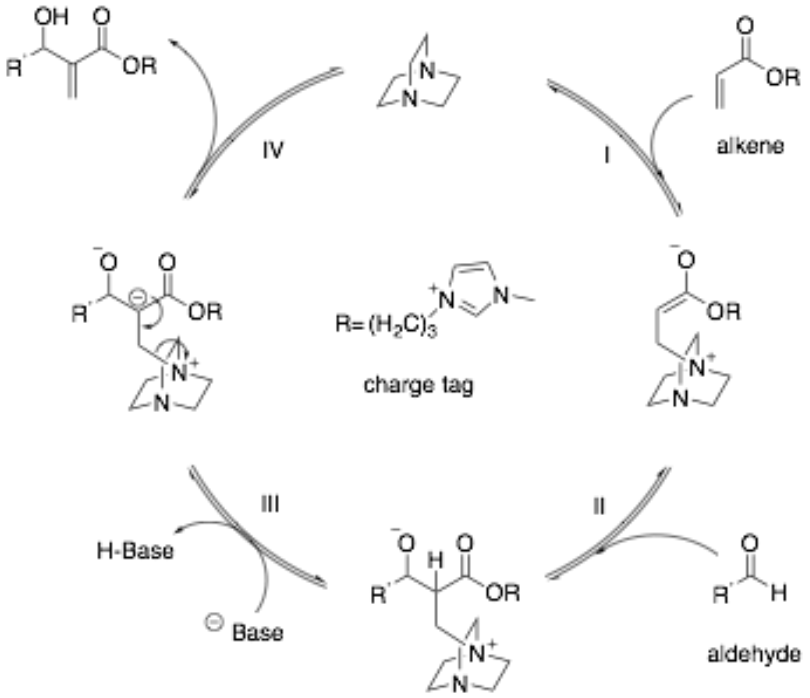

Scheme III.4: Generalized catalytic cycle for MBH reaction where a methylimidazolium ion was used as a charged tag. Modified from reference [40].

The initial mechanism was described by Hoffmann and Rabe,[39] and further mechanistic details were proposed by Aggarwal[40] and McQuade[41] and their co-workers. First step involves 1,4-addition of catalyst DABCO and alkene to give enolate product, followed with aldolic addition to give aldol product in step II, step III and step IV is actually much more complicate rather than normal proton transfer, however, it yields product and regenerate catalyst. Again, the point here is not to discuss the mechanism of MBH reaction, but to show the addition of charge tag reagent for visualization by MS. Most of the intermediates can be observed by ESI-MS as shown in Figure 1.13, *m/z* 195.11 stands for the charge tagged starting material alkene. The enolate intermediate after step I appears at *m/z* 154.11 due to protonation meaning that it possesses two positive charges; the aldol intermediate at

m/z 229.62 is also protonated and dicationic; and the final product appears at *m/z* 346.14 and catalyst at *m/z* 113.33.

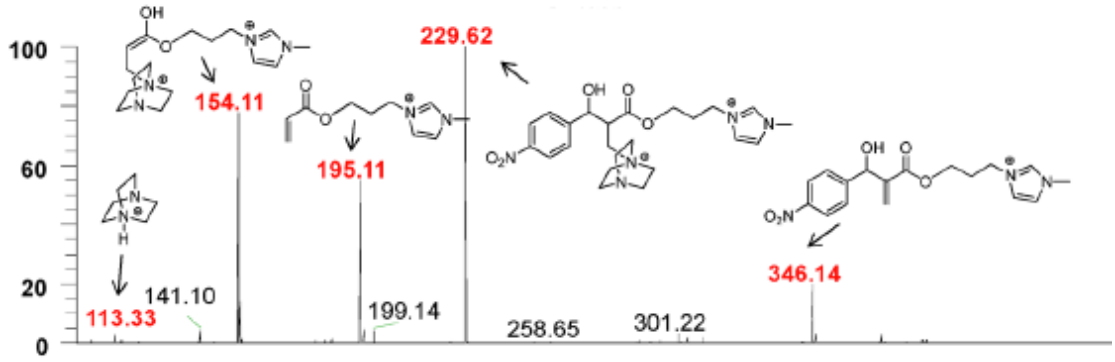

Figure III.13: Selected ESI (+)-MS of MBH reaction with starting material alkene charge tagged by methylimidazolium ion. Modified from reference [40].

1.10 Conclusion

To conclude, mass spectrometry is a rapidly developing, highly informative technique that can applied to many fields. With electrospray ionization being a soft ionization method, it is perfect even in cases where the species of interest involve labile ligands and reactive species.

Chapter 2: Ring Closing Olefin Metathesis (RCM)

2.1 Intruduction

Olefin is an an old but commonly used word for alkene, which derives from two Latin words: *oleum* (oil) and *fiacre* (to make). To describe reactions that can form a liquid (or 'oil') from gas, the word "metathesis" is generated from two Greek words: *meta* (change) and *thesis* (position) to describe the swapping of substituent groups around the carbon-carbon double bond in the reaction.[42] Olefin metathesis reactions cleave carbon-carbon double bonds and reassemble them to generate products containing new carbon-carbon double bonds. It can cleave C=C bonds from identical alkenes or from two different alkenes and reassemble them, the newly assembled C=C bond could be either the same or different from original C=C bonds (see Scheme 2.1).

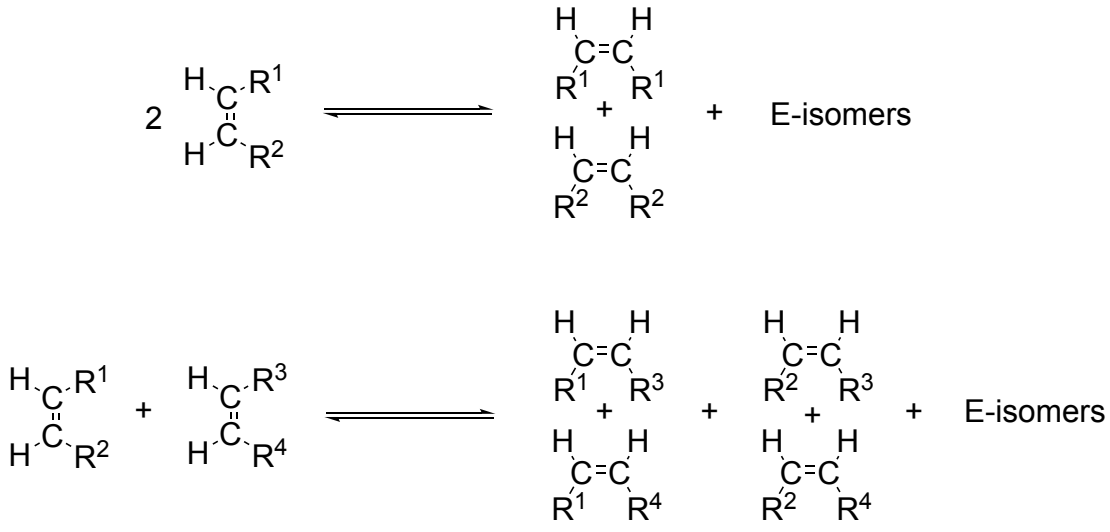

Scheme IV.1: General reactions for olefin metathesis.

Olefin metathesis was first discovered back in the mid-1950s by workers at DuPont, Standard Oil of Indiana,[43] and Phillips Petroleum.[44] The process requires a catalyst and is largely controlled by thermodynamics, and was initially conducted with heterogeneous

catalysts. It can also be conducted homogeneously, primarily by complexes of Ru, Mo, W, Re, and some Group 4 and Group 5 metals. Today we understand that many transition metal complexes can catalyze such reactions with fast rate, but at the time it was remarkable to observe strong carbon-carbon double bonds (the strongest bonds in the molecule) being cleaved in the catalytic process.

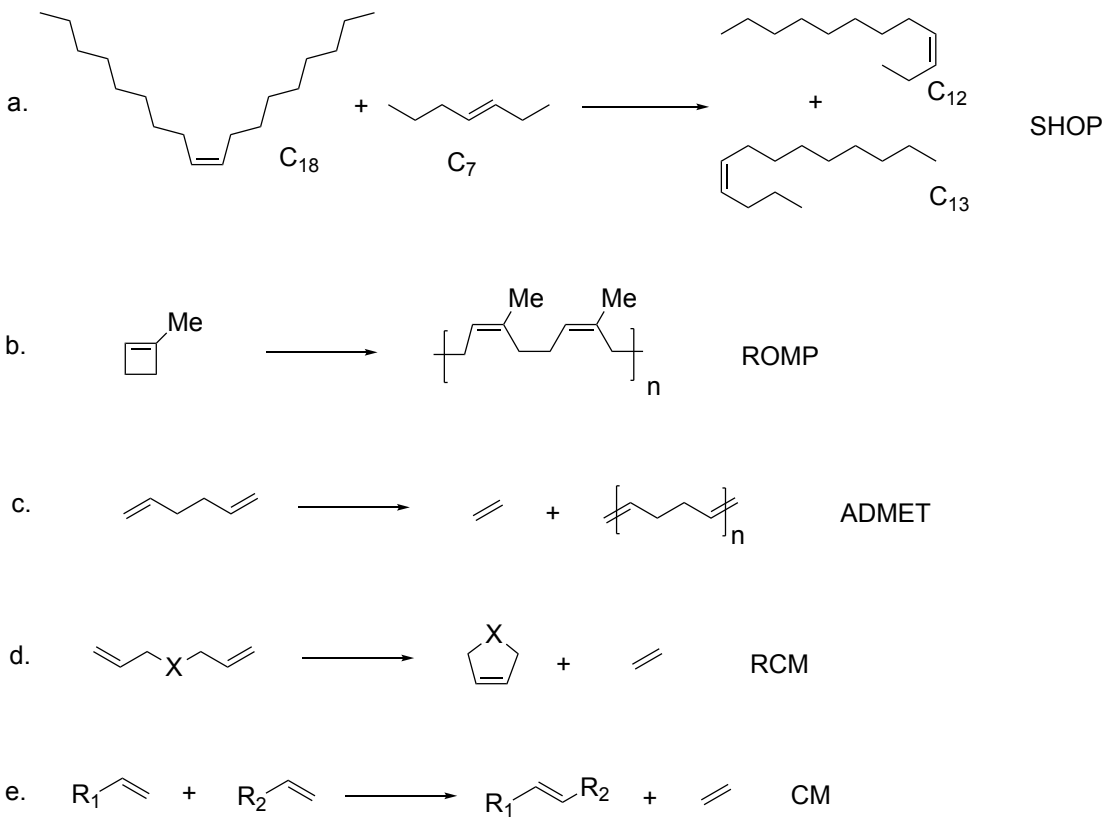

Scheme IV.2: Five types of olefin metathesis. a), Shell Higher Olefin Process (SHOP), b), Ring-Opening Metathesis Polymerization (ROMP), c), Addition Metathesis Polymerization (ADMET), d), Ring-Closing Metathesis (RCM), X = halogen, NTs, $C(CO_2R)_2$. e), Cross Metathesis (CM).

Olefin metathesis is involved in different types of reaction (see Figure 2.2). Some of them have industrial uses, and by far the most important application of metathesis is SHOP (Shell Higher Olefin Process), which is used to produce medium length olefins (of most ultimate value) from short and long chain olefins (less valuable). It was developed more than 40 years ago by the Shell Oil Company and produces about a million metric tons per year of linear C_{12}-C_{15} alcohols derived from C_{11}-C_{14} alkenes.[45,46,47,48,49] Most of these alcohols are subsequently converted into detergents and plasticizers. Another remarkable reaction used today in chemical industry is ROMP (Ring Opening Metathesis Polymerization). Most cyclic alkenes undergo metathesis, but instead of forming cyclodiene through dimerization (see Scheme 2.3), they usually undergo polymerization to form very interesting materials such as those shown in Scheme 2.2 (b).

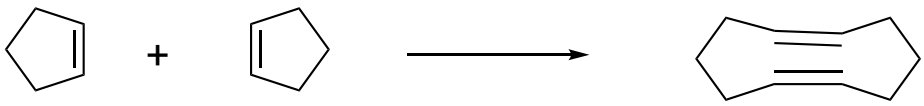

Scheme IV.3: Two cyclopentene go through dimerization to form 1,6-cyclodecadiene.

Over the past several decades, another type of olefin metathesis – Ring-Closing metathesis (RCM, Scheme 2.2 (d)), has become more and more popular and widespread in the synthesis of cyclic compounds thanks to the design of well-defined and robust catalysts. The first RCM reaction was reported by Didier Villemin in 1980[50] to make a 16-membered ring by closing two chain end C=C bonds and releasing one equivalent of ethylene. After nearly four decades, RCM has been developed as a powerful methodology that has revolutionized the way in which chemists approached the synthesis of ring systems. It has

also become a key step in many synthetic sequences such as reactions involving heterocyclic rings containing phosphorus,[51] oxygen,[52] nitrogen,[53] including aromatic heterocyclic rings,[54] cyclophanes,[55] and some spirocyclic natural products (see Scheme 2.4).

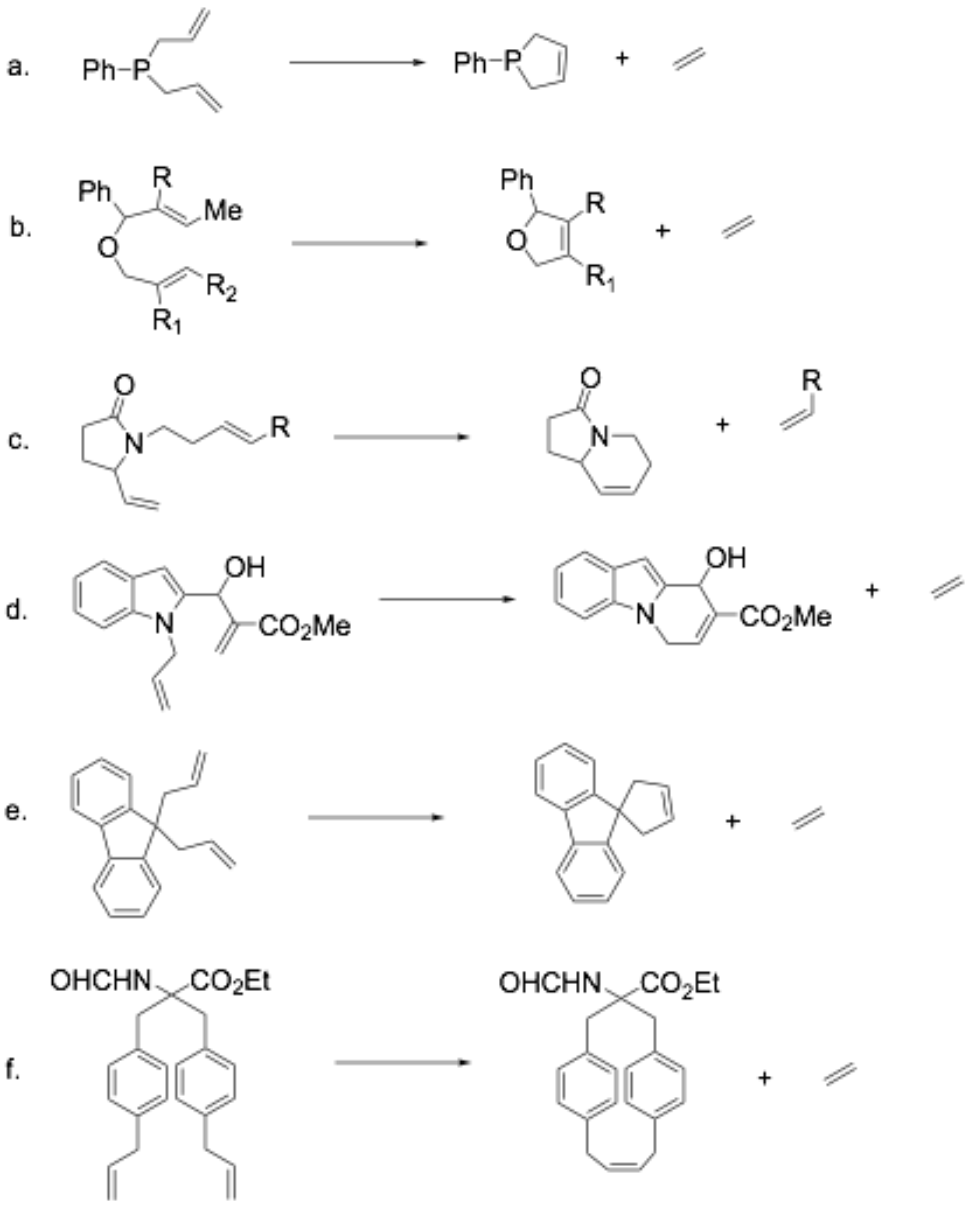

Scheme IV.4: Selected formation of heterocyclic ring containing halogen atoms or aromatic ring undergo RCM. a.) contains phosphorus, b.) contains oxygen, c.)

contains nitrogen, d.) contains aromatic ring, e.) contains spirocyclic ring, f.) cyclophane derivative.

Over the past decade, there have been many new applications of RCM in the synthesis of compounds used for medical and biological purposes, such as peptidomimetics[56] carbonhydride derivatives[57,58,59] alkaloids[60,61] and bioactive cyclic compounds.[62,63] One example is the synthesis of a type I β-turn mimic (Scheme 2.5). β-turn mimics play an important role in protein studies because of their ability to stabilize short peptides and protein-protein interactions. RCM made an important contribution to the construction of the 10-membered rings, the key step in this synthetic sequence.

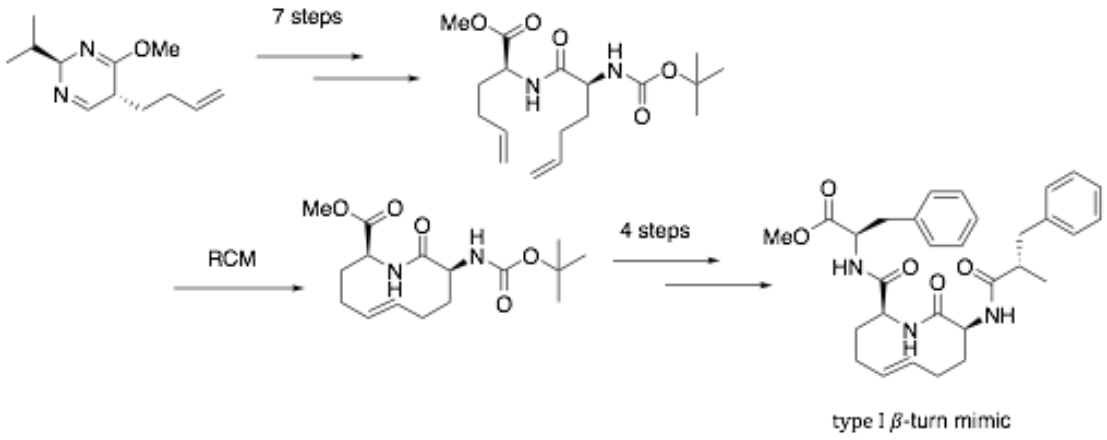

Scheme IV.5: Synthesis of type I β-turn mimic via RCM. Modified from reference [56].

Another application of RCM is the synthesis of a natural product Aristeromycin form carbohydrates. Aristeromycin is an important carbocyclic nucleoside compound containing a five-membered carbocycle that exhibits significant antitumor as well as antiviral activity and is also used in cancer chemotherapy.[64] The key step of the synthesis is about how to

obtain the cyclopentene. At the early stage (1990), it required 10 steps to obtain the cyclopentene from a simple sugar D-glucose and go forward to Aristeromycin.[65] However, with the help of RCM, the diene was made easily from Ribofuranoside and the ring closed to give the cyclopentene intermediate, and Ribofuranoside is available in two steps from ribose, a simple sugar with linear form $CHO(CHOH)_3CH_2OH$ (see Scheme 2.6).

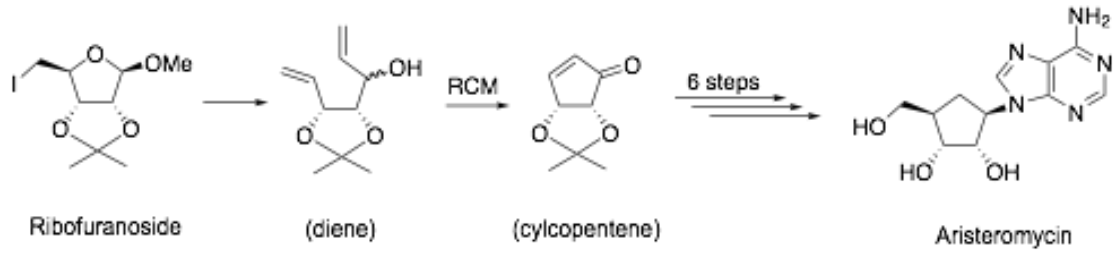

Scheme IV.6: Synthesis of Aristeromycin via RCM from ribose. Modified from reference [60].

2.2 Mechanism of RCM

In 2005, Yves Chauvin, Robert Grubbs, and Richard Schrock were awarded the Nobel Prize in Chemistry for their fundamental work on the mechanism of metathesis. Their work led to the widely accepted hypothesis that metathesis occurs by a sequence of [2+2] cycloaddition and cycloreversion reactions, and the key intermediates in this mechanism are metal-carbene and metallacyclobutane complex. In brief, one ligand on the carbene complex catalyst precursor disassociates to give an open coordination site, necessary for coordination of olefin C=C bond before the [2+2] cycloaddition step. After coordination of olefin, the complex containing the olefin and the metal-carbene generates a metallacyclobutane complex, which reverts to complex containing a new metal carbene and new olefin that dissociate the new olefin (see Scheme 2.7).

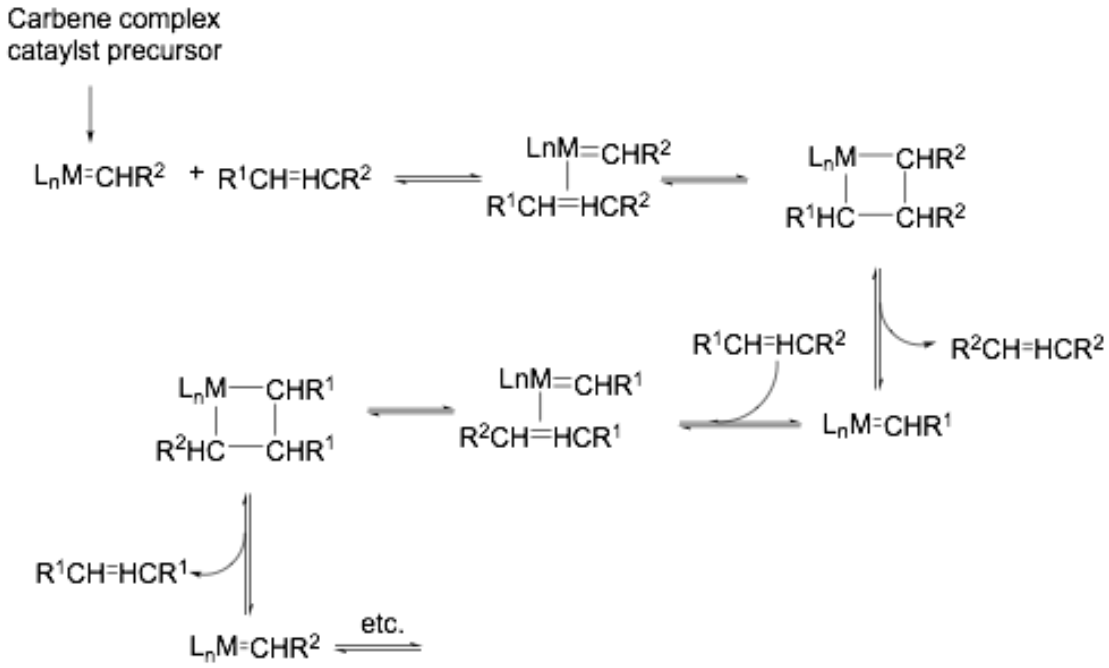

Scheme IV.7: Widely accepted mechanism of the olefin metathesis reaction.[66,67]

This sequence of reactions showed in Scheme 11 represent the general mechanism for all types of metathesis. With suitable modification, it can be adopted to describe RCM specifically (see Scheme 2.8).

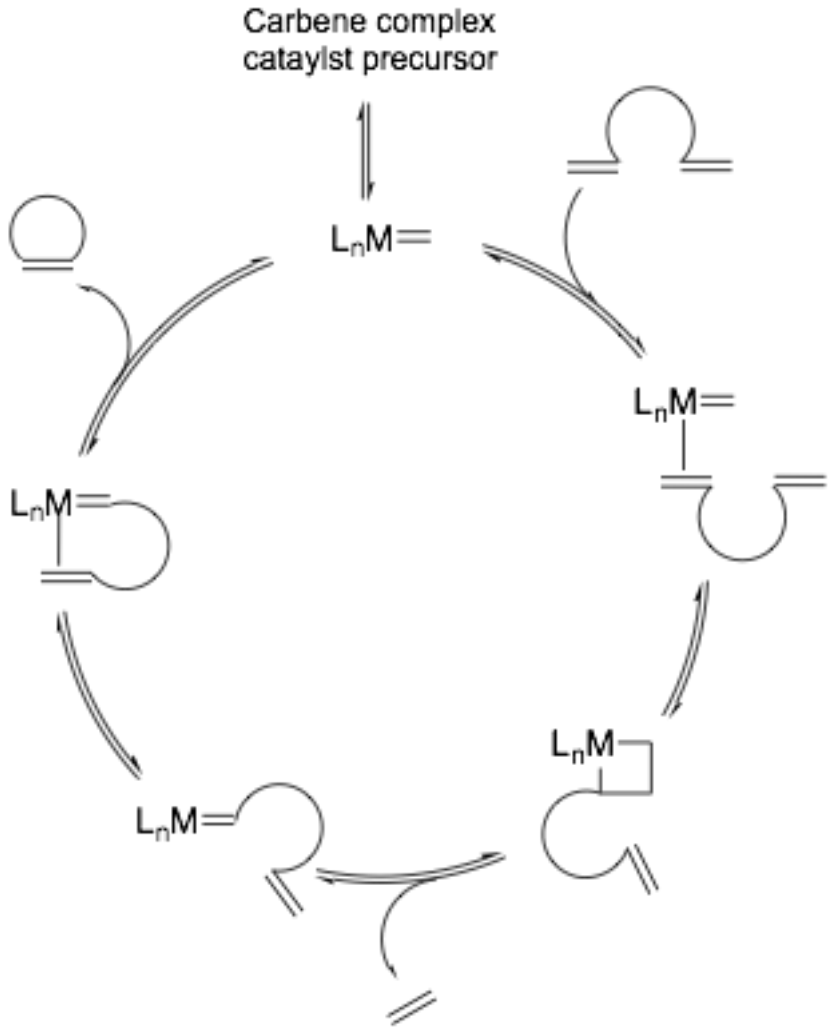

Scheme IV.8: Mechanism cycle of RCM. The reaction is generally driven by ethylene loss.

2.3 Development of the catalyst

Although RCM has become powerful tool for organic synthesis in many areas, it has no advantage over other methodologies when it was first discovered because of the limitations of the catalyst. Metathesis catalysts can be either homogenous or heterogeneous. Homogenous catalysts include complexes of Ru, Mo and W, and heterogeneous catalysts such as WO_3/silica or MoO_3 supported on alumina are used on an industrial scale. In early

mechanism studies during 1970s, the catalyst often was some mixture of compounds, such as $WCl_6/AlEt_2Cl$ or $WCl_6/BuLi$, and the turnover rate and ratio had no advantage over other methods. At that time, investigators didn't understand that it was metal carbene and metallacyclobutane complexes actually catalyzing the metathesis reaction. The first well-defined catalyst that showed that metal carbene complexes could catalyze metathesis was reported by Casey and Burkhardt.[68] They synthesized the tungsten carbene complex $(CO)_5W{=}CPh_2$ and demonstrated the exchange process of it with $H_2C{=}C(Ph)(OMe)$ to give $(CO)_5W{=}C(Ph)(OMe)$ and $H_2C{=}CPh_2$ (see Scheme 2.9).

Scheme IV.9: Reactions between a well-defined carbene complex and an alkene demonstrating metathesis

Based on this catalyst, further work done by Katz and coworkers showed that this complex could catalyze metathesis reactions: not only cross metathesis,[69] but also ROMP of small-ring cycloalkenes.[70,71] Although this result clearly demonstrated that metal-carbene complexes could be the true catalytically active specie, it was not an especially active catalyst. Continued worked by Schrock's group led to some very active catalysts by using different metals (see Figure 2.1).

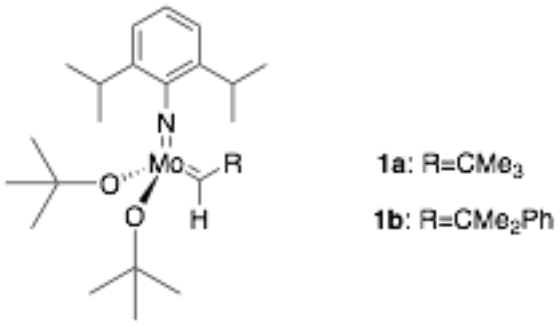

Figure IV.1: Mo involved metal-carbene complex constructed by Schrock.

Further work by Schrock's group led to another version of an alkylidene catalyst based on Mo complex **2** (also known as Schrock's second-generation catalyst, see Scheme 2.10) that was effective in giving metathesis products with high yield and excellent % ee values under mild condition.[72]

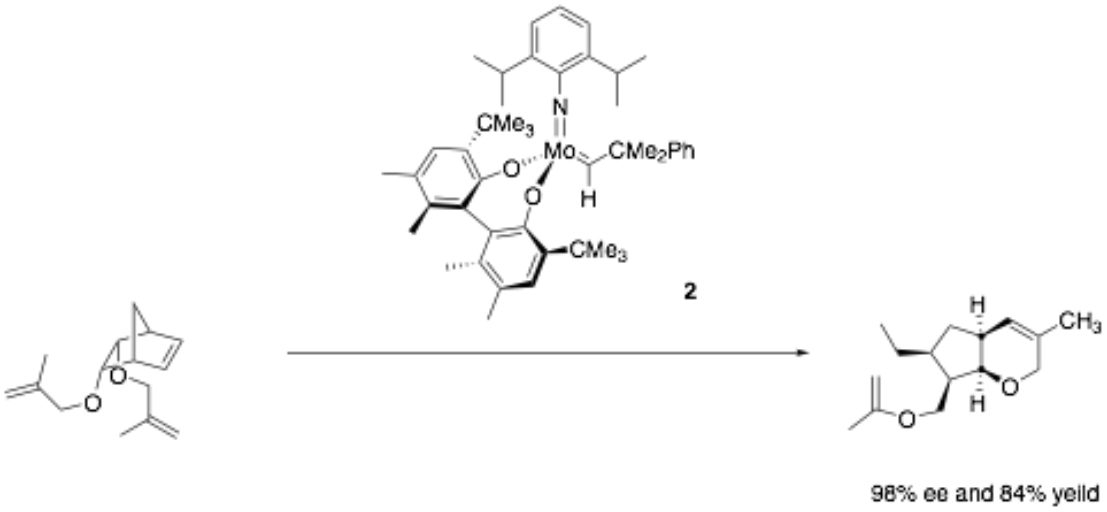

Scheme IV.10: Metathesis catalyzed by Schrock's second-generation catalyst with high yield and high % ee value.

At the same time, Grubbs and coworkers were also working to uncover the mechanism and to introduce an effective catalyst.[73] They studied Tebbe's reagent, an organometallic

compound with formula $(C_5H_5)_2TiCH_2ClAl(CH_3)_2$, and found that the titanacyclobutanes derived from the reagent could be in the direct equilibrium with the metal carbene (see Scheme 2.11), and that Tebbe's reagent can promote Ring-Opening Metathesis Polymerization by forming four-membered ring metallacyclic intermediates.[74] This system of Ti-based complexes was not an active metathesis process, but the work showed that both intermediates – metal-carbene and metallacycle – were important in the metathesis pathway.

Scheme IV.11: Titanacyclobutane equilibrium with titana-carbene.

Although the Ti complexes helped to illustrate the true nature of metathesis catalysts, they were not widely applicable in practical use because these complexes were not as active as other catalysts and Ti (as a metal in early transition group) limited their use in metathesis of alkenes containing oxygen functional groups.

Grubbs and coworkers discovered the Ru complex that led to numerous metathesis catalysts that proved to be especially useful in the field of organic synthesis: a Ru-alkylidene complex (also known as Grubbs' first-generation catalyst as shown in Figure 2.2).[75] However, the instability of this catalyst in air and water limited its use, and the lifetime of this catalyst was insufficient to give high yield of products with reasonable catalyst loadings.

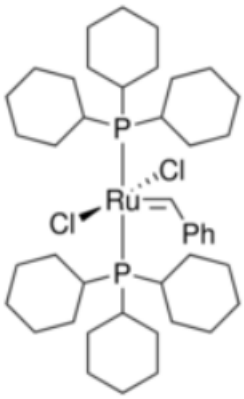

Figure IV.2: Grubbs' first-generation catalyst 3.

It was understood by Grubbs that catalyst activation was the loss of one of the neutral ligands from the catalyst precursor to produce a 14-electron species. For the ligand system in **3**, phosphines less bulky than PCy_3 would coordinate too strongly to the metal and were not susceptible to dissociation, but phosphines bulkier than PCy_3 (i.e. with larger cone angle) were too labile to produce a stable 14-electron complex intermediate. To improve the use of the Ru-alkylidene complex, a new ligand system was required. Further modification by Grubbs involved replacement of one PCy_3 ligand with an N-heterocyclic carbene (NHC) ligand to produce a more active yet more stable complex that posseed a wide range of metathesis activity. The Ru-alkylidene is known as Grubbs' second-generation catalyst (see Figure 2.3).[76]

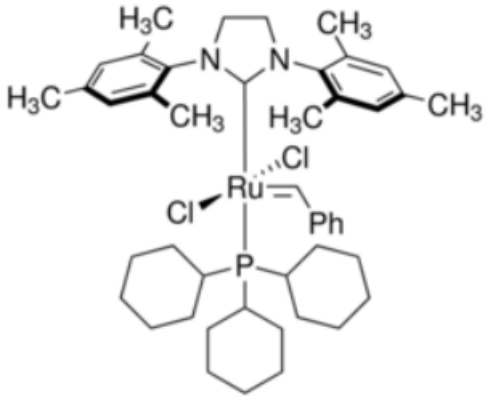

Figure IV.3: Grubbs' second-generation catalyst.

The development of Ru-based catalysts continues as new types of catalyst have been disclosed, such as the first- and second-generation Hoveyda-Grubbs catalyst,[77] the third generation of Grubbs catalyst,[78] and the second generation of Piers' catalyst.[79] It is apparent that no one catalyst is suitable for all type of metathesis reactions or for every application of metathesis in organic or polymer synthesis.

2.4 Equilibrium of RCM and other metathesis

As in many cyclization methods, the competition between intermolecular oligomerization reactions and intramolecular ring closing reactions limits the efficiency of RCM (though Fogg has shown that oligomerization is not irreversible[82]). As shown in Scheme 2.7, olefin metathesis involves a series of fully reversible [2+2] cycloaddition and cycloreversion reactions, which means that "living" metathesis products are distributed thermodynamically in the whole metathesis process.[80,81] In many other cases, RCM and oligomerization are irreversible, but in such cases that is mainly due to high activity but short lifetime catalyst that generate a kinetic distribution of all metathesis products. As the

reactivity and lifetime of catalyst has been improved (discussed above), it is possible to establish a ring-chain equilibrium system for diene metathesis.[82]

The relationship between RCM and ROM are mirror images, which is evident from comparison of Scheme 2.12a and 2.12b. For 2.12a, the metallacycobutane cycloaddition, it will close the ring, and 2.12b involves cycloreversion which will open the ring. For RCM, the formation of strained ring structures is enthalpically unfavorable, which makes it a thermodynamically controlled reaction, generally driven by loss of ethylene gas as shown in 2.12c, and its reversible. However, the product of RCM can act as the monomer of ROMP, and any ring strain energy can create an enthalpic driving force to give oligomers such as dimers, trimers etc. as shown in 2.12d. Htheighly strained rings do not usually form via RCM, so monomers for ROMP (such as dicyclopentadiene or norbornene) are made via other methods. ROMP can reversibly break down oligomers to give RCM product in a process known as cyclodepolymerization (CDP). Oligomers can ring-close to form cyclic oligomers (twice as large for dimer, three times large for trimer, etc.) as shown in 2.12f, and this process is reversible, similar to 2.12c. Oligomers can also be formed direct from precursors via intermolecular metathesis, also known as ADMET polymerization as shown in 2.12e. The reversible reaction of ADMET polymerization is to break the carbon chain of the oligomer through metathesis to give monomer, which is the starting material of RCM.

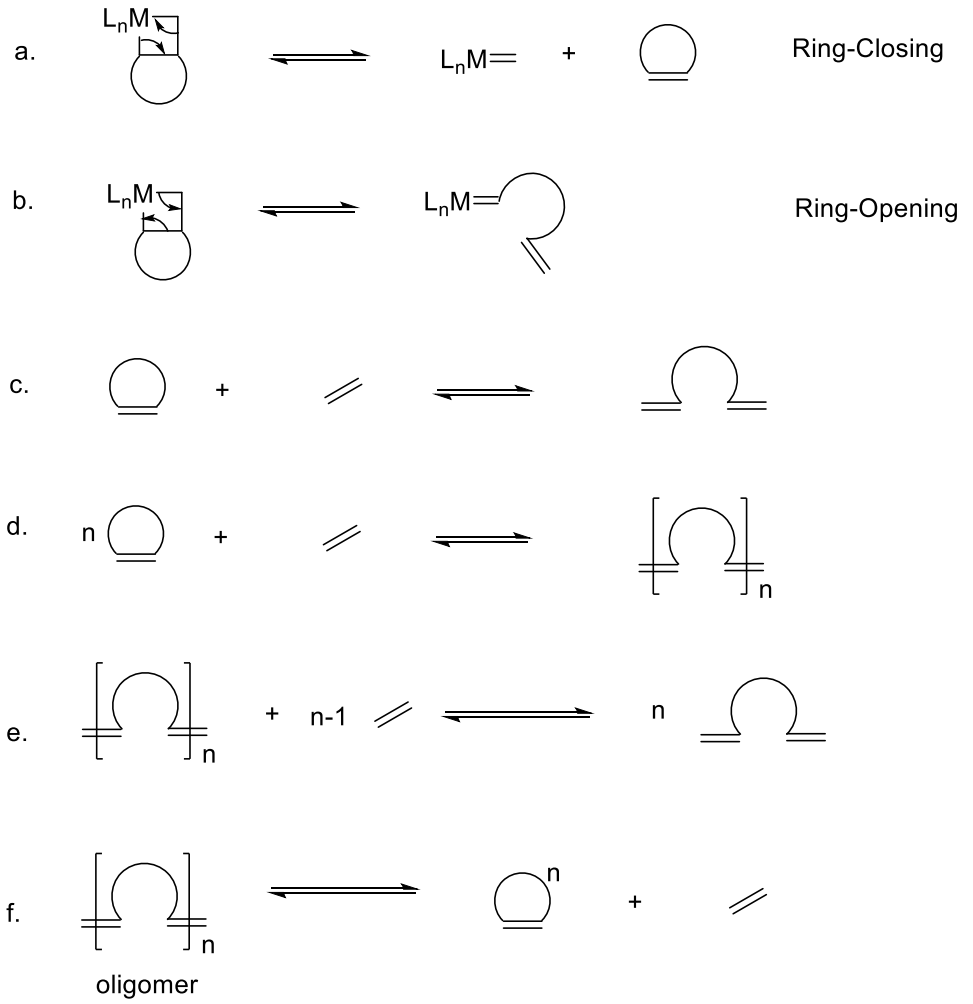

Scheme IV.12: Possible metathesis pathways in RCM.

However, the most common reactions of RCM occur in refluxing nonpolar organic solvents such as dichloromethane or toluene, and under such condition, ethylene is efficiently swept out if the reaction mixture. As such, ADMET and RCM are effectively irreversible. In summary of ring-chain equilibrium in RCM, precursors undergo intra- or inter-molecular metathesis which are irreversible, while equilibrium can be established between the product of RCM (ring compound) and oligomers (chain compound), see Scheme 2.13.

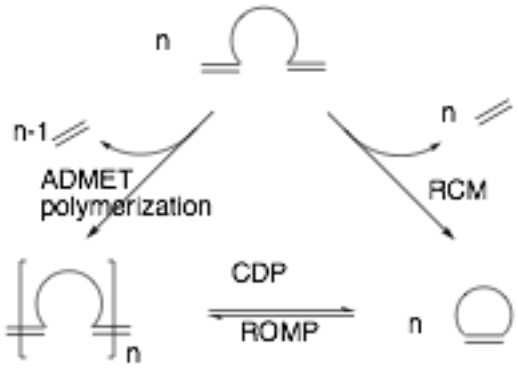

Scheme IV.13: Olefin metathesis pathways involving irreversible loss of ethylene.

2.5 Decomposition of Grubbs second generation (GuII) catalyst

As do many other catalysts, the extensively used ruthenium-based olefin catalyst would decompose during the catalytic cycle. It is important to understand the decomposition pathways of the existing catalyst in order to design new and more efficient catalysts. To discover the decomposition pathways, chemists seek to understand what and why byproducts may be formed during metathesis reactions and also some potential competition of catalyst with different chemical environments. Even though numerous modification on ruthenium-based catalysts have been developed in literature (as discussed above) in order to balance between stability and reactivity, the second-generation Grubbs catalyst is one of the most used olefin catalyst and will be discussed here.

As discussed in chapter 2.2, the proposed mechanism shows that activation of GuII via dissociation of tricyclohexylphosphine (PCy_3) forms methylidene complexes after a catalytic turnover with a terminal alkene. PCy_3 can be further protonated in ESI condition and observed at *m/z* 281 as $[HPCy_3]^+$. Methylidene complexes are considered as the most fragile species in metathesis reactions and prone to rapid decomposition. Their instability

was first proposed by Grubbs, where he suggest that the dissociated phosphine can not only recapture the methylidene complex to give a 16 electron coordinated Ru species (resting state), but also can react with the alkylidene moiety to form methyltricyclohexylphosphonium chloride $[CH_3PCy_3]^+Cl^-$ and dinuclear ruthenium hydride species (see Scheme 2.14).[83,84] The dissociated phosphine can react with the alkylidene, first forming the phosphine ylide ($Cy_3P=CH_2$) and a 12 electron Ru complex. This 12 electron ruthenium product can then C-H activate the mesityl ring of the 14 electron species to form a dinuclear complex through two chloride bridges between two ruthenium centers. Then phosphine ylide can abstract HCl and migration of the two chlorides can generate the final dinuclear ruthenium hydride species. The final decomposition product is also believed be responsible for the undesired isomerization in olefin metathesis reactions.[83,85]

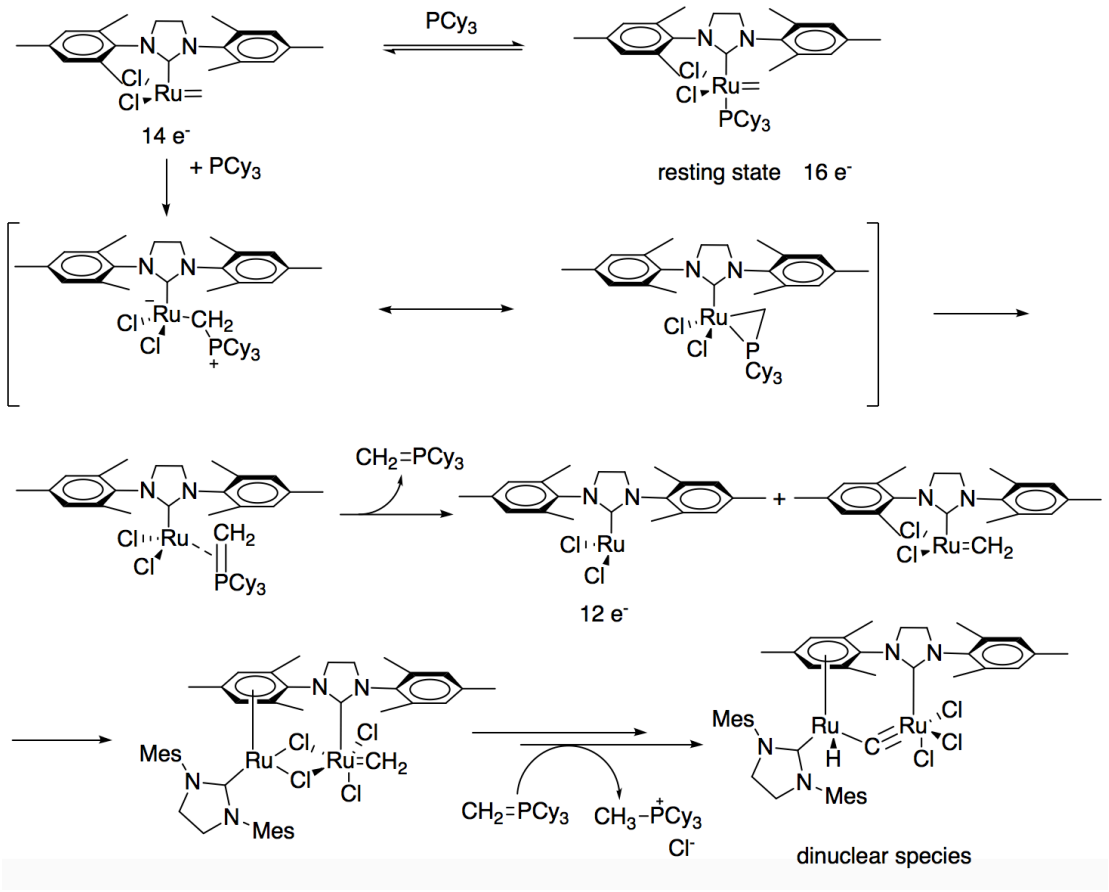

Scheme IV.14: Decomposition mechanism proposed by Grubbs. Modified from reference [84].

The dinuclear ruthenium hydride complex had been shown to be active for the isomerization by Grubbs, but Fogg questioned whether the activity of this species can account for all the observed isomerization in metathesis.[86] Fogg pointed out that the isomerization happened in metathesis could be attributed to decomposed ruthenium nanoparticles which appear to contribute significantly rather than molecular ruthenium species [87] and proposed a pathway of GuII decomposition recently (2016) (see Scheme 2.15).

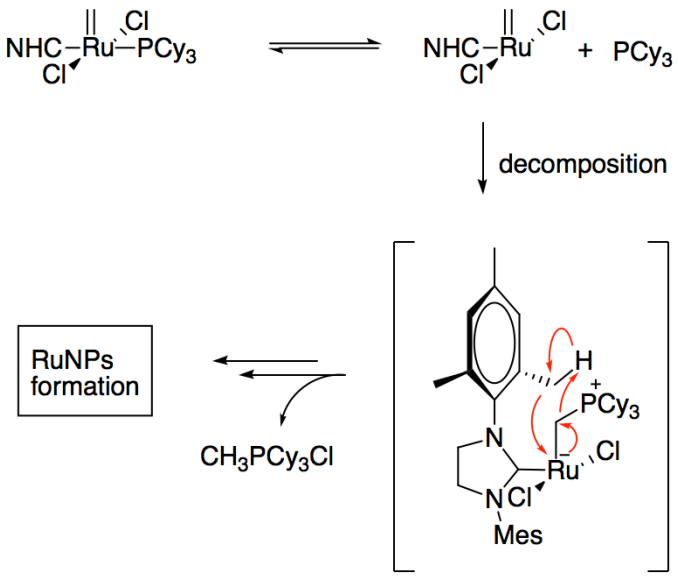

Scheme IV.15: Proposed decomposition pathway for formation of ruthenium nanoparticles by Fogg. Modified from references [87,88].

Similar to Grubbs' proposal, this pathway is also established for when free PCy_3 attacks the alkylidene moiety of active 14 electron species, but the elimination of phosphine occurs by abstraction of a proton (from the NHC ligand) and bound chloride to form $[CH_3PCy_3]Cl$. A net loss of three ligands per Ru center yield low-coordinated Ru species providing a starting point for the formation of Ru nanoparticles.

2.6 Isomerization

As mentioned above, isomerization could have happened due to the decomposition of GuII catalyst. It is unintended but commonly observed in most olefin metathesis[89,90,91,92] and several examples are shown in Scheme 2.16.

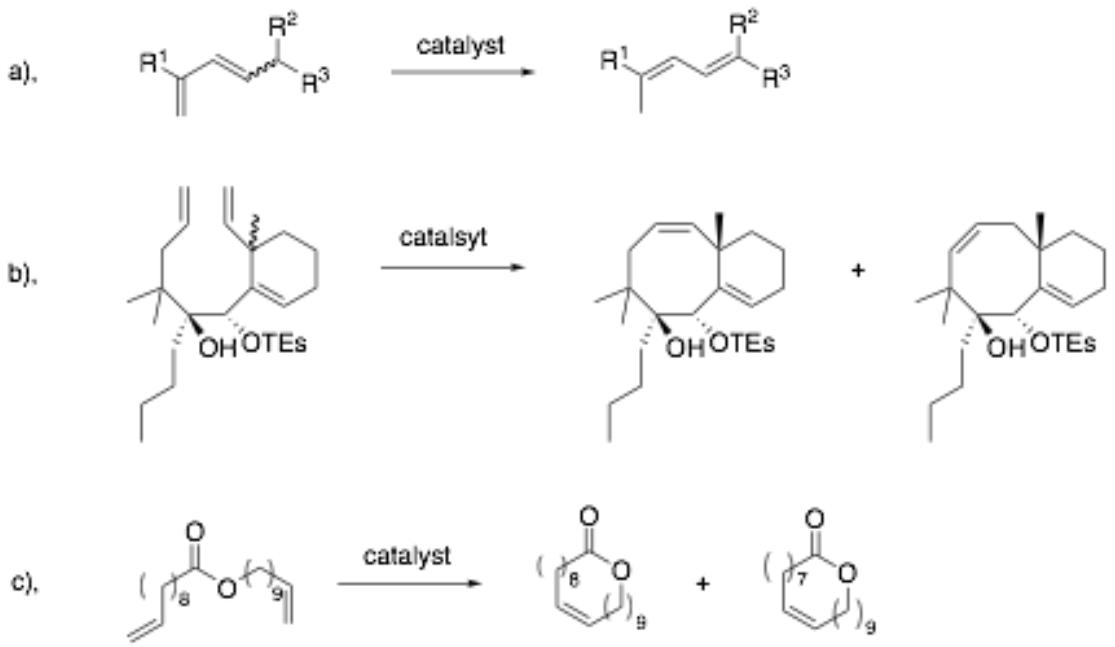

Scheme IV.16: Examples of isomerization occur in RCM. a), b), c) modified from references [93], [94] and [95] respectively.

An early overview by Bernd Schmidt showed a potential mechanism that may contribute to isomerization via a π-allyl complex (see Scheme 2.17).[96]

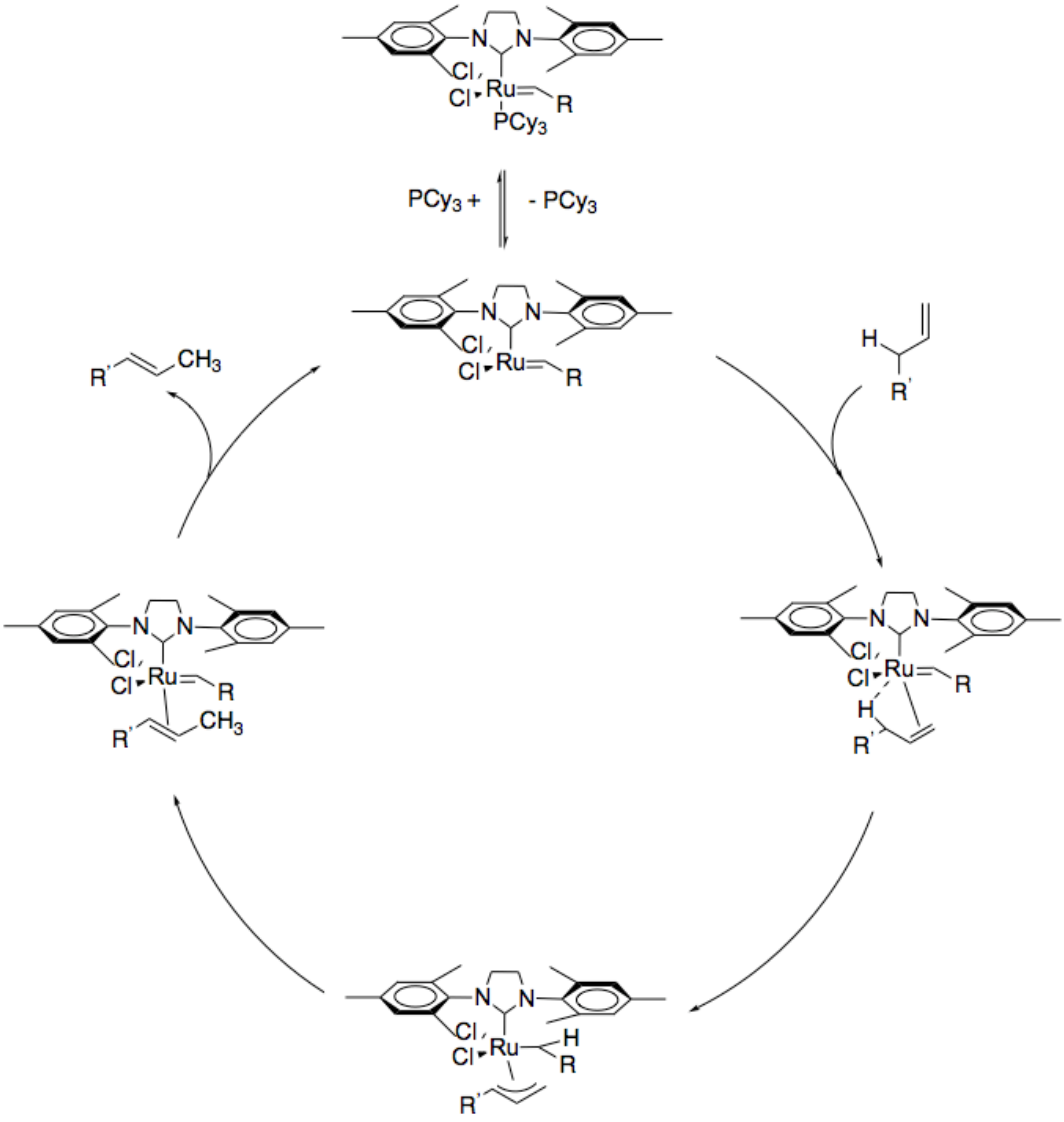

Scheme IV.17: Proposed mechanism of isomerization via π-allyl complexes.

Again, the catalyst is activated by dissociate PCy_3 to form a 14 electron Ru species, but instead of alkene coordination, an agnostic interaction (indicated by a dashed line) might occur and cause deprotonation of the alkene to form a σ-alkyl/π-allyl complex, which can rearrange to generate an isomerized alkene. Dissociation of the isomerized alkene regenerates the active 14 electron Ru species.

2.7 Conclusion

To conclude, metathesis is used in the production of specialty chemicals, agricultural chemicals, drugs, and polymers with unique properties, and interest in using it to generate other new materials remains strong. However, the finer details of the process remain under study, in the hope of continuing to be able to improve catalyst performance, lifetime and scope.

Chapter 3: Results and discussions

3.1 Presursors

To investigate the ring-closing metathesis reaction, we planned to probe it using a combination of a charge-tagged substrate and the real-time mass spectrometric analysis method of pressurized sample infusion (PSI) electrospray ionization mass spectrometry (ESI-MS), which is described in detail in chapter 1.

We prepared a range of dibutyldialkenylammonium hexafluorophosphate compounds of general formula $[Bu_2N(\{CH_2\}_nCH=CH_2)(\{CH_2\}_mCH=CH_2)]^+PF_6^-$ as precursors and exposed them to Grubb's second generation catalyst (GuII). For n=m=1-6 to make five-, seven-, nine-, eleven-, thirteen- and fifteen- membered ring, plus two cases: n=1, m=2 and n=1, m=4 to make six- and eight-membered rings. The positive charge on nitrogen created inherent charge that makes these ions visible by ESI-MS. The synthesis and isolation of these compounds was straightforward via a two step synthesis: double alkylation of dibutylamine followed by a salt metathesis with $Na[PF_6]$ (Scheme 3.1a). Precursors were characterized by ESI-MS, ^1H NMR (see Appendix I and IV), and in two cases, by X-ray structure determinations (Figure 3.1, and see full report in appendix II). One problem for proton NMR is that the salt metathesis was done in deionized water, and it is very hard to completely remove water, all precursors had been dried under vacuum for 3 days but still some water residue showed up in their ^1H NMR (δ 1.56 for $CDCl_3$ and δ 1.52 for CD_2Cl_2). H_2O as a weak donor can degrade catalyst productivity in RCM proved by Fogg,[88] however, the amount of H_2O residue was too low to worry about compare to 10 and 100 equivalent of H_2O used in Fogg's experiment. To try to make the numbering of the different charged

compounds as transparent as possible, we have named them according to the ring size formed in each case, with the prefix "**R**" for "reactant" and "**P**" for "product". So, when n=1, the product formed is a five-membered ring, **P5**, and the reacting diene from which it was formed is correspondingly named as **R5**. The $[Bu_2N(\{CH_2\}_nCH{=}CH_2)(\{CH_2\}_mCH{=}CH_2)]^+PF_6^-$ compounds prepared are named as **R5**, **R6**, **R7**, **R8**, **R9**, **R11**, **R13** and **R15**.

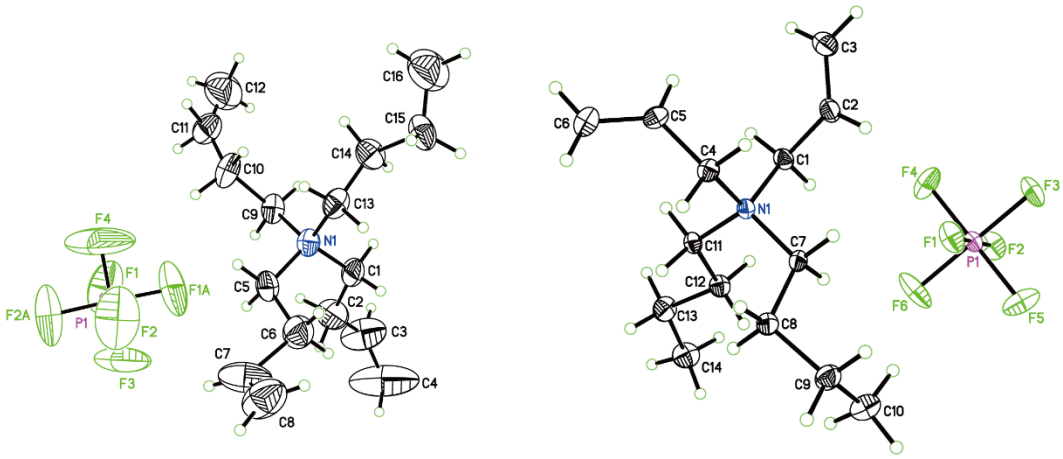

Figure 3.1: Left, crystal structure of R7. Right, crystal structure of R5.

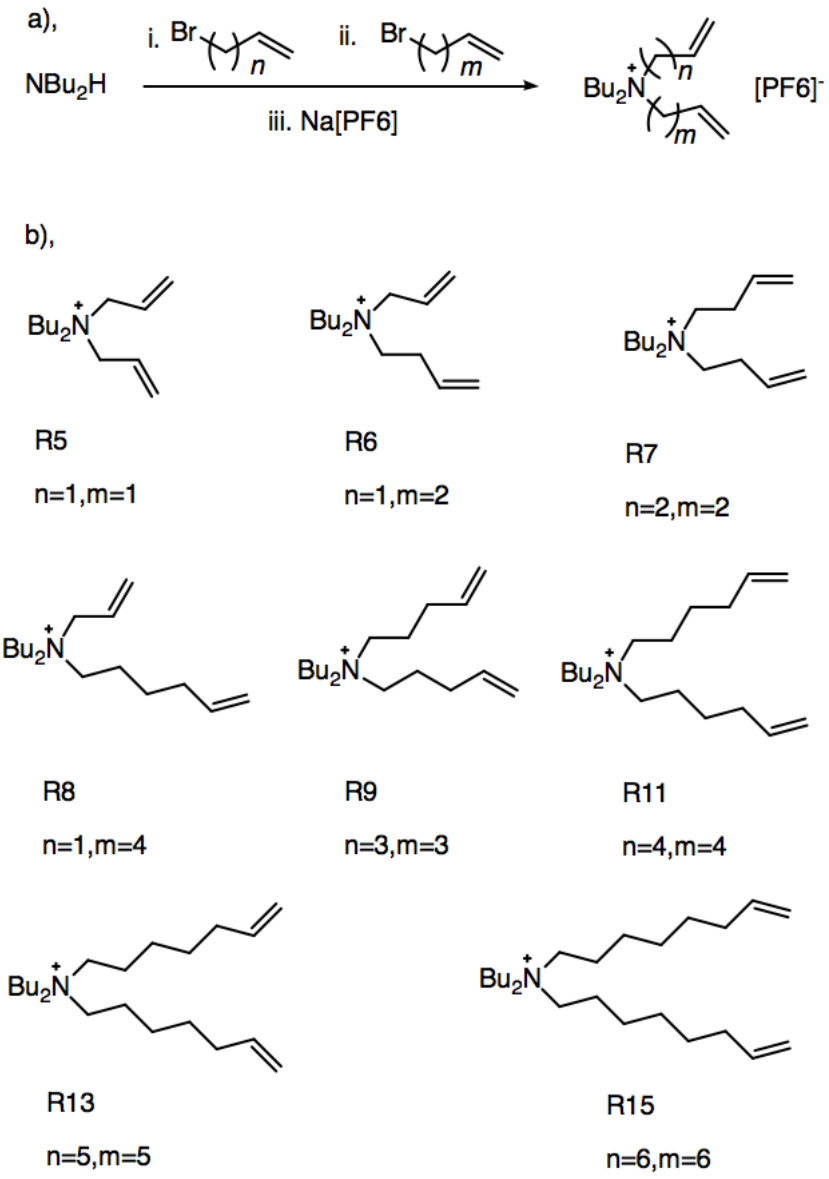

Scheme 3.1: a), General synthetic route to the charged precursors used in this study. b), structure of each precursor.

3.2 Reactions

To maximize our chances of observing intermediates, we ran the RCM reactions under relatively high catalyst loadings (20 mol%) at precursors' concentration 0.035 mM (to

approach to this low concentration, we made stock solution for both starting material and the catalyst). This concentration was optimized to suit our instrument (the micro Q-ToF, mentioned in chapter 1) to obtain satisfactory signal and to avoid potential aggregations or instrument saturation at the early stage of this work and kept it consistent for each precursor. Compared to experiments carried out in other RCM study, this concentration was ultra low, most experiments were talking about 5 mM of starting material (including Fogg's group [97,98]) which is unsuitable for MS. Conditions of high catalyst loading had the beneficial side effect of accelerating the reaction, and in some cases (depending on the ring size of the product) all starting material was consumed in less than ten minutes.

The reaction rate for the disappearance of different precursors was very different (see Figure 3.2). The disappearance of each starting material was plotted together and color-coded. It is believed that ring strain energy plays an important role in RCM process for the enthalpic cost of the reaction.[错误! 未定义书签。] For simple carbocycles, strain energy is at minimum for five- to seven-membered rings. It increases sharply in the medium-ring regime and then declines again (see Figure 3.3).[99] Thus, for small strain energy, reactions tend to be fast such as **R5**-**R7**, for **R8** and **R9** it would be slowest and from **R11** to **R15** tend to be faster and faster. However, based on our observations, **R7** and **R15** was the fastest reactions that is reasonable, but **R6** was far slower than **R7** and **R5** was surprisingly the slowest one. Note that Figure 3.3 showed here are carbocycles without heteroatoms, with installation of a N, it could affect the strain energy of the ring because there are two butyl group designed to minimize aggregation which could bring steric effect to the ring. However, we've found a collaborator to calculate the strain energy for those nitrogen contained carboncycles.

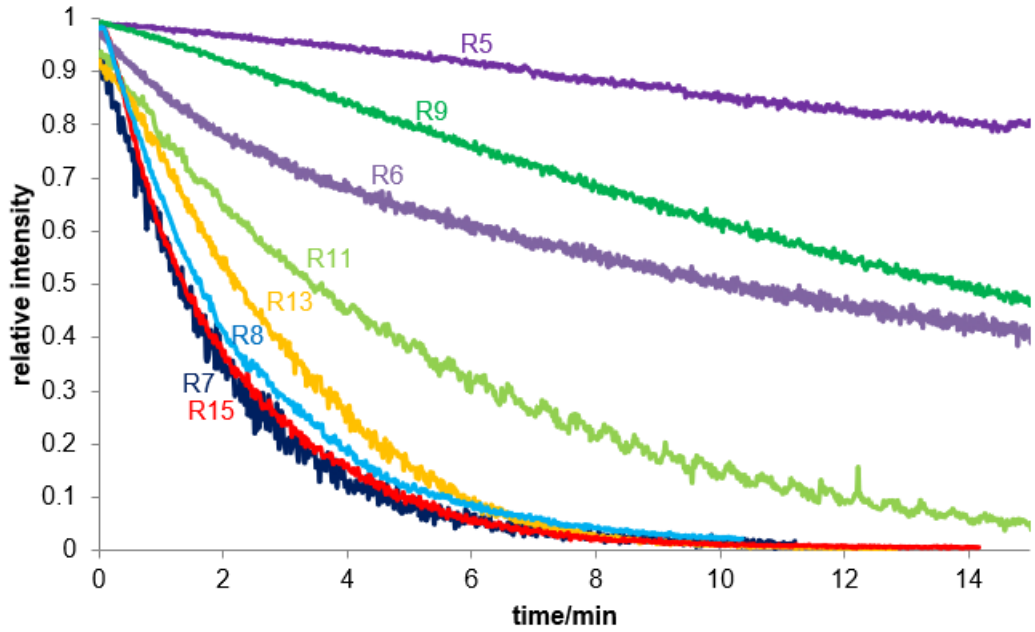

Figure 3.2: Disappearance rate of precursors over time.

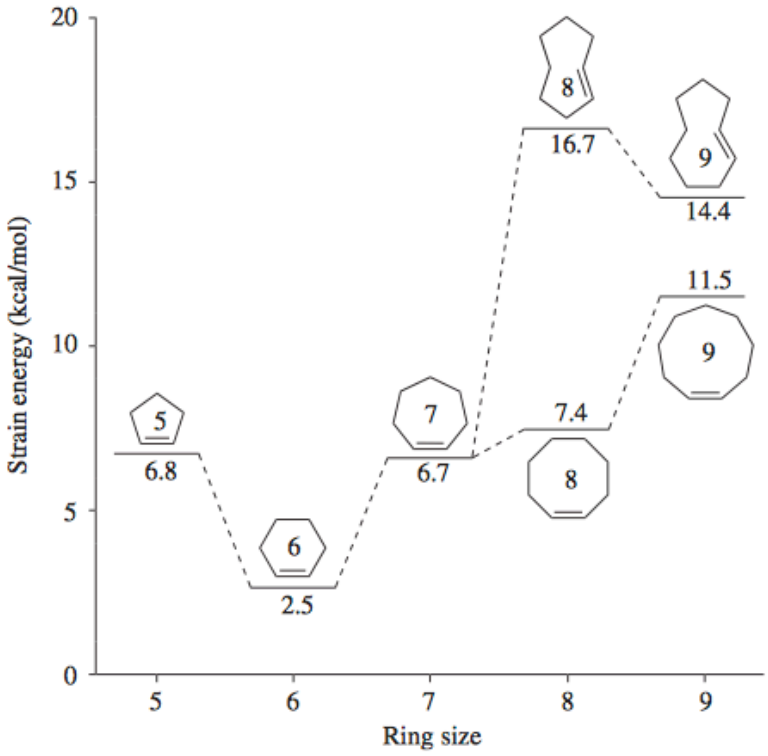

Figure 3.3： Ring strain energy for different size carbocycles. Modified from reference [98].

By examination of the disappearance of precursors, we can show that the metathesis reaction is first order in catalyst, as seen in Figure 3.4, plotted using Bures' method of time normalization.[100] We chose **R7** because it is the fastest. All three lines for 5, 10 and 20 mol% should overlap perfectly if first order. The 5% catalyst loading line deviates slightly from others, but we found this is not an uncommon occurrence for low catalyst loadings under mass spectrometric conditions: even low levels of contaminants in the solvent can influence reactions where concentrations are very low (as in MS analyses). In a previous study, for example, we observed impurities including the amines added in trace quantities to the dichloromethane solvent used, and these affect the effective concentration of the catalyst.[101] Even at 20 mol% loading, the catalyst concentration under the condition employed was only 7×10^{-6} M.

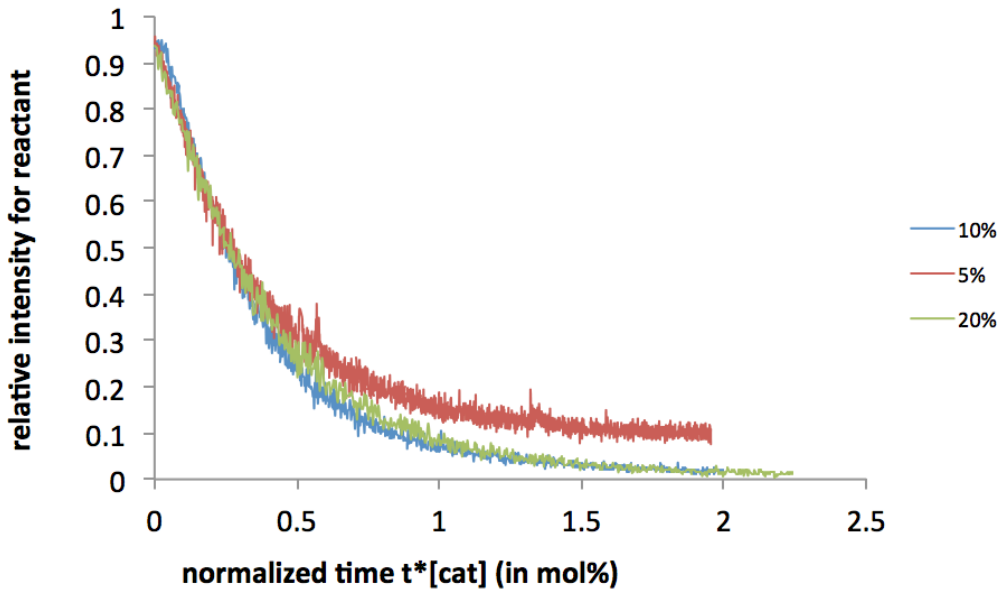

Figure 3.4: Reaction rates for 7-membered ring starting material at 5, 10 and 20% catalyst loading, plotted with time normalized method.

Also, reaction rate constants were calculated through the following equation:

$$\ln\left(\frac{[A]_t}{[A]_0}\right) = -kt \qquad \text{Equation (5)}$$

where $[A]_t$ can be represented by the ion counts at the *m/z* for each precursor and $[A]_0$ can be represented by the total ion counts for each reaction in mass spectrometric analysis method. All calculated rate constants were plotted in a line graph (Figure 3.5).

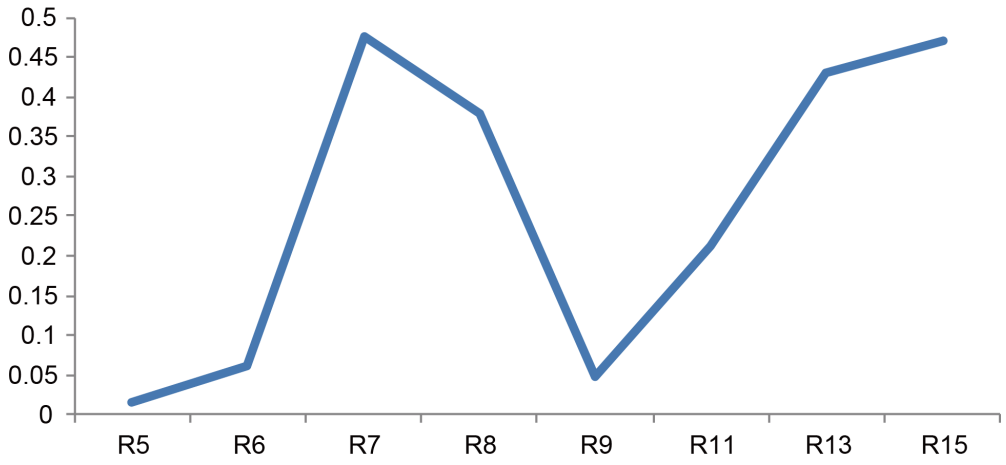

Figure 3.5: Reaction rate constants for disappearance of the starting material in each case.

3.3 Byproducts

Examination of the product distribution of each reaction revealed some interesting byproducts in some of the slower reactions. Mapping the product distribution and reaction rate by ring size, we observe a clear relationship between amount of byproduct formed and the rate of reaction (see Figure 3.6). For **R7**, **R8**, **R13**, **R15**, reactions are clean and also

faster as noted above, but for **R5**, **R6**, **R9** and **R11**, the reaction is slower, and some byproducts appear.

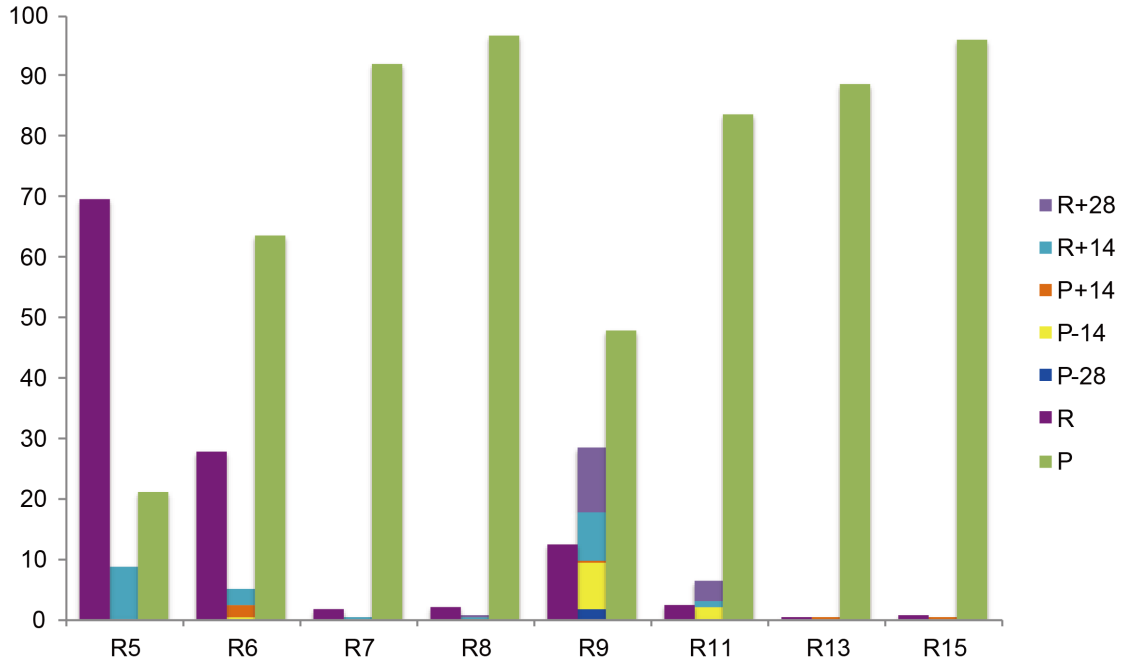

Figure 3.6: Product distribution after 45 minutes for each precursor, for each one, purple column stands for leftover reactant, middle column indicate different byproducts, green column stands for main product.

The most abundance of byproducts was observed in the formation of 9-membered ring product where **R9** as the precursor. Substantial quantities of ions with masses 14 Da above (and to a lesser extent, below) the starting material and the product were observed. Starting material **R9** observed at *m/z* 266 and expected product **P9** observed at *m/z* 238, however, other mass of ions also be observed such as *m/z* 210 (**P9** – 28), *m/z* 224 (**P9** – 14), *m/z* 280 (**R9** + 14) and *m/z* 294 (**R9** + 28). These ions were always minor – single figure percentages – but reliably and reproducibly there (see Figure 3.7).

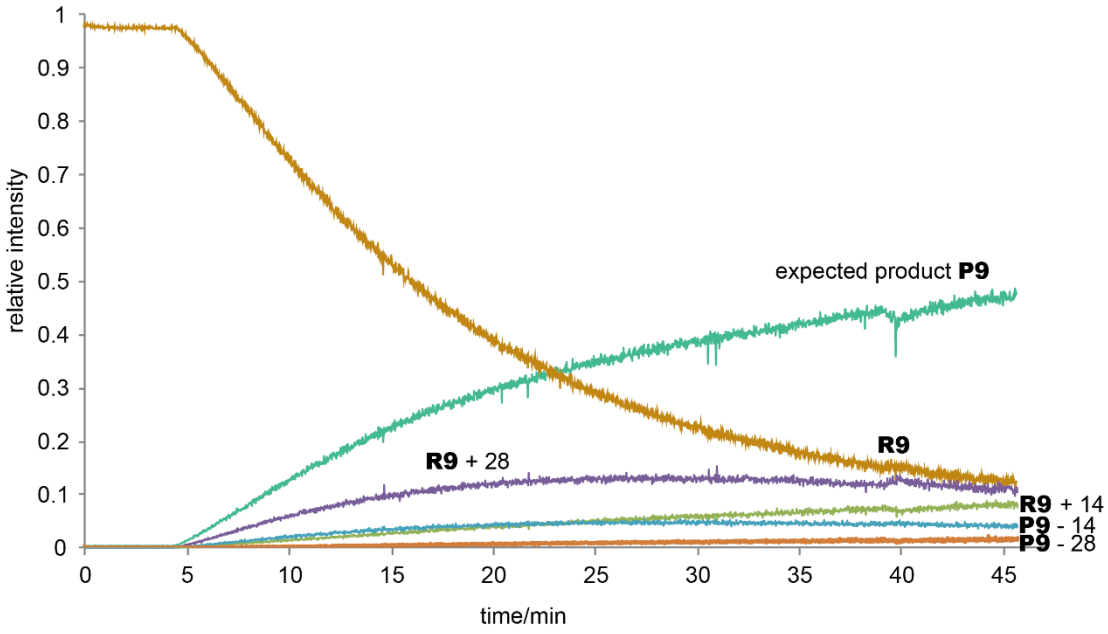

Figure 3.7: Relative abundance for R9 and all products at 45 minutes.

For the reactions that produce byproducts, we examined the byproducts and noticed that all byproducts are 14 Da mass units different from starting material or the dominant product. MS/MS studies (discussed in chapter 1.4) of these byproducts implies that they are related to starting material and product rather than from the catalyst. A 14 Da mass difference usually indicates CH_2, and to confirm that, we examined the product mixture using high resolution mass spectrometry (Orbitrap MS), and the differences universally corresponded to 14.01565 (the exact mass of CH_2) within 4 ppm (see appendix III for detail).

It is important to understand where the CH_2 comes from, one possibility is that CH_2 is from the solvent CH_2Cl_2. An obvious experiment that can be run is to use CD_2Cl_2 as the solvent. If the source of the CH_2 is solvent, then deuterium inclusion would be observed by MS with larger *m/z* differences. However, due to the very high price of CD_2Cl_2 (CAD 239.5 per 10 mL, *sigma-aldrich*), we decided to run the experiment in small vial and higher

concentration, so we compare the reaction in a small vial by using normal dichloromethane and deuterated dichloromethane to examine the difference, if any (see Figure 3.8). We chose the precursor **R5** as it only gives one byproduct which is easy to observe. The byproducts showed up at *m/z* 196 and *m/z* 224 (instead of *m/z* 198 and *m/z* 226 if deuterium was involved), which means that the source of CH_2 is not the solvent.

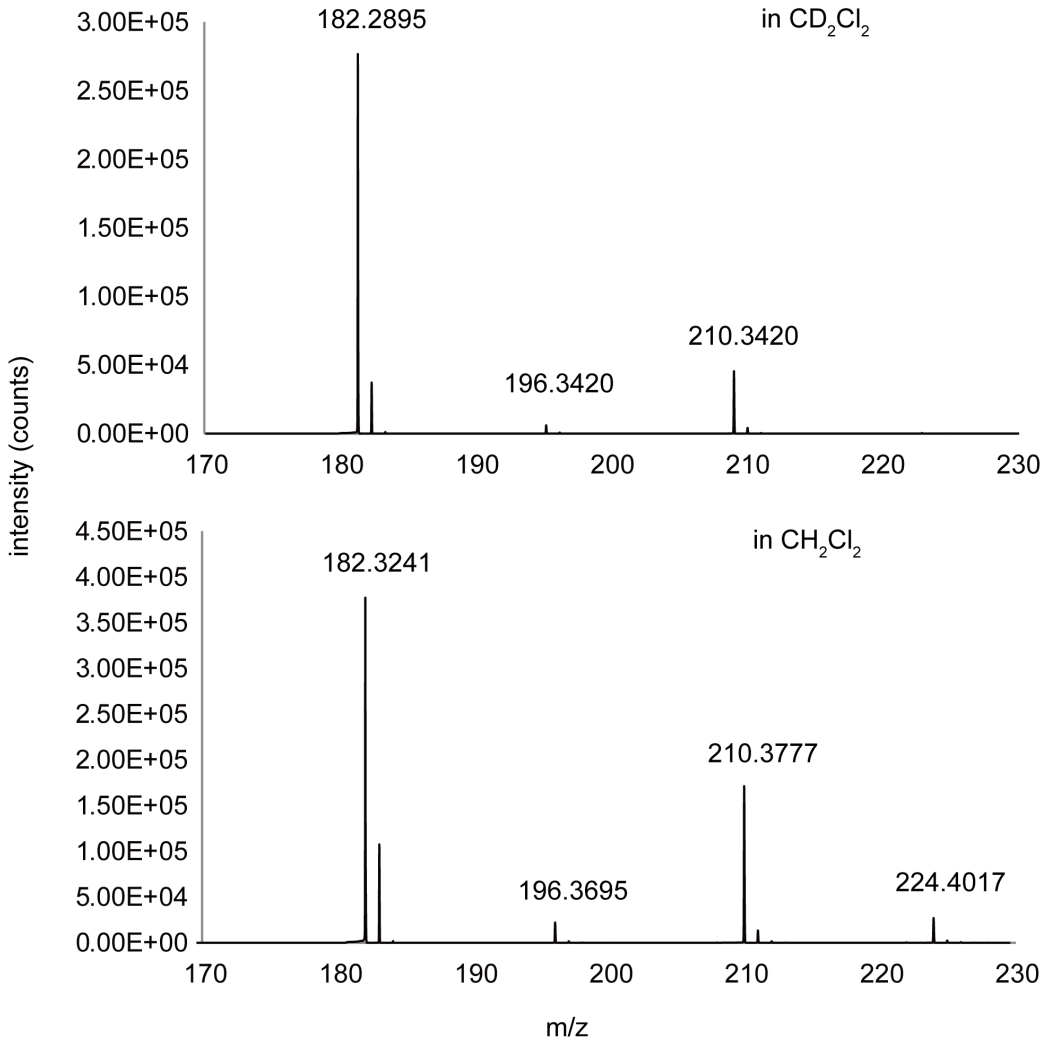

Figure 3.8: Top is R5 with GuII 20 mol% loading in deuterated DCM. Bottom is R5 with GuII 20 mol% in normal DCM.

3.4 Proposed isomerization pathways for byproducts

The most plausible explanation for these byproducts are that they show up through olefin isomerization. This process is readily catalyzed by a variety of metal complexes, most often through the sequence migratory insertion to beta hydride elimination of a different alkene.[102] Migration of the double bond creates the opportunity for different products to arise via cross-metathesis (Scheme 3.2), the example used is for the n=3 case, for which we observed the greatest percentage of byproducts. Note that there is some ambiguity, because we cannot distinguish between some of the species based on *m/z*, because they have identical empirical formulae.

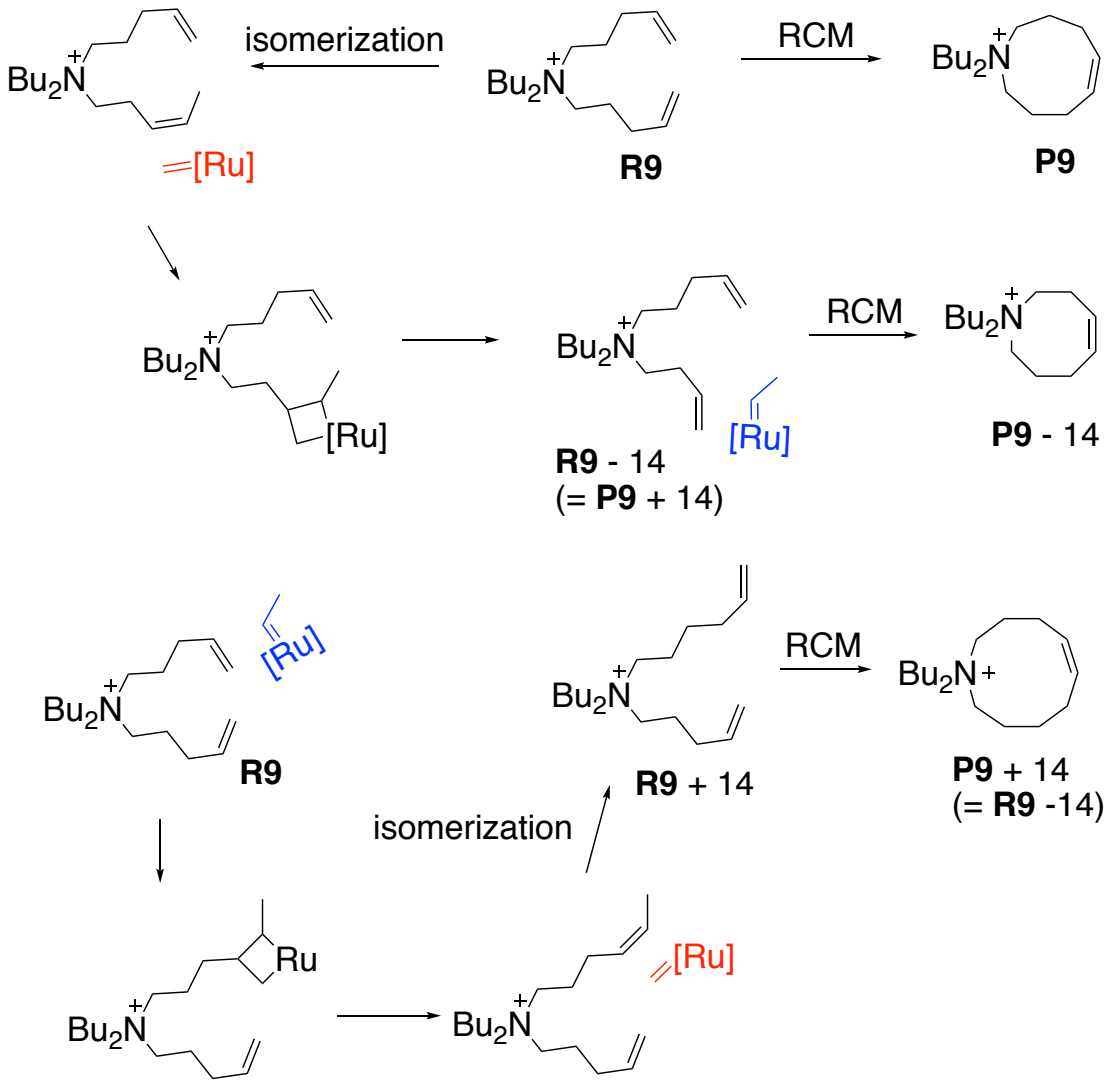

Scheme 3.2: Isomerization leading to creation of byproducts differing in mass by +/− 14 Da from the expected product.

The isomerization can affect not only the starting material, but also the ring-closed product. The example used is for **R7** case, for which has 95% conversion ratio and in short time (less than 10 minutes). We successfully isolated **P7**, the ring-closed product: a symmetric 7-membered ring including an N atom and a C=C bond (Figure 3.10, bottom right, blue). The MS spectrum shows only one peak for this product which indicate there

is no other significant impurities (Figure 3.9). However, we can't distinguish them based on mass if isomerization happened because they have exactly the same formula, so ^{1}H-COSY NMR experiment was carried out to help identify products (Figure 3.10). The protons in the butyl groups overlapped, but the proton in the ring would be different if isomerization happened and the symmetry would be broken.

Based on the NMR spectrum, we can clearly distinguish two different products, symmetric product coded as blue, asymmetric product coded as red, light purple stands for protons at butyl group for both, and green stands for H_2O residue (samples already dried under vacuum for 5 days).

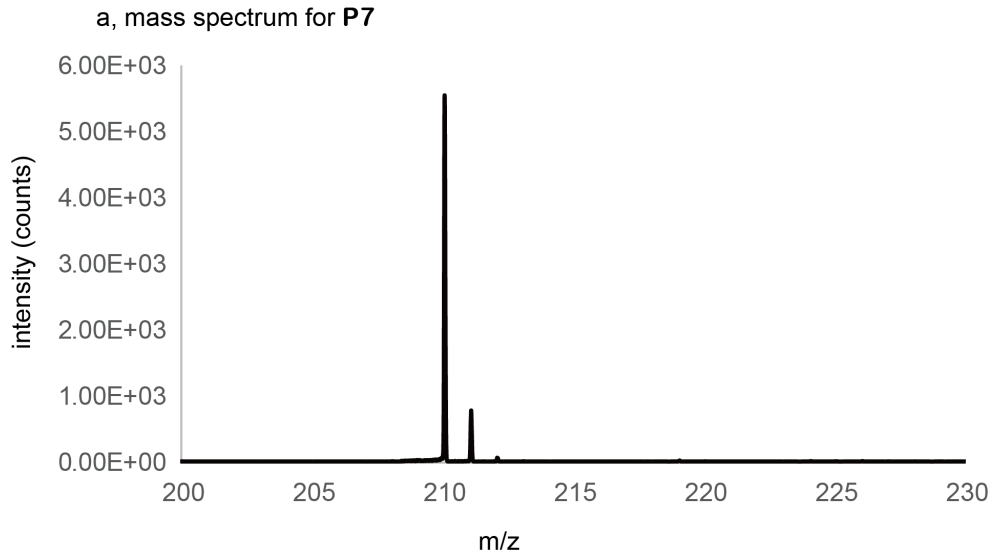

Figure 3.9: MS characterization of P7, at *m/z* 210.4170.

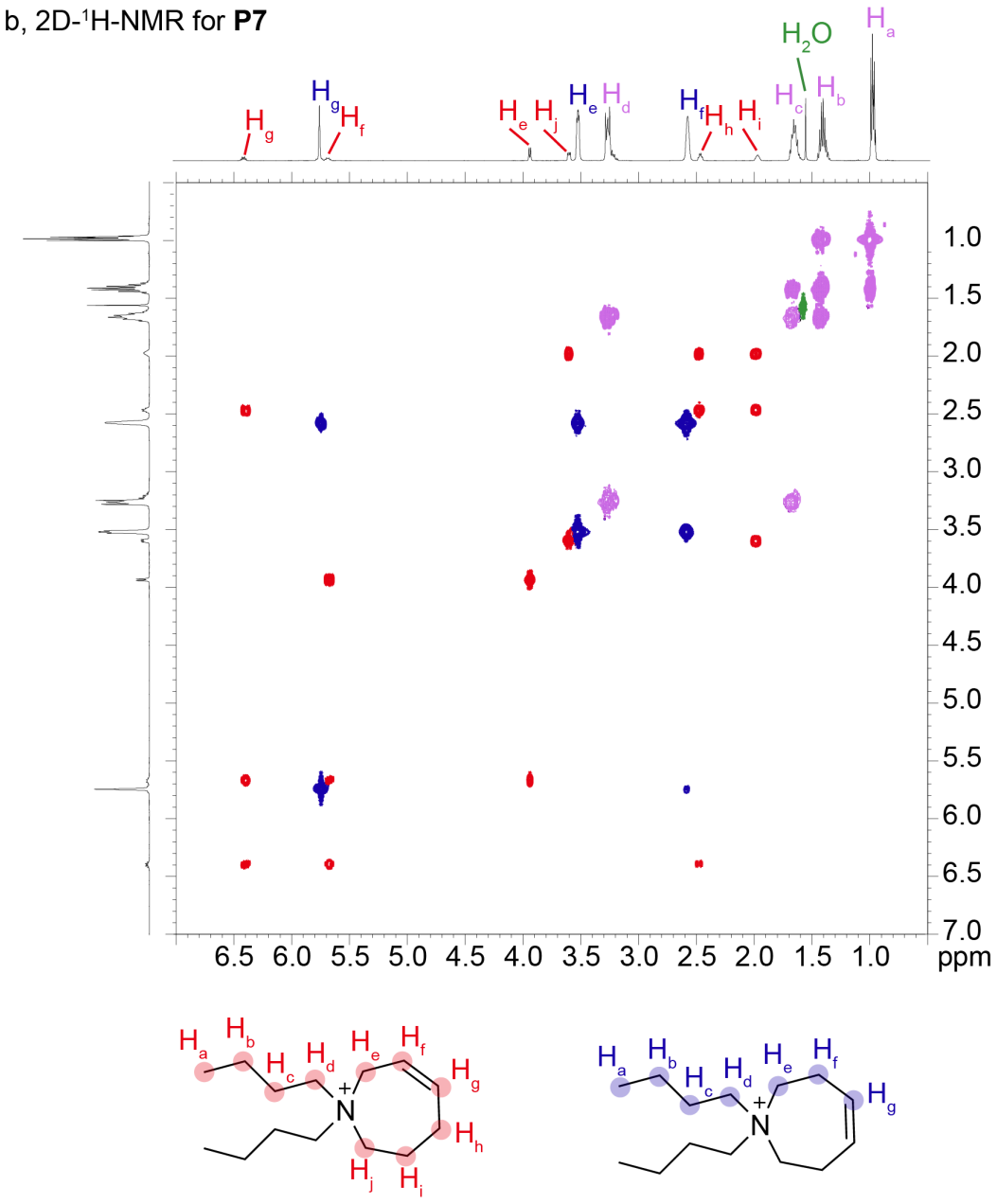

Figure 3.10: COSY-^{1}H-NMR spectrum for P7.

3.5 Oligomeric species

It is also possible that oligomeric species were formed as mentioned in Chapter 2. It is believed by Fogg that oligomerization is unlike to occur in the synthesis of small ring (particularly those of five or six members) under normal conditions of concentration and temperature, but highly possible to occur in the synthesis of medium and large rings.[82] Oligomerization will be disfavored in solutions as dilute as those employed in ESI-MS studies, but oligomers are very diagnostic if they did exist. Dimers will appear with 2^+ charge and hence have an isotope pattern whose peak are separated by $m/z = 0.5$ units and trimers will be separated by $m/z = 0.333$, and so on. Close inspection of each reaction revealed no appreciable amounts of dimer for the precursors to 5, 6, 7, 8 and 9-membered rings, but we did observe trace levels of dimers for the larger ring sizes, maximizing for the precursor to the 15-memberd ring (see Figure 3.11 for **R15** reaction). The abundance as plotted reached a maximum of 0.5% of the total ion current. The dynamic of the oligomer is largely as might be expected, maximizing after about 2 half-lives then slowly diminishing over time as further metathesis restored the monomeric product. We could detect no signs of a dimeric product nor of any trimers in any experiment.

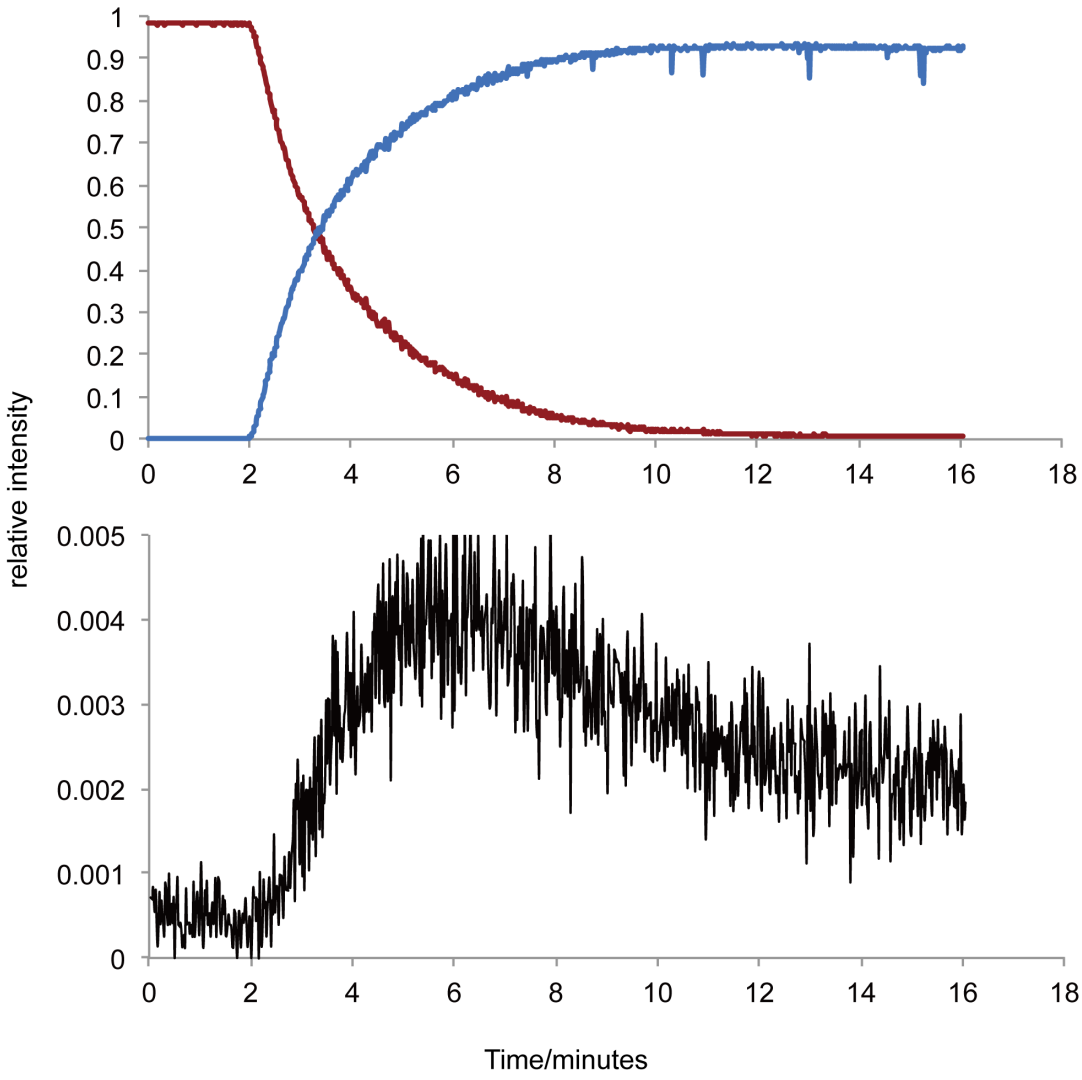

Figure 3.11: Top is overall progress for R15 forming of P15 and bottom is oligomer trace (dimer, observed at *m/z* 336).

3.6 Catalyst decomposition species

The isomerization catalyst is believed form via Grubbs' second-generation catalyst decomposition as discussed in Chapter 2. However, given that ESI-MS is only capable of detecting charged species, we would need to be able to capture the period where the charged tag is coordinated to the ruthenium complex. We were unable to detect any such

species, suggesting that the residence time for the charged alkene on the ruthenium complex is low (i.e. the catalyst does not rest with the charge-tagged alkene bound to it, which might be the case if the ring-closing metathesis step is relatively fast) and/or relatively small fraction of the pre-catalyst finds its way into the active form. But we were able to obtain some evidence that indicated that the catalyst decomposed. The ligand used in Grubbs' catalyst themselves can be charged via protonation (or related processes), and these charged substances will show up in the mass spectrum. There are three main decomposition species observed: an imidazolium ion derived from protonating the NHC ligand, $[C_{21}H_{27}N_2]^+$ (*m/z* 307), protonated PCy_3, $[HPCy_3]^+$ (*m/z* 281), and $[ClPCy_3]^+$ (*m/z* 315), (Figure 3.12, example used here is **R11**).

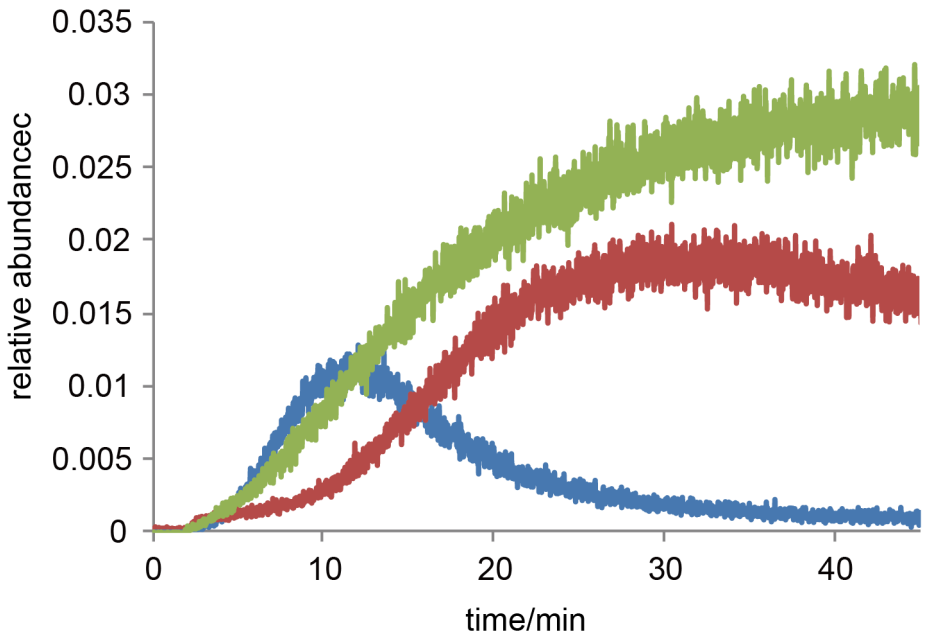

Figure 3.12: Abundance traces for catalyst decomposition products. Green is $[C_{21}H_{27}N_2]^+$ *m/z* 307, red is $[HPCy_3]^+$ *m/z* 281 and blue is $[ClPCy_3]^+$ *m/z* 315.

It turns out that the ion from NHC ligand is the dominant decomposed species from the catalyst as observed in our experiments. This is surprising because the NHC is considered as a strong sigma-donating ligand capable of effectively stabilizing 14 electron ruthenium intermediate species. Also, trace level ions at *m/z* 295 ware detected that were believed correspond to phosphonium ylide $[CH_3PCy_3]^+$, which formed after HCl removal by the reaction of CH_2=PCy_3 with ruthenium complex (discussed in Chapter 2.5). A signal at *m/z* 297 was also observed, MS/MS experiments helped ascribed these to hydride product of the $[CH_3PCy_3]^+$.[103] However, it is inconvenient to monitor for middle to large ring size precursors because signal at *m/z* 295 will overlap with the isotope pattern of precursors or products. But we can still clearly see this species for small ring size reactions. Abundance of ions at *m/z* 297 are almost twice that of ions at *m/z* 295, so we plotted ions at *m/z* 297 for 5, 6, and 7-membered ring precursor (see Figure 3.13). The signal was very noisy which indicate that *m/z* 295 was not an important species here, the catalyst could go through other different pathway of decomposition.

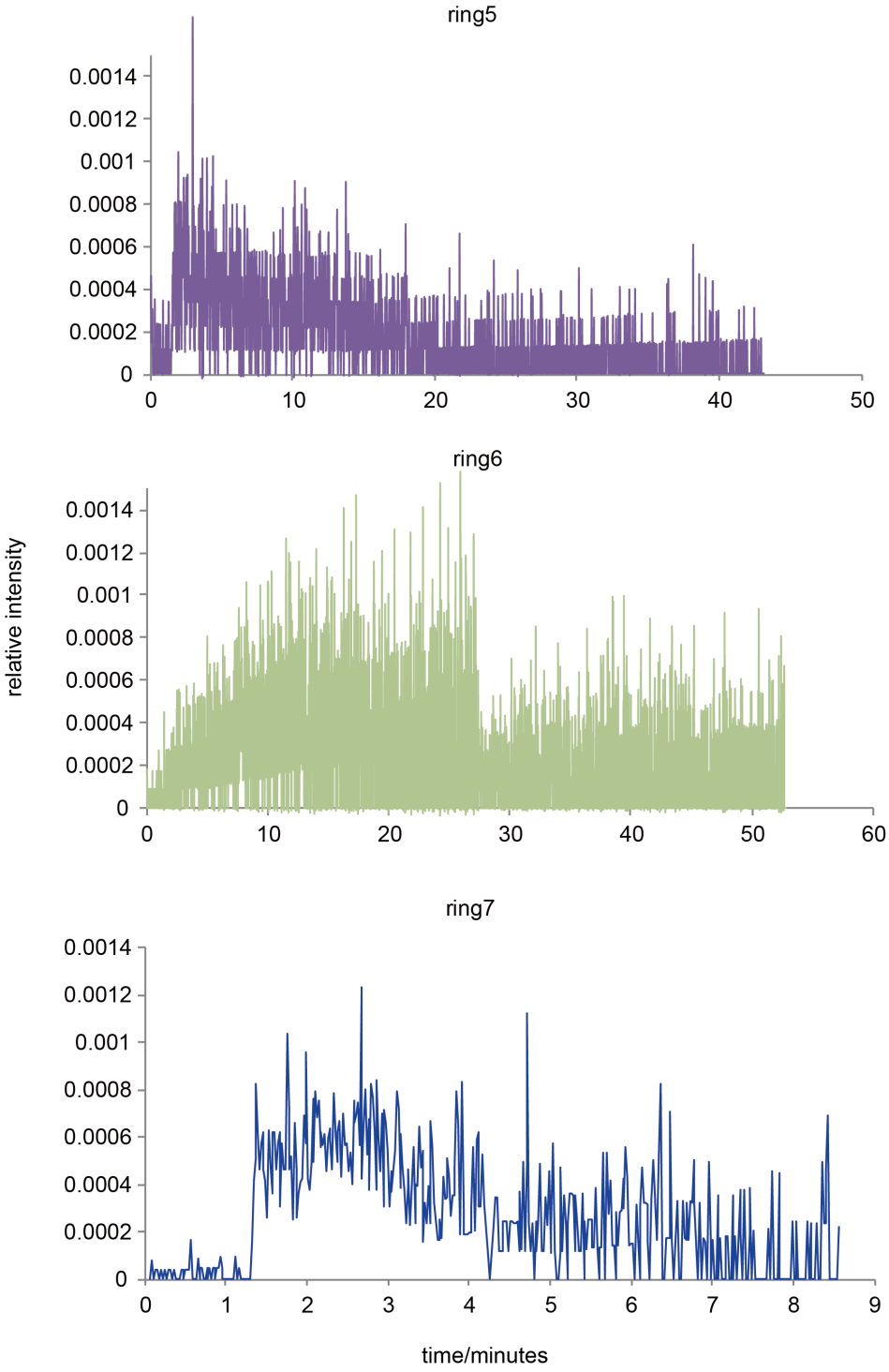

Figure 3.13: Abundance of *m/z* 297 during 5, 6 and 7-membered ring forming. Note that time scale is different because they have different reaction rate constant.

It is unclear why the abundance of $[CH_3PCy_3]^+$ is very low (more close to noise level), as discussed above in Chapter 2.5, it is believed that $[CH_3PCy_3]^+$ would be the most significant species through catalyst decomposition pathway. There was an signal observed at *m/z* 281 which corresponded to $[HPCy_3]^+$ (protonated PCy_3). However, we also detected an unexpected decomposed species $[ClPCy_3]^+$ at *m/z* 315 which was confirmed by Orbitrap analysis with 5.7 ppm (the Orbitrap MS was recently installed in our department and wasn't optimized when I used it for our sample testing, see appendix III for detail data). The exact mass of $[ClPCy_3]^+$ is 315.20084 Da compared with the observed mass 315.19904 Da. The isotopic pattern also matched with the characteristic chlorine M+2 peak present (see Figure 3.14).

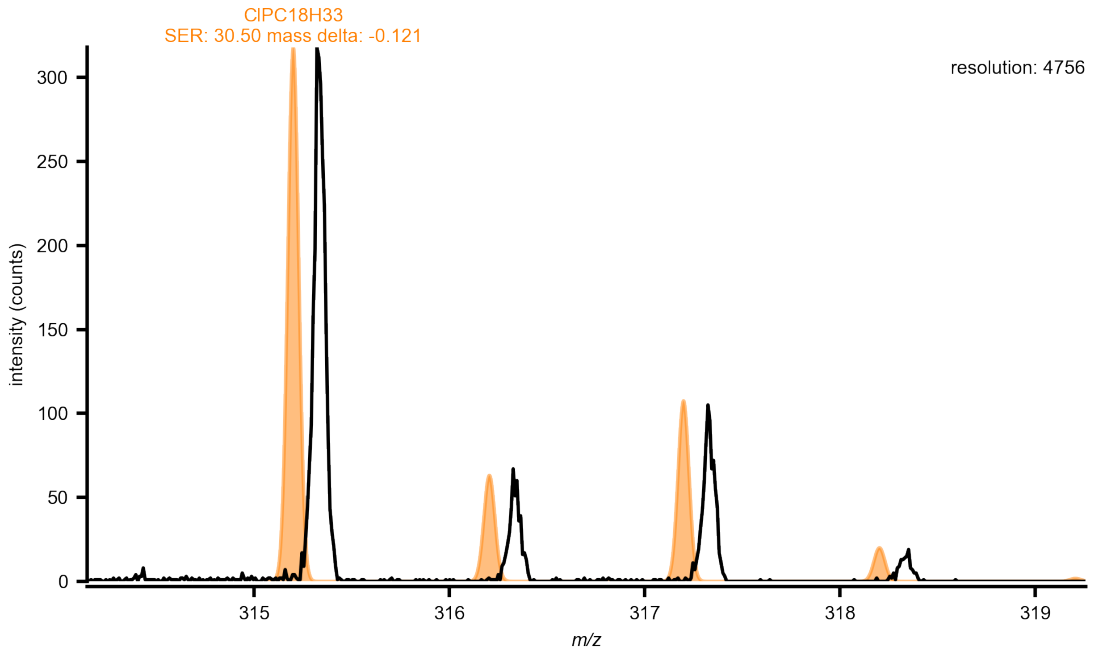

Figure 3.14: Isotope pattern of *m/z* 315 which we believed to be $[ClPCy_3]^+$. Black line stands for experimental and yellow line stands for predicted.

3.7 Deliberately isomerization catalyst added experiment

So, assuming that isomerization of precursor was a possible process, it was only noticeable for slow reaction precursors because it takes time for Grubbs' catalyst to decompose and the slow reaction rate makes starting material hang round long enough for isomerization to occur. There is an obvious experiment that suggest itself: we deliberately added an isomerization catalyst with metathesis catalyst same time with same loading at the very beginning for some fast and clean reaction, addition of the isomerization catalyst would hopefully generate some byproduct species if the isomerization hypothesis is correct. Here, we chose **R7**, since this was the fastest and cleanest reaction with no byproducts to speak of, presumably because the reaction is quick enough that isomerization does not have time to occur. The isomerization catalyst chosen was a commercially available, ruthenium hydride complex $RuHCl(CO)(PPh_3)_3$, which can cause isomerization in refluxed dichloromethane.[104] And we observed big increase of byproducts that have similar distribution as **R9**, which are 14 Da mass difference from product or precoursor (see Figure 3.15).

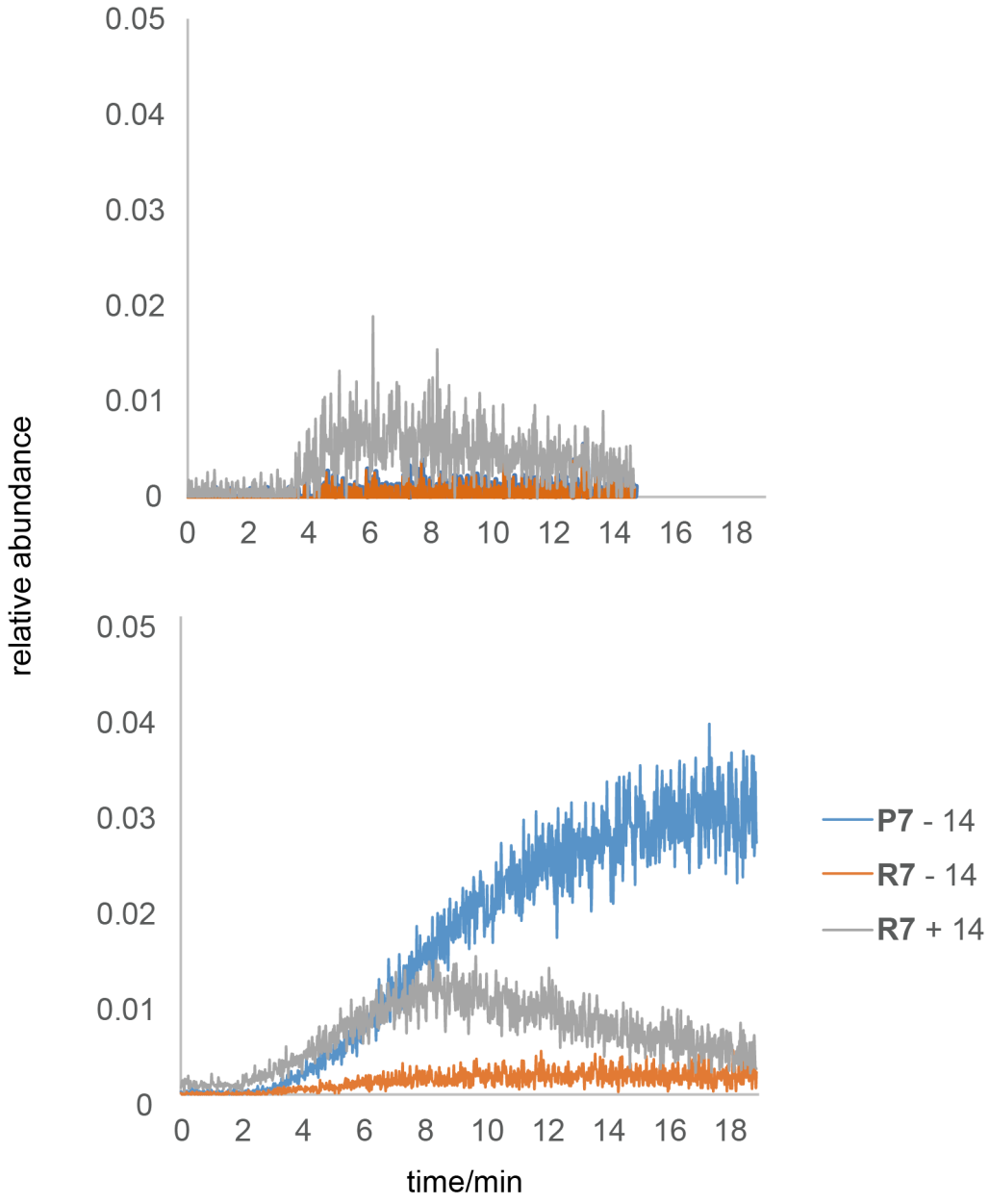

Figure 3.15: Top is expected byproducts in reaction R7 with 20 mol% GuII and bottom is expected byproducts in R7 with 20 mol% of GuII and 20 mol% of Ru-H.

3.8 Conclusion

These studies into RCM using PSI-ESI-MS allowed detailed insight into the kinetics of the reaction beyond the main productive cycle, in particular the importance of

isomerization. Isomerization leads to the formation of byproducts, which in nearly all cases are undesirable (one possible exception is the isomerization of the product to move the position of the alkene in the new ring system, because there are some syntheses for which this bond is hydrogenated at the next step anyway). The byproduct obvious to mass spectrometry were those with different masses, universally a mass change of units of ± 14 Da from the expected product. These arose from isomerization of the starting material diene and of the product cycloene, and could be rationalized on the basis of separate metathesis and isomerization catalytic cycles operating simultaneously. Isomerization was only found to be problematic when the reaction was slow, i.e. when forming strained rings (such as the smallest ring, which requires the installation of a double bond with ideal, angles of 120^{o} in a five-membered ring which would normally have bond angles of 108^{o}; and for the medium-sized rings, especially the nine-membered ring, for which it is hard to find stable conformers).

Proof of isomerization being the reason as far as byproduct formation was concerned was proved by addition of an isomerization catalyst, which produced appreciable amounts of the expected byproducts. The source of the actual isomerization catalyst is almost certainly the precatalyst itself, because it was shown that various charged species formed from the precatalyst's ligands. One of those, $[ClCy_3]^+$, had never been previously detected as a decomposition product of Grubbs' catalyst before, so a new pathway may have been revealed, and this will be the subject of future studies. Further studies should focus on other metathesis catalysts, given the success of this work – the charge-tagged ligands expressly designed for this project will be equally applicable to any RCM catalyst capable of tolerating the tetralkylammonium functional group. Any experimenter interested in

unlocking mechanistic details about their reactions will be able to employ our methodologies, both synthetic and kinetic. The complementarity between MS and NMR will also be appealing to many chemists, as the strengths of the two techniques are quite different but they work together to provide information not obtainable by either one alone.

Our insights may help chemists in the short term in catalyst selection, e.g. when forming a strained ring, a catalyst that is not prone to decomposition may be preferable to a more active catalyst. Ultimately, complete mechanistic insight will hopefully allow the rational design of better metathesis catalyst for which the problematic decomposition processes observed here are effectively shut down.

3.9 Experiments and synthesis of precursors

All glassware involved are cleaned with base bath then rinsed with tap water followed with distilled water (including funnel and stir bar), dried in air overnight, and dried in oven at least 1 hour before use. All plastic syringes and needles were obtained commercially and used once only. All diene synthesis reactions were carried out in fume hood under air. All off-line metathesis reactions were carried out under N_2 using standard Schlenk flask and glovebox techniques. The catalysts were obtained from *Sigma-Aldrich*, amines and halogen carbenes were obtained from *Oakwood Chemical*. Dichloromethane was freshly distilled over calcium hydride before use.

NMR spectra were recorded on a Bruker Avance 300/500 NMR at standard condition and referenced to the residual proton of the solvent. Signals are reported in ppm relative to TMS at 0 ppm.

MS spectra were recorded on a Micro Q-ToF mass spectrometer. To obtain consistent MS condition for each experiment, capillary voltage was set at 3 kV, cone voltage 15 V, extraction voltage 2.5 V, source temperature 80^{o}C, and desolvation gas temperature 180^{o}C. To obtain the best signal for each experiment, cone and desolvation gas flow, probe head position and MCP detector voltage were optimized.

Synthesis of R5: allyl bromide (4.86 g, 40.2 mmol) in diethyl ether (20 mL) was added slowly to dibutylamine (10.05 g, 77.82 mmol) in a 100 mL round bottom flask (RBF) at room temperature (RT) over a period of 5 min and the solution was stirred overnight at RT, followed by filtration to remove white precipitate (Bu_2NH_2Br), diethyl ether and exceed allyl bromide was removed by vacuum, followed by filtration through celite again direct into a 50 mL RBF to obtain one alkene substituted $Bu_2NC_3H_5$, another portion of allyl bromide (4.80 g, 39.7 mmol) was added into 50 mL RBF, the solution was stirred for 2 days with a silica oil bath applied (75~80^{o}C) The brownish liquid was then washed with diethyl ether (3 × 25 mL) followed by salt metathesis with $NaPF_6$ in deionized water and recrystallization from ethanol to give a white powder product (1.03 g, 2.90 mmol, 7.46 % yield). ^{1}H NMR (300 Mz, $CDCl_3$) δ 5.96-5.82 (2H, m), 5.75-5.68 (4H, m), 3.83 (4H, d), 3.16-3.10 (4H, m), 1.75-1.65 (4H, m), 1.40 (4H, sex), 0.99 (6H, t). +ve *m/z* 210.2, -ve *m/z* 145.1.

Synthesis of R6: allyl bromide (5.10 g, 42.5 mmol) in diethyl ether (20 mL) was added slowly to dibutylamine (9.81 g, 76.0 mmol) in a 100 mL RBF at RT over a period of 5 min, the solution was stirred overnight at room temperature, followed by filtration through celite

to remove white precipitate (Bu_2NH_2Br), diethyl ether and exceed allyl bromide was removed by vacuum, followed by filtration through celite again, direct into a 50 mL RBF without washing to obtain one alkene substituted $Bu_2NC_3H_5$, another portion of 4-bromo-1-butene (7.10 g, 52.6 mmol) was added slowly, the mixture was stirred for 2~3 days with a silica oil bath applied (75~80^oC). The brownish liquid was washed with diethyl ether (3 × 25 mL) to remove exceed 4-bromo-1-butene, followed by salt metathesis with $NaPF_6$ in deionized water and recrystallization with ethanol to give a white powder product (0.891 g, 2.4 mmol, 11.4 % yeild). ^1H NMR (300 Mz, $CDCl_3$) δ 5.91-5.78 (1H, m) 5.79-5.65 (3H, m), 5.28-5.19 (2H, m), 3.88 (2H, d), 3.23-3.15 (6H, m), 2.52-2.45 (2H, m), 1.73-1.62 (4H, m), 1.42 (4H, sex), 1.00 (6H, t). MS (qToF) +ve *m/z* 224.3, -ve *m/z* 145.0.

Synthesis of R7: 4-bromo-1-butene (6.40 g, 46.1 mmol) in diethyl ether (20 mL) was added slowly to dibutylamine (9.90 g, 76.7 mmol) in a 100 mL RBF at RT over a period of 5 min, the solution was refluxed overnight with silica oil bath applied, followed by filtration through celite to remove white precipitation (Bu_2NH_2Br), diethyl ether and exceed 4-bromo-1-butene was removed by vacuum, followed by filtration through celite again, directly into a 50 mL RBF without washing to obtain one alkene substituted $Bu_2NC_4H_7$, another portion of 4-bromo-1-butene (7.10 g, 52.6 mmol) was added slowly, the solution was stirred for 2~3 days with silica oil bath applied (75~80^oC). The brownish and oily mixture was washed with diethyl ether (3 × 25 mL) followed by salt metathesis with $NaPF_6$ in deionized water and recrystallization with ethanol to give white powder product (1.15 g, 3.00 mmol, 20.4 % yeild). ^1H NMR (300 Mz) δ 5.80-5.67 (2H, m), 5.28-

5.20 (4H, m), 3.28-3.19 (8H, m), 2.50-2.42 (4H, m), 1.69-1.59 (4H, m), 1.44 (4H, sex), 1.00 (6H, t). MS (qToF) +ve *m/z* 238.4, -ve *m/z* 145.1.

Synthesis of R8: allyl bromide (5.02 g, 41.8 mmol) in diethyl ether (20 mL) was added slowly into dibutylamine (6.82 g, 52.9 mmol) in a 100 mL RBF at RT over period of 5 min, the solution was stirred overnight, followed by filtration through celite to remove white precipitation (Bu_2NH_2Br), diethyl ether and exceed allyl bromide was removed by vacuum, followed by filtration through celite again directly into a 50 mL RBF without washing to obtain one substituted $Bu_2NC_3H_5$, a portion of 6-bromo-1-butene (6.98 g, 43.1 mmol) was added, the solution was then stirred for 2~3 days with a silica oil bath applied (75~80^oC). The brownish oily mixture was washed with diethyl ether (3 × 25 mL) followed by salt metathesis with $NaPF_6$ in deionized water and recrystallization with ethanol to give white powder product (1.35 g, 3.40 mmol, 12.9 % yield). ^1H NMR (300 Mz, $CDCl_3$) δ 5.92-5.66 (4H, m), 5.09-5.00 (2H, m), 3.84 (2H, d), 3.17-3.11 (6H, m), 2.14 (2H, q), 1.73-1.60 (6H, m), 1.53-1.35 (6H, m), 0.99 (6H, t). MS (Q-ToF) +ve *m/z* 252.4, -ve *m/z* 145.2.

Synthesis of R9: 5-bromo-1-pentene (5.60g, 36.6 mmol) was added slowly into dibutylamine (8.14 g, 63.1 mmol) in a 100 mL RBF at RT over a period of 5 min without any solvent. The mixture was stirred overnight with with silica oil bath applied (60~65^oC), followed with filtration through celite to remove white precipitation (Bu_2NH_2Br), directly into a 50 mL RBF without washing to obtain one alkene substituted $Bu_2NC_5H_9$ (mixed with exceed 5-bromo-1-pentene), another portion of 5-bromo-1-pentene (6.05 g, 39.5 mmol) was added into the brownish mixture and stirred for 3~5 days at (75~80^oC). The dark brown

mixture was washed with diethyl ether (3×25 mL) followed by salt metathesis with $NaPF_6$ in deionized water and recrystallization with 1-butanol to give white powder product (1.55 g, 3.77 mmol, 12.0% yield). ^{1}H NMR (300 Mz, CD_2Cl_2) δ 5.86-5.72 (2H, m), 5.18-5.11 (4H, m), 3.14-3.08 (8H, m), 2.18 (4H, q), 1.78-1.68 (4H, m), 1.65-1.54 (4H, m), 1.42 (4H, sex), 1.01 (6H, t). MS (Q-ToF) +ve *m/z* 266.4, -ve *m/z* 145.0.

Synthesis of R11: 6-bromo-1-hexene (6.23 g, 36.9 mmol) was added into dibutylamine (7.03 g, 54.5 mmol) in a 100 mL RBF slowly at RT over a period of 5 min without any solvent. The mixture was stirred about 36 hours with silica oil bath applied (75~80^{o}C), followed with filtration through celite to remove white precipitation (Bu_2NH_2Br) directly into a 50 mL RBF without washing to obtain one alkene substituted $Bu_2NC_6H_{11}$, another portion of 6-bromo-hexene (6.85 g, 42.28 mmol) was added into the brownish mixture and stirred for 3~5 days at (75~80^{o}C). The dark brown mixture was washed with diethyl ether (3×25 mL) followed by salt metathesis with $NaPF_6$ in deionized water and recrystallization with 1-butanol to give white powder product (1.71 g, 3.90 mmol, 14.3% yield). ^{1}H NMR (300 Mz, $CDCl_3$) δ 5.82-5.68 (2H, m), 5.10-5.00 (4H, m), 3.18-3.11 (8H, m), 2.15 (4H, q), 1.68-1.56 (8H, m), 1.52-1.36 (8H, m), 1.00 (6H, t). MS (Q-ToF) +ve *m/z* 294.5, -ve *m/z* 145.0.

Synthesis of R13: 7-bromo-1-heptene (6.56 g, 37.27 mmol) was slowly added into dibutylamine (6.01 g, 46.59 mmol) in a 100 mL RBF at RT over a period of 5 min without any solvent, the mixture was stirred for 2 days with silica oil bath applied (75~80^{o}C), followed with filtration through celite to remove white precipitation (Bu_2NH_2Br) directly

into a 50 mL RBF to obtain one alkene substituted $Bu_2NC_7H_{13}$ (mixed with exceed 7-bromo-1-heptene), another portion of 7-bromo-1-heptene (7.06 g, 40.1 mmol) was added into the brownish mixture and stirred for 3~5 days at 75~80^oC. The dark mixture was washed with diethyl ether (3×25 mL) followed by salt metathesis with $NaPF_6$ in deionized water and recrystallization with 1-butanol to give white product (1.53 g, 3.27 mmol, 14.1% yield). ^1H NMR (300 Mz, $CDCl_3$) δ 5.84-5.71 (2H, m), 5.05-4.95 (4H, m), 3.19-3.11 (8H, m), 2.08 (4H, q), 1.68-1.56 (8H, m), 1.52-1.35 (12H, m), 1.00 (6H, t). MS (Q-ToF) +ve *m/z* 322.6, -ve *m/z* 145.2.

Synthesis of R15: 8-bromo-1-octene (7.18 g, 37.59 mmol) was added slowly into dibutylamine (6.23 g, 48.3 mmol) in a 100 mL RBF at RT over a period of 5 min without any solvent, the mixture was stirred for 2 days with silica oil bath applied (75~80^oC), followed with filtration through celite to remove white precipitation (Bu_2NH_2Br) directly into a 50 mL RBF without washing to obtain one alkene substituted $Bu_2NC_7H_{13}$ mixed with exceed 8-bromo-1-octene), another portion of 8-bromo-1-octene (7.20 g, 37.70 mmol) was added into the brownish mixture and stirred for 3~5 days at 75~80^oC. The dark mixture was washed with diethyl ether (3×25 mL) followed by salt metathesis with $NaPF_6$ in deionized water and recrystallization with 1-butanol to give white product (1.68 g, 3.39 mmol, 14.1% yield). ^1H NMR (300 Mz, $CDCl_3$) δ 5.86-5.72 (2H, m), 5.04-4.94 (4H, m), 3.19-3.12 (8H, m), 2.06 (4H, q), 1.68-1.57 (8H, m), 1.50-1.35 (16H, m), 1.01 (6H, t). MS (Q-ToF) +ve *m/z* 350.7, -ve *m/z* 145.3.

Appendix I

^{1}H NMR of all precursors in $CDCl_3$

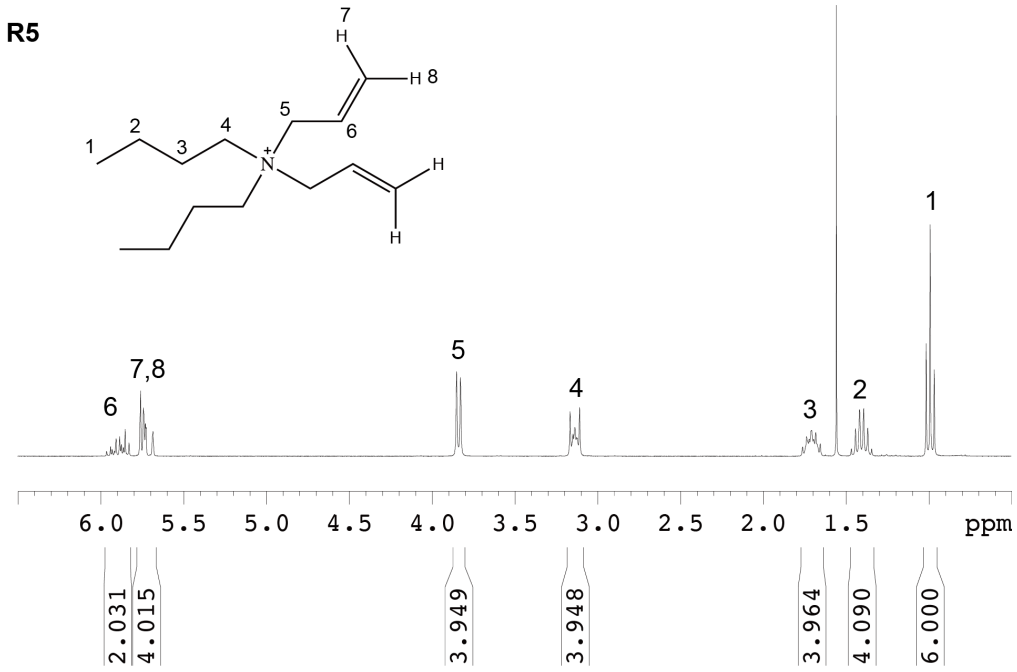

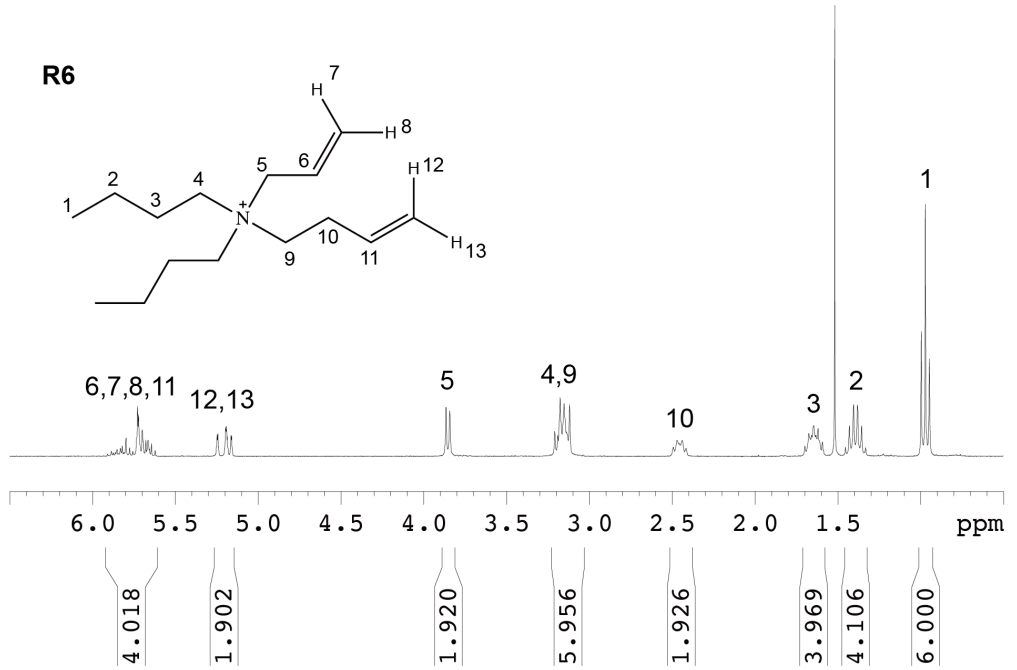

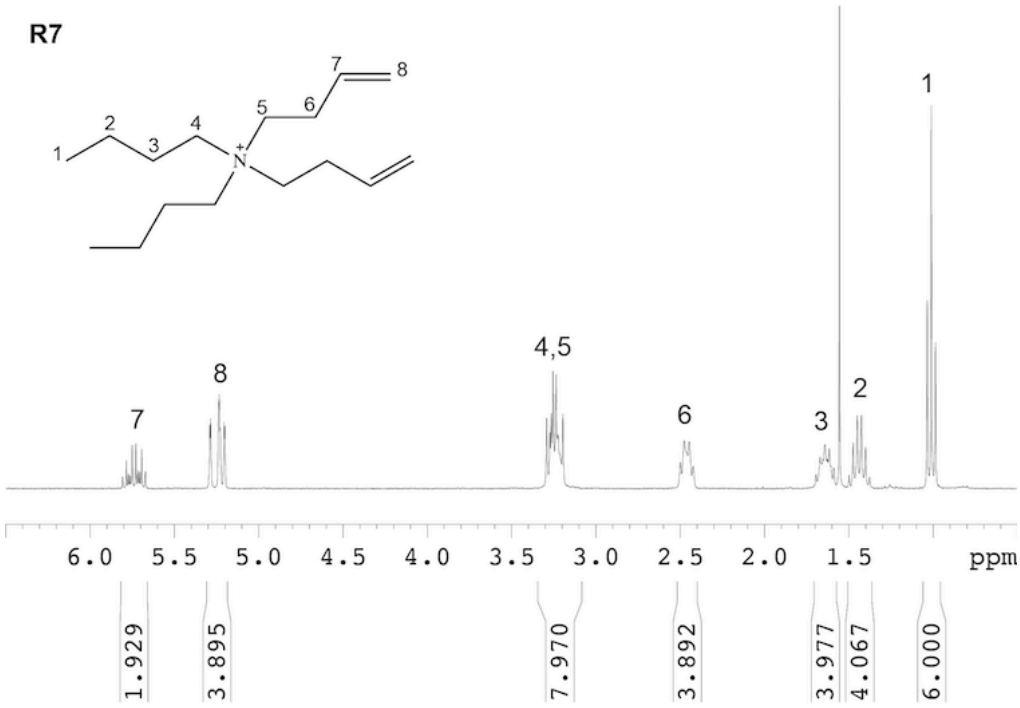
R7
7
8
5
6
2
4
3
1
N+
1
4,5
8
2
7
6
3
6.0
5.5
5.0
4.5
4.0
3.5
3.0
2.5
2.0
1.5
ppm
1.929
3.895
7.970
3.892
3.977
4.067
6.000

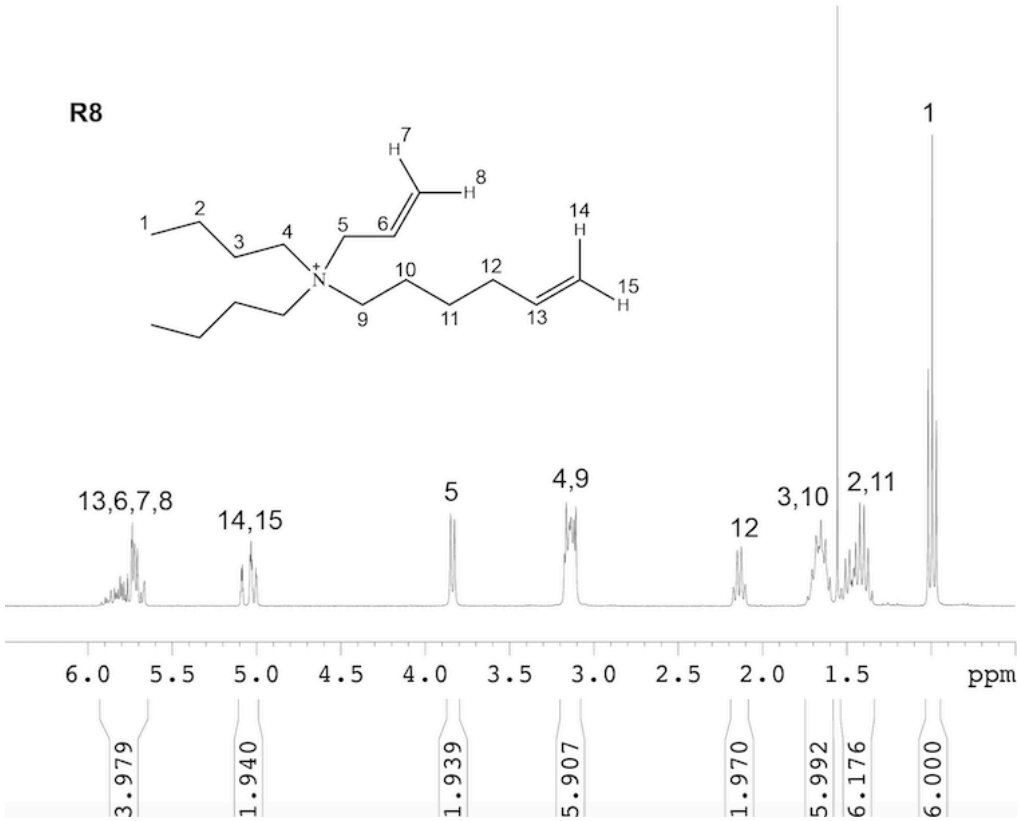
R8
1
H7
H8
2
3
4
5
6
14
H
1
N+
10
12
15
H
9
11
13
13,6,7,8
14,15
5
4,9
12
3,10
2,11
6.0
5.5
5.0
4.5
4.0
3.5
3.0
2.5
2.0
1.5
ppm
3.979
1.940
1.939
5.907
1.970
5.992
6.176
6.000

R9 in CD_2Cl_2

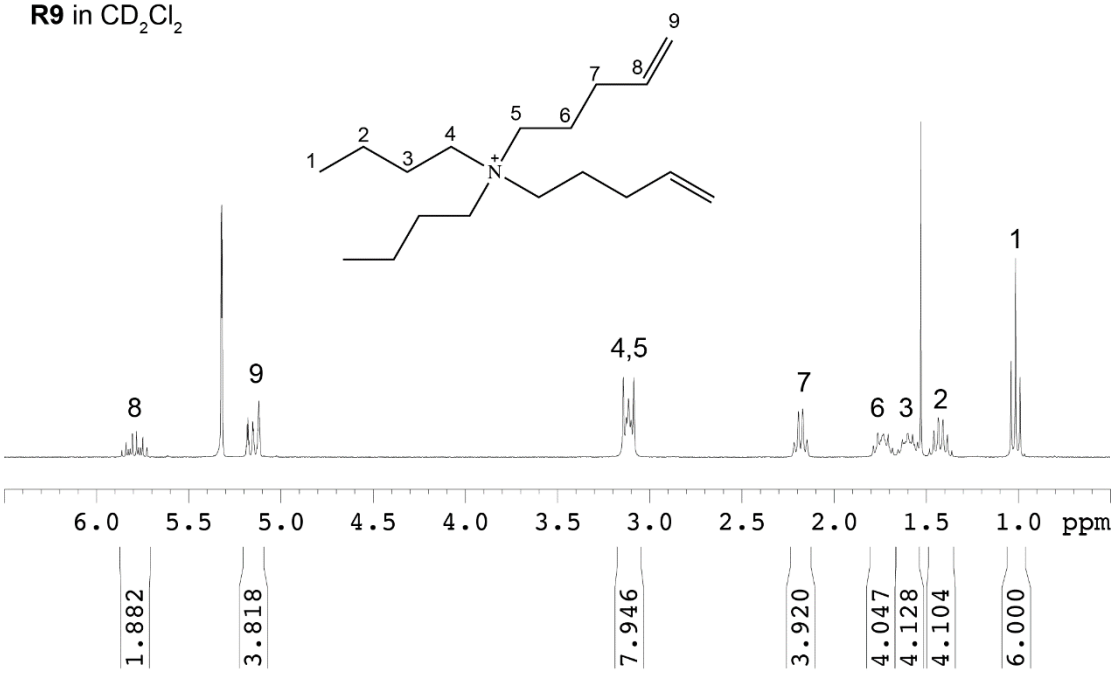

R11

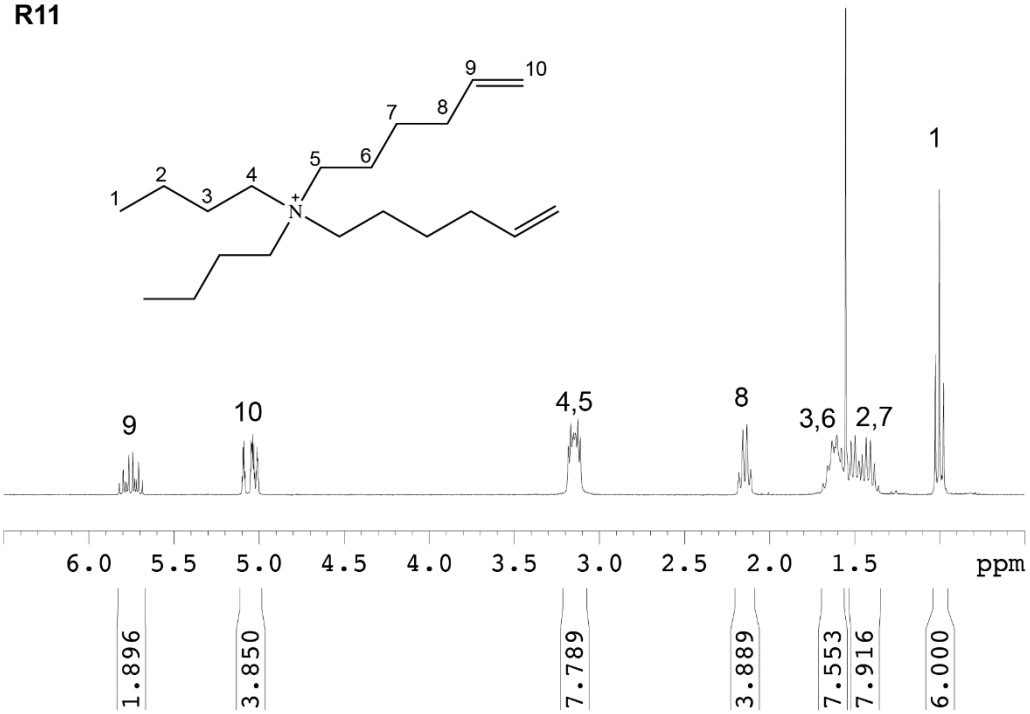

R13

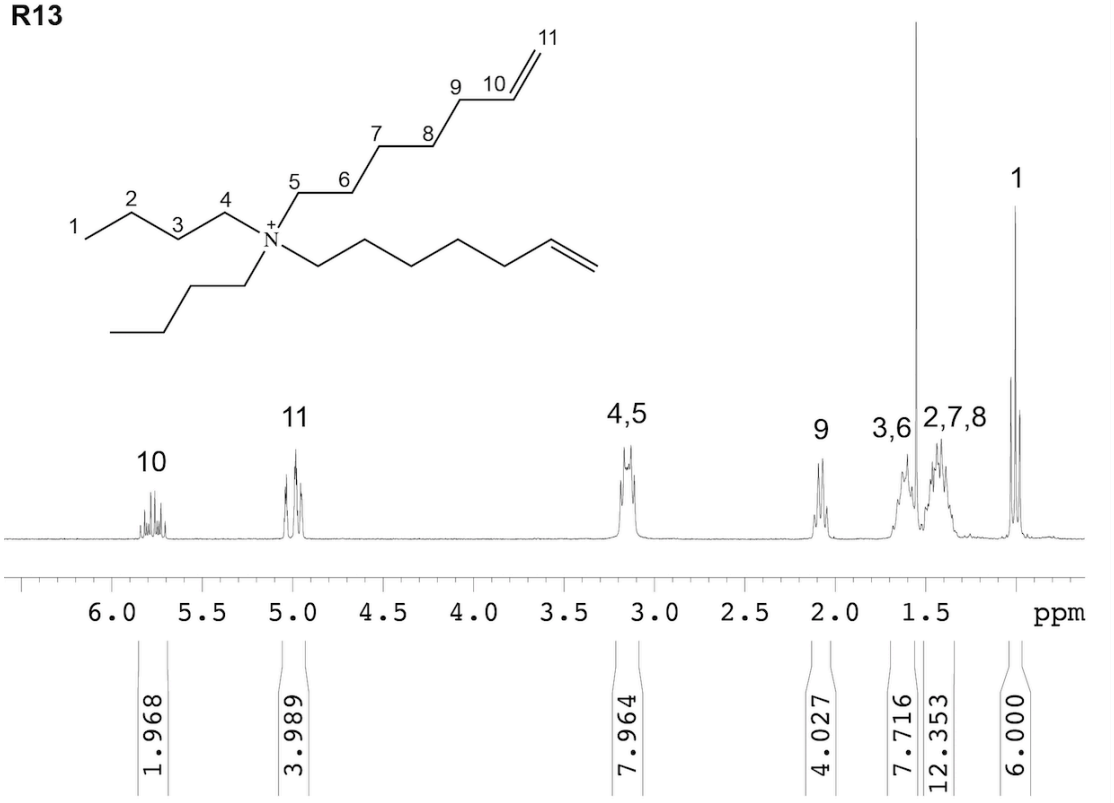
11
9
10
7
8
5
6
2
4
1
3
N+
1
10
11
4,5
9
3,6
2,7,8
6.0
5.5
5.0
4.5
4.0
3.5
3.0
2.5
2.0
1.5
ppm
1.968
3.989
7.964
4.027
7.716
12.353
6.000

R15

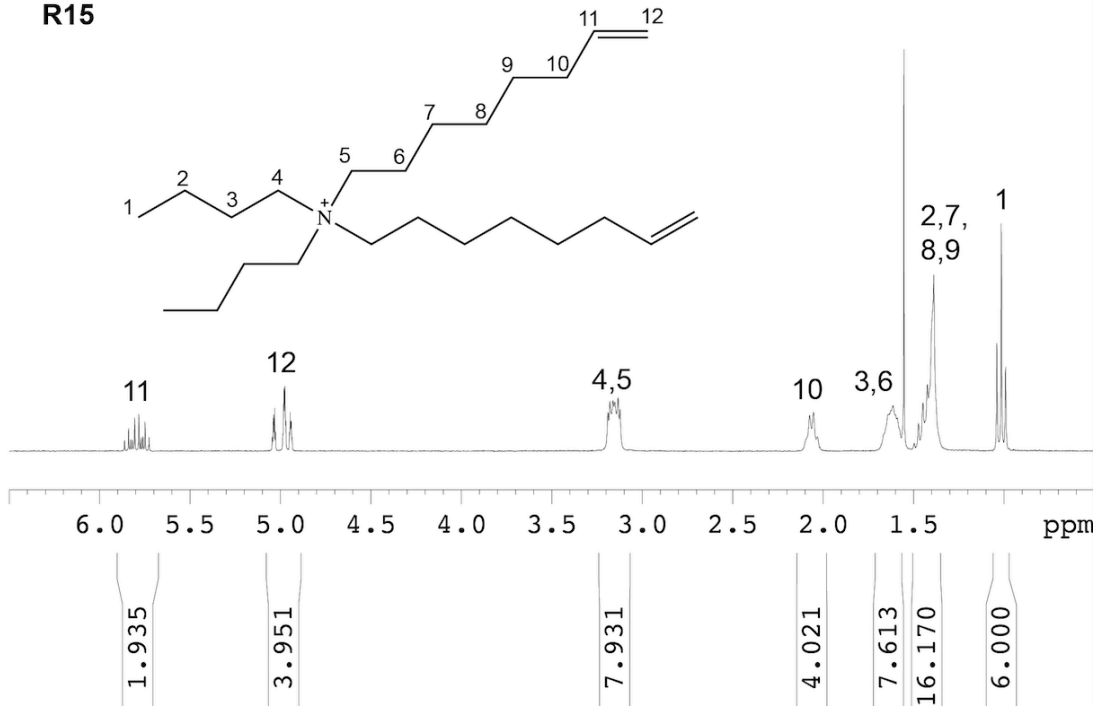
11
12
9
10
7
8
5
6
2
4
1
3
N+
2,7,
8,9
1
11
12
4,5
10
3,6
6.0
5.5
5.0
4.5
4.0
3.5
3.0
2.5
2.0
1.5
ppm
1.935
3.951
7.931
4.021
7.613
16.170
6.000

Appendix II

X-ray report for **R5**:

DISCUSSION

The compound crystallizes as colorless block-like crystals from an ethanol solution. There are four molecules of the di-butyl, di-propylene ammonium cation and associated PF_6 anion in the unit cell of the primitive, centrosymmetric, monoclinic space group $P2_1/c$.

The structures of the two molecules are as expected (see Figures). Bond distances and angles are otherwise unexceptional.

CRYSTAL SUMMARY

Crystal data for $C_{14}H_{28}F_6NP$; $M_r = 355.34$; Monoclinic; space group $P2_1/c$; $a = 9.4663(13)$ Å; $b = 13.2301(18)$ Å; $c = 14.178(2)$ Å; $\alpha = 90°$; $\beta = 93.998(2)°$; $\gamma = 90°$; $V = 1771.4(4)$ $Å^3$; $Z = 4$; $T = 120(2)$ K; λ(Mo-Kα) = 0.71073 Å; μ(Mo-Kα) = 0.207 mm^{-1}; d_{calc} = 1.332g.cm^{-3}; 41285 reflections collected; 4431 unique ($R_{int} = 0.0332$); giving $R_1 = 0.0331$, $wR_2 = 0.0844$ for 3751 data with [$I>2\sigma(I)$] and $R_1 = 0.0417$, $wR_2 = 0.0890$ for all 4431 data. Residual electron density ($e^-.Å^{-3}$) max/min: 0.686/-0.277.

An arbitrary sphere of data were collected on a colorless block-like crystal, having approximate dimensions of 0.198 × 0.196 × 0.108 mm, on a Bruker APEX-II diffractometer using a combination of ω- and φ-scans of 0.5° [1]. Data were corrected for absorption and polarization effects and analyzed for space group determination. The structure was solved by intrinsic phasing methods and expanded routinely [2]. The model was refined by full-matrix least-squares analysis of F^2 against all reflections [3]. All non-hydrogen atoms were refined with anisotropic atomic displacement parameters. Unless otherwise noted,

hydrogen atoms were included in calculated positions. Atomic displacement parameters for the hydrogens were tied to the equivalent isotropic displacement parameter of the atom to which they are bonded (U_{iso}(H) = 1.5U_{eq}(C) for methyl, 1.2U_{eq}(C) for all others).

REFERENCES

[1] Bruker AXS. (2014). *APEX-2*. Bruker-Nonius AXS, Madison, Wisconsin, USA.
[2] G. M. Sheldrick, *Acta Cryst.*, **2015**, *A71*, 3.
[3] G. M. Sheldrick, *Acta Cryst.*, **2015**, *C71*, 3.

Table R5-1. Crystal data and structure refinement for uvic1601.

Identification code	uvic1601	
Empirical formula	$C_{14}H_{28}F_6NP$	
Formula weight	355.34	
Temperature	120(2) K	
Wavelength	0.71073 Å	
Crystal system	Monoclinic	
Space group	$P2_1/c$	
Unit cell dimensions	*a* = 9.4663(13) Å	α = 90°
	b = 13.2301(18) Å	β = 93.998(2)°
	c = 14.178(2) Å	γ = 90°
Volume	1771.4(4) Å^3	
Z	4	
Density (calculated)	1.332 g.cm^{-3}	
Absorption coefficient (μ)	0.207 mm^{-1}	
F(000)	752	
Crystal color, habit	colorless, block	
Crystal size	0.198 × 0.196 × 0.108 mm^3	
θ range for data collection	2.108 to 28.370°	
Index ranges	$-12 \le h \le 12$, $-17 \le k \le 17$, $-18 \le l \le 18$	
Reflections collected	41285	
Independent reflections	4431 [R_{int} = 0.0332]	
Completeness to θ = 25.242°	100.0 %	
Absorption correction	Numerical	
Max. and min. transmission	1.0000 and 0.9382	
Refinement method	Full-matrix least-squares on F^2	
Data / restraints / parameters	4431 / 0 / 201	
Goodness-of-fit on F^2	1.045	
Final R indices [I>2σ(I)]	R_1 = 0.0331, wR_2 = 0.0844	
R indices (all data)	R_1 = 0.0417, wR_2 = 0.0890	
Extinction coefficient	n/a	

Largest diff. peak and hole 0.686 and -0.277 $e^{-}.Å^{-3}$

Table R5-2. Atomic coordinates and equivalent isotropic displacement parameters ($Å^2$) for uvic1601. U(eq) is defined as one third of the trace of the orthogonalized U_{ij} tensor.

	x	y	z	U(eq)
N(1)	0.74964(10)	0.39789(7)	0.83079(7)	0.015(1)
C(1)	0.61674(12)	0.33267(9)	0.81847(9)	0.018(1)
C(2)	0.55585(13)	0.30466(10)	0.90948(9)	0.022(1)
C(3)	0.53151(16)	0.20992(11)	0.93216(11)	0.030(1)
C(4)	0.85630(13)	0.35118(9)	0.90363(8)	0.018(1)
C(5)	0.90463(14)	0.24779(9)	0.87682(9)	0.021(1)
C(6)	1.03791(15)	0.22791(11)	0.86299(10)	0.027(1)
C(7)	0.70738(12)	0.50213(9)	0.86504(8)	0.016(1)
C(8)	0.82542(13)	0.58030(9)	0.87297(9)	0.019(1)
C(9)	0.76939(14)	0.68215(10)	0.90648(10)	0.024(1)
C(10)	0.65807(16)	0.72995(11)	0.83882(11)	0.030(1)
C(11)	0.81733(12)	0.40345(9)	0.73696(8)	0.016(1)
C(12)	0.73413(13)	0.46065(10)	0.65848(9)	0.020(1)
C(13)	0.81166(16)	0.45296(11)	0.56784(9)	0.026(1)
C(14)	0.74688(17)	0.52043(11)	0.48932(10)	0.031(1)
P(1)	0.25852(3)	0.53499(2)	0.82557(2)	0.017(1)
F(1)	0.38800(8)	0.53640(7)	0.90504(5)	0.028(1)
F(2)	0.12929(8)	0.53368(7)	0.74665(6)	0.030(1)
F(3)	0.15485(8)	0.50086(7)	0.90402(6)	0.031(1)
F(4)	0.29096(10)	0.42005(7)	0.80370(7)	0.039(1)
F(5)	0.22639(11)	0.65057(7)	0.84820(7)	0.043(1)
F(6)	0.36346(10)	0.56954(9)	0.74800(6)	0.044(1)
H(1A)	0.5440	0.3696	0.7785	0.022
H(1B)	0.6398	0.2700	0.7846	0.022
H(2)	0.5341	0.3568	0.9522	0.026
H(3A)	0.5527	0.1570	0.8901	0.036
H(3B)	0.4927	0.1946	0.9905	0.036
H(4A)	0.9398	0.3962	0.9121	0.021
H(4B)	0.8130	0.3469	0.9651	0.021
H(5)	0.8369	0.1949	0.8696	0.025
H(6A)	1.1070	0.2799	0.8699	0.033
H(6B)	1.0649	0.1615	0.8461	0.033
H(7A)	0.6300	0.5283	0.8212	0.020
H(7B)	0.6691	0.4945	0.9279	0.020
H(8A)	0.8649	0.5890	0.8106	0.023
H(8B)	0.9024	0.5564	0.9183	0.023
H(9A)	0.7287	0.6722	0.9683	0.029
H(9B)	0.8500	0.7296	0.9163	0.029

H(10A)	0.6411	0.7997	0.8585	0.045
H(10B)	0.5699	0.6912	0.8393	0.045
H(10C)	0.6911	0.7299	0.7748	0.045
H(11A)	0.8330	0.3336	0.7148	0.020
H(11B)	0.9114	0.4357	0.7479	0.020
H(12A)	0.7247	0.5325	0.6766	0.024
H(12B)	0.6380	0.4315	0.6481	0.024
H(13A)	0.9120	0.4722	0.5817	0.032
H(13B)	0.8093	0.3819	0.5458	0.032
H(14A)	0.7952	0.5088	0.4314	0.046
H(14B)	0.7576	0.5914	0.5082	0.046
H(14C)	0.6461	0.5045	0.4778	0.046

Table R5-3. Anisotropic displacement parameters ($Å^2$) for uvic1601.
The anisotropic displacement factor exponent takes the form:
$-2\pi^2[h^2a^{*2}U_{11} + ... + 2hka^*b^*U_{12}]$

	U_{11}	U_{22}	U_{33}	U_{23}	U_{13}	U_{12}
N(1)	0.0128(4)	0.0158(5)	0.0155(5)	-0.0008(4)	0.0016(4)	0.0002(4)
C(1)	0.0147(5)	0.0189(6)	0.0205(6)	-0.0011(4)	0.0016(4)	-0.0031(4)
C(2)	0.0186(6)	0.0225(6)	0.0243(6)	-0.0018(5)	0.0065(5)	-0.0021(5)
C(3)	0.0347(8)	0.0258(7)	0.0321(7)	0.0024(6)	0.0138(6)	-0.0017(6)
C(4)	0.0176(6)	0.0193(6)	0.0156(5)	0.0005(4)	-0.0009(4)	0.0020(4)
C(5)	0.0241(6)	0.0178(6)	0.0191(6)	0.0011(4)	-0.0018(5)	0.0021(5)
C(6)	0.0266(7)	0.0261(7)	0.0283(7)	-0.0029(5)	-0.0004(5)	0.0068(5)
C(7)	0.0155(5)	0.0156(5)	0.0186(6)	-0.0020(4)	0.0038(4)	0.0017(4)
C(8)	0.0178(6)	0.0173(6)	0.0232(6)	-0.0012(5)	0.0028(5)	-0.0004(4)
C(9)	0.0240(6)	0.0196(6)	0.0292(7)	-0.0040(5)	0.0013(5)	-0.0001(5)
C(10)	0.0358(8)	0.0228(7)	0.0319(7)	0.0011(6)	-0.0013(6)	0.0024(6)
C(11)	0.0155(5)	0.0198(6)	0.0146(5)	-0.0005(4)	0.0037(4)	0.0007(4)
C(12)	0.0203(6)	0.0228(6)	0.0167(5)	0.0006(5)	0.0014(4)	0.0006(5)
C(13)	0.0332(7)	0.0292(7)	0.0174(6)	0.0003(5)	0.0055(5)	0.0046(6)
C(14)	0.0411(8)	0.0333(8)	0.0185(6)	0.0020(5)	0.0028(6)	0.0007(6)
P(1)	0.0148(2)	0.0198(2)	0.0169(2)	0.0008(1)	0.0022(1)	-0.0013(1)
F(1)	0.0183(4)	0.0438(5)	0.0215(4)	0.0003(3)	-0.0015(3)	-0.0024(3)
F(2)	0.0219(4)	0.0416(5)	0.0242(4)	0.0022(3)	-0.0049(3)	-0.0018(3)
F(3)	0.0190(4)	0.0483(5)	0.0256(4)	0.0072(4)	0.0076(3)	-0.0026(4)
F(4)	0.0381(5)	0.0280(5)	0.0501(6)	-0.0133(4)	-0.0013(4)	0.0109(4)
F(5)	0.0610(6)	0.0199(4)	0.0459(5)	-0.0022(4)	-0.0095(5)	0.0060(4)
F(6)	0.0310(5)	0.0787(7)	0.0217(4)	0.0063(4)	0.0066(4)	-0.0227(5)

Table R5-4. Bond lengths [Å] for uvic1601.

atom-atom	distance	atom-atom	distance
N(1)-C(11)	1.5182(14)	N(1)-C(4)	1.5240(15)
N(1)-C(7)	1.5246(15)	N(1)-C(1)	1.5256(15)
C(1)-C(2)	1.4961(17)	C(1)-H(1A)	0.9900
C(1)-H(1B)	0.9900	C(2)-C(3)	1.3183(19)
C(2)-H(2)	0.9500	C(3)-H(3A)	0.9500
C(3)-H(3B)	0.9500	C(4)-C(5)	1.4996(17)
C(4)-H(4A)	0.9900	C(4)-H(4B)	0.9900
C(5)-C(6)	1.3168(19)	C(5)-H(5)	0.9500
C(6)-H(6A)	0.9500	C(6)-H(6B)	0.9500
C(7)-C(8)	1.5210(17)	C(7)-H(7A)	0.9900
C(7)-H(7B)	0.9900	C(8)-C(9)	1.5356(17)
C(8)-H(8A)	0.9900	C(8)-H(8B)	0.9900
C(9)-C(10)	1.5131(19)	C(9)-H(9A)	0.9900
C(9)-H(9B)	0.9900	C(10)-H(10A)	0.9800
C(10)-H(10B)	0.9800	C(10)-H(10C)	0.9800
C(11)-C(12)	1.5196(16)	C(11)-H(11A)	0.9900
C(11)-H(11B)	0.9900	C(12)-C(13)	1.5271(17)
C(12)-H(12A)	0.9900	C(12)-H(12B)	0.9900
C(13)-C(14)	1.5221(19)	C(13)-H(13A)	0.9900
C(13)-H(13B)	0.9900	C(14)-H(14A)	0.9800
C(14)-H(14B)	0.9800	C(14)-H(14C)	0.9800
P(1)-F(4)	1.5862(9)	P(1)-F(5)	1.5960(9)
P(1)-F(3)	1.5988(8)	P(1)-F(6)	1.5993(9)
P(1)-F(2)	1.5993(8)	P(1)-F(1)	1.6062(8)

Symmetry transformations used to generate equivalent atoms:

X-ray report for **R7**:

DISCUSSION

The compound crystallizes as colourless tablet-like crystals. There are four molecules of the di-n-butyl, di-butylene ammonium hexafluorophosphate salt in the unit cell of the primitive, centrosymmetric, orthorhombic space group Pnma.

Both the cation and the anion crystallize on the crystallographic mirror planes, perpendicular to the b axis. Because of this location, only half of each molecule is Both the cation and the anion crystallize on the crystallographic mirror planes, perpendicular to the b axis. Because of this location, only half of each molecule is observed within the asymmetric unit. Furthermore, the cation is disordered about the mirror plane. It was ultimately modeled with a half occupancy molecule with the two parts of the disorder decoupled from each other. Due to this decoupling, C12 and C16 are directly related and refined poorly. Thus they were restrained to have the same atomic displacement parameters and constrained to have similar C-C distances to their respective bonding methylene carbon atom. This disorder also disguises the true location of the ethylene functionality. The model depicted here was developed comparing bond distances and angles of residual density to the gamma carbon of the butyl chains. It is likely that all four sites have some character of methyl and terminal ethylinic character. Furthermore, the PF_6 anion also exhibits typical elongation, bordering on positional disorder, of the fluorine atoms.

Attempts to solve the structure in lowewr symmetry space groups (primarily $Pna2_1$, the acentric isomorph of Pnma) did not yield satisfactory results and were abandoned.

Bond distances and angles are generally reliable. However, as noted above there is the real possibility that the terminal groups (methyl and ethylene) are scrambled.

CRYSTAL SUMMARY

Crystal data for $C_{16}H_{32}F_6NP$; M_r = 383.39; Orthorhombic; space group Pnma; a = 15.2010(18) Å; b = 9.7668(12) Å; c = 13.4419(16) Å; α = 90°; β = 90°; γ = 90°; V = 1995.7(4) $Å^3$; Z = 4; T = 120(2) K; λ(Mo-Kα) = 0.71073 Å; μ(Mo-Kα) = 0.189 mm^{-1}; d_{calc}

= 1.276g.cm^{-3}; 33098 reflections collected; 2168 unique (R_{int} = 0.0510); giving R_1 = 0.0867, wR_2 = 0.2361 for 1582 data with [I>2σ(I)] and R_1 = 0.1111, wR_2 = 0.2583 for all 2168 data. Residual electron density (e^-.Å^{-3}) max/min: 0.723/-0.515.

An arbitrary sphere of data were collected on a colorless tablet-like crystal, having approximate dimensions of 0.138 × 0.132 × 0.078 mm, on a Bruker APEX-II diffractometer using a combination of ω- and φ-scans of 0.5° [1]. Data were corrected for absorption and polarization effects and analyzed for space group determination. The structure was solved by intrinsic phasing methods and expanded routinely [2]. The model was refined by full-matrix least-squares analysis of F^2 against all reflections [3]. All non-hydrogen atoms were refined with anisotropic atomic displacement parameters. Unless otherwise noted, hydrogen atoms were included in calculated positions. Atomic displacement parameters for the hydrogens were tied to the equivalent isotropic displacement parameter of the atom to which they are bonded (U_{iso}(H) = 1.5U_{eq}(C) for methyl, 1.2U_{eq}(C) for all others).

Table R7-1. Crystal data and structure refinement for uvic1602.

Identification code	uvic1602	
Empirical formula	$C_{16}H_{32}F_6NP$	
Formula weight	383.39	
Temperature	120(2) K	
Wavelength	0.71073 Å	
Crystal system	Orthorhombic	
Space group	Pnma	
Unit cell dimensions	*a* = 15.2010(18) Å	α = 90°
	b = 9.7668(12) Å	β = 90°
	c = 13.4419(16) Å	γ = 90°
Volume	1995.7(4) Å^3	
Z	4	
Density (calculated)	1.276 g.cm^{-3}	
Absorption coefficient (μ)	0.189 mm^{-1}	
F(000)	816	
Crystal color, habit	colorless, tablet	

Crystal size	0.138 × 0.132 × 0.078 mm^3
θ range for data collection	2.022 to 26.374°
Index ranges	$-19 \leq h \leq 19$, $-12 \leq k \leq 12$, $-16 \leq l \leq 16$
Reflections collected	33098
Independent reflections	2168 [$R_{int} = 0.0510$]
Completeness to θ = 25.242°	100.0 %
Absorption correction	Numerical
Max. and min. transmission	1.0000 and 0.9488
Refinement method	Full-matrix least-squares on F^2
Data / restraints / parameters	2168 / 1 / 183
Goodness-of-fit on F^2	1.055
Final R indices [I>2σ(I)]	$R_1 = 0.0867$, $wR_2 = 0.2361$
R indices (all data)	$R_1 = 0.1111$, $wR_2 = 0.2583$
Extinction coefficient	n/a
Largest diff. peak and hole	0.723 and -0.515 $e^-.Å^{-3}$

Table R7-2. Atomic coordinates and equivalent isotropic displacement parameters ($Å^2$) for uvic1602. U(eq) is defined as one third of the trace of the orthogonalized U_{ij} tensor.

	x	y	z	U(eq)
N(1)	0.1904(2)	0.7500	0.4714(3)	0.034(1)
C(1)	0.2816(4)	0.8002(7)	0.4461(5)	0.043(2)
C(2)	0.3578(4)	0.7074(9)	0.4727(6)	0.064(3)
C(3)	0.4427(5)	0.724(3)	0.4373(7)	0.082(9)
C(4)	0.5203(6)	0.758(5)	0.4767(7)	0.151(8)
C(5)	0.1845(4)	0.7036(6)	0.5805(5)	0.040(2)
C(6)	0.2111(6)	0.8142(9)	0.6548(6)	0.057(2)
C(7)	0.2046(5)	0.741(4)	0.7614(6)	0.081(5)
C(8)	0.1883(7)	0.8379(13)	0.8159(8)	0.086(3)
C(9)	0.1734(4)	0.6210(6)	0.4059(5)	0.037(1)
C(10)	0.0804(5)	0.5626(7)	0.4142(6)	0.048(2)
C(11)	0.0495(9)	0.4757(18)	0.3399(12)	0.054(3)
C(12)	0.0505(13)	0.4550(17)	0.2350(14)	0.098(5)
C(13)	0.1237(5)	0.8588(6)	0.4515(5)	0.040(2)
C(14)	0.1128(5)	0.9006(7)	0.3448(5)	0.047(2)
C(15)	0.0764(9)	1.0563(17)	0.3411(14)	0.053(4)
C(16)	0.0216(13)	1.0611(18)	0.2555(14)	0.098(5)
P(1)	0.19523(8)	0.2500	0.61424(9)	0.038(1)
F(1)	0.2338(2)	0.1395(3)	0.5425(3)	0.110(1)
F(2)	0.1586(3)	0.3587(4)	0.6889(3)	0.131(2)
F(3)	0.2835(3)	0.2500	0.6704(3)	0.137(3)
F(4)	0.1079(3)	0.2500	0.5581(4)	0.200(4)
H(1A)	0.2907	0.8890	0.4801	0.052
H(1B)	0.2839	0.8178	0.3736	0.052

H(2A)	0.3621	0.7082	0.5461	0.076
H(2B)	0.3397	0.6136	0.4537	0.076
H(3)	0.4466	0.7080	0.3677	0.098
H(4A)	0.5247	0.7767	0.5459	0.181
H(4B)	0.5710	0.7631	0.4357	0.181
H(5A)	0.1233	0.6749	0.5948	0.048
H(5B)	0.2229	0.6228	0.5900	0.048
H(6A)	0.1707	0.8934	0.6511	0.069
H(6B)	0.2719	0.8461	0.6418	0.069
H(7)	0.2116	0.6467	0.7779	0.097
H(8A)	0.1831	0.9273	0.7887	0.103
H(8B)	0.1807	0.8240	0.8853	0.103
H(9A)	0.1848	0.6449	0.3355	0.044
H(9B)	0.2159	0.5489	0.4251	0.044
H(10A)	0.0767	0.5125	0.4781	0.058
H(10B)	0.0392	0.6409	0.4187	0.058
H(11A)	-0.0144	0.4755	0.3538	0.065
H(11B)	0.0704	0.3857	0.3641	0.065
H(12A)	0.0357	0.3595	0.2203	0.147
H(12B)	0.1092	0.4758	0.2090	0.147
H(12C)	0.0072	0.5155	0.2037	0.147
H(13A)	0.1399	0.9409	0.4905	0.048
H(13B)	0.0661	0.8264	0.4764	0.048
H(14A)	0.0708	0.8385	0.3111	0.056
H(14B)	0.1700	0.8948	0.3098	0.056
H(15A)	0.0423	1.0779	0.4019	0.064
H(15B)	0.1255	1.1222	0.3351	0.064
H(16A)	0.0049	1.1562	0.2420	0.147
H(16B)	-0.0315	1.0064	0.2673	0.147
H(16C)	0.0535	1.0239	0.1983	0.147

Table R7-3. Anisotropic displacement parameters ($Å^2$) for uvic1602.
The anisotropic displacement factor exponent takes the form:
$-2\pi^2[h^2a^{*2}U_{11} + ... + 2hka^*b^*U_{12}]$

	U_{11}	U_{22}	U_{33}	U_{23}	U_{13}	U_{12}
N(1)	0.0318(19)	0.0309(18)	0.040(2)	0.000	0.0081(15)	0.000
C(1)	0.034(3)	0.045(4)	0.050(3)	0.009(3)	0.006(3)	-0.011(2)
C(2)	0.033(3)	0.094(9)	0.064(4)	0.023(4)	0.006(3)	-0.003(3)
C(3)	0.036(3)	0.13(3)	0.080(5)	-0.033(11)	0.009(3)	0.015(7)
C(4)	0.051(5)	0.32(2)	0.076(6)	-0.06(2)	-0.001(4)	0.051(19)
C(5)	0.046(3)	0.039(3)	0.037(3)	0.007(2)	0.010(3)	-0.004(2)
C(6)	0.064(5)	0.060(4)	0.048(4)	0.001(4)	0.003(4)	-0.012(4)
C(7)	0.070(5)	0.125(12)	0.046(4)	-0.029(12)	-0.010(4)	0.035(14)

C(8)	0.084(7)	0.104(8)	0.069(6)	-0.026(6)	0.005(6)	-0.023(6)
C(9)	0.036(3)	0.028(3)	0.047(3)	-0.003(3)	0.013(3)	0.004(2)
C(10)	0.045(4)	0.036(3)	0.063(4)	-0.013(3)	0.017(3)	-0.011(3)
C(11)	0.043(8)	0.061(9)	0.058(6)	-0.005(5)	0.007(6)	-0.010(6)
C(12)	0.088(12)	0.089(5)	0.117(8)	0.024(7)	-0.007(8)	0.018(5)
C(13)	0.039(3)	0.027(3)	0.054(4)	-0.010(3)	0.003(3)	0.002(3)
C(14)	0.052(4)	0.040(4)	0.049(4)	0.000(3)	0.002(3)	0.011(3)
C(15)	0.040(8)	0.048(7)	0.071(6)	0.023(5)	0.013(6)	0.009(5)
C(16)	0.088(12)	0.089(5)	0.117(8)	0.024(7)	-0.007(8)	0.018(5)
P(1)	0.0388(7)	0.0356(7)	0.0386(7)	0.000	-0.0056(5)	0.000
F(1)	0.131(3)	0.0613(18)	0.138(3)	-0.0506(18)	0.055(2)	-0.0237(18)
F(2)	0.160(3)	0.084(2)	0.148(3)	-0.038(2)	0.080(3)	0.013(2)
F(3)	0.071(3)	0.281(8)	0.061(3)	0.000	-0.028(2)	0.000
F(4)	0.052(3)	0.454(14)	0.093(4)	0.000	-0.029(3)	0.000

Table R7-4. Bond lengths [Å] for uvic1602.

atom-atom	distance	atom-atom	distance
N(1)-C(13)	1.493(7)	N(1)-C(1)	1.510(7)
N(1)-C(5)	1.538(7)	N(1)-C(9)	1.558(6)
C(1)-C(2)	1.514(10)	C(1)-H(1A)	0.9900
C(1)-H(1B)	0.9900	C(2)-C(3)	1.385(10)
C(2)-H(2A)	0.9900	C(2)-H(2B)	0.9900
C(3)-C(4)	1.334(19)	C(3)-H(3)	0.9500
C(4)-H(4A)	0.9500	C(4)-H(4B)	0.9500
C(5)-C(6)	1.525(10)	C(5)-H(5A)	0.9900
C(5)-H(5B)	0.9900	C(6)-C(7)	1.61(2)
C(6)-H(6A)	0.9900	C(6)-H(6B)	0.9900
C(7)-C(8)	1.22(3)	C(7)-H(7)	0.9500
C(8)-H(8A)	0.9500	C(8)-H(8B)	0.9500
C(9)-C(10)	1.528(9)	C(9)-H(9A)	0.9900
C(9)-H(9B)	0.9900	C(10)-C(11)	1.392(18)
C(10)-H(10A)	0.9900	C(10)-H(10B)	0.9900
C(11)-C(12)	1.424(15)	C(11)-H(11A)	0.9900
C(11)-H(11B)	0.9900	C(12)-H(12A)	0.9800
C(12)-H(12B)	0.9800	C(12)-H(12C)	0.9800
C(13)-C(14)	1.501(10)	C(13)-H(13A)	0.9900
C(13)-H(13B)	0.9900	C(14)-C(15)	1.619(19)
C(14)-H(14A)	0.9900	C(14)-H(14B)	0.9900
C(15)-C(16)	1.421(14)	C(15)-H(15A)	0.9900
C(15)-H(15B)	0.9900	C(16)-H(16A)	0.9800
C(16)-H(16B)	0.9800	C(16)-H(16C)	0.9800
P(1)-F(4)	1.528(4)	P(1)-F(3)	1.539(4)
P(1)-F(1)	1.562(3)	P(1)-F(1)#1	1.562(3)
P(1)-F(2)#1	1.563(3)	P(1)-F(2)	1.563(3)

Symmetry transformations used to generate equivalent atoms:
#1 x,-y+1/2,z

Table R7-5. Bond angles [°] for uvic1602.

atom-atom-atom	angle	atom-atom-atom	angle
C(13)-N(1)-C(1)	110.6(4)	C(13)-N(1)-C(5)	109.9(4)
C(1)-N(1)-C(5)	111.3(4)	C(13)-N(1)-C(9)	111.2(4)
C(1)-N(1)-C(9)	106.8(4)	C(5)-N(1)-C(9)	106.9(3)
N(1)-C(1)-C(2)	117.1(5)	N(1)-C(1)-H(1A)	108.0
C(2)-C(1)-H(1A)	108.0	N(1)-C(1)-H(1B)	108.0
C(2)-C(1)-H(1B)	108.0	H(1A)-C(1)-H(1B)	107.3
C(3)-C(2)-C(1)	124.1(13)	C(3)-C(2)-H(2A)	106.3
C(1)-C(2)-H(2A)	106.3	C(3)-C(2)-H(2B)	106.3
C(1)-C(2)-H(2B)	106.3	H(2A)-C(2)-H(2B)	106.4
C(4)-C(3)-C(2)	135.7(10)	C(4)-C(3)-H(3)	112.1
C(2)-C(3)-H(3)	112.1	C(3)-C(4)-H(4A)	120.0
C(3)-C(4)-H(4B)	120.0	H(4A)-C(4)-H(4B)	120.0
C(6)-C(5)-N(1)	113.6(5)	C(6)-C(5)-H(5A)	108.9
N(1)-C(5)-H(5A)	108.9	C(6)-C(5)-H(5B)	108.9
N(1)-C(5)-H(5B)	108.9	H(5A)-C(5)-H(5B)	107.7
C(5)-C(6)-C(7)	104.5(13)	C(5)-C(6)-H(6A)	110.8
C(7)-C(6)-H(6A)	110.8	C(5)-C(6)-H(6B)	110.8
C(7)-C(6)-H(6B)	110.8	H(6A)-C(6)-H(6B)	108.9
C(8)-C(7)-C(6)	101(2)	C(8)-C(7)-H(7)	129.3
C(6)-C(7)-H(7)	129.3	C(7)-C(8)-H(8A)	120.0
C(7)-C(8)-H(8B)	120.0	H(8A)-C(8)-H(8B)	120.0
C(10)-C(9)-N(1)	114.5(5)	C(10)-C(9)-H(9A)	108.6
N(1)-C(9)-H(9A)	108.6	C(10)-C(9)-H(9B)	108.6
N(1)-C(9)-H(9B)	108.6	H(9A)-C(9)-H(9B)	107.6
C(11)-C(10)-C(9)	119.2(8)	C(11)-C(10)-H(10A)	107.5
C(9)-C(10)-H(10A)	107.5	C(11)-C(10)-H(10B)	107.5
C(9)-C(10)-H(10B)	107.5	H(10A)-C(10)-H(10B)	107.0
C(10)-C(11)-C(12)	142.5(17)	C(10)-C(11)-H(11A)	101.3
C(12)-C(11)-H(11A)	101.3	C(10)-C(11)-H(11B)	101.3
C(12)-C(11)-H(11B)	101.3	H(11A)-C(11)-H(11B)	104.6
C(11)-C(12)-H(12A)	109.5	C(11)-C(12)-H(12B)	109.5
H(12A)-C(12)-H(12B)	109.5	C(11)-C(12)-H(12C)	109.5
H(12A)-C(12)-H(12C)	109.5	H(12B)-C(12)-H(12C)	109.5
N(1)-C(13)-C(14)	116.1(5)	N(1)-C(13)-H(13A)	108.3
C(14)-C(13)-H(13A)	108.3	N(1)-C(13)-H(13B)	108.3
C(14)-C(13)-H(13B)	108.3	H(13A)-C(13)-H(13B)	107.4
C(13)-C(14)-C(15)	108.8(8)	C(13)-C(14)-H(14A)	109.9

Table R7-6. Torsion angles [°] for uvic1602.

atom-atom-atom-atom	angle	atom-atom-atom-atom	angle
C(13)-N(1)-C(1)-C(2)	173.5(6)	C(5)-N(1)-C(1)-C(2)	51.0(7)
C(9)-N(1)-C(1)-C(2)	-65.3(7)	N(1)-C(1)-C(2)-C(3)	166.3(12)
C(1)-C(2)-C(3)-C(4)	113(4)	C(13)-N(1)-C(5)-C(6)	-66.6(7)
C(1)-N(1)-C(5)-C(6)	56.4(7)	C(9)-N(1)-C(5)-C(6)	172.6(5)
N(1)-C(5)-C(6)-C(7)	-177.2(6)	C(5)-C(6)-C(7)-C(8)	-151.8(10)
C(13)-N(1)-C(9)-C(10)	-53.9(7)	C(1)-N(1)-C(9)-C(10)	-174.7(5)
C(5)-N(1)-C(9)-C(10)	66.0(6)	N(1)-C(9)-C(10)-C(11)	161.1(9)
C(9)-C(10)-C(11)-C(12)	-39(2)	C(1)-N(1)-C(13)-C(14)	64.8(7)
C(5)-N(1)-C(13)-C(14)	-171.8(5)	C(9)-N(1)-C(13)-C(14)	-53.6(7)
N(1)-C(13)-C(14)-C(15)	-154.1(6)	C(13)-C(14)-C(15)-C(16)	-146.7(12)

Symmetry transformations used to generate equivalent atoms:
#1 x,-y+1/2,z

Appendix III

Orbitrap data

Table 0.1: Catalyst decomposition species in R5**. Mass determined by Orbitrap MS.**

R5	m_{obs}	m_{em}	$\Delta=m_{obs}-m_{em}$
$C_{21}H_{27}N_2^+$ NHC^+ (*m/z* 307)	307.21542	307.21688	0.00146
$C_{18}H_{34}P+$ $[HPCy_3]^+$ (*m/z* 281)	281.23853	281.23926	0.00073
$C_{18}H_{33}PCl^+$ $[ClPCy_3]^+$ (*m/z* 315)	315.19904	315.20084	0.00180

Table 0.2: Orbitrap data for R9, m_{obs} indicate observed data from mass spectrum, m_{em} indicate calculated exact mass, $\Delta=m_{obs}-m_{em}$ indicate the mass difference between observed and calculated and Δ 14 Da indicate the mass difference between each product and adjacent byproduct.

	m_{obs}	m_{em}	$\Delta=m_{obs}-m_{em}$	Δ 14 Da
$C_{16}H_{32}N^+$ product	238.25230	238.25348	0.00118	N/A
$C_{17}H_{34}N^+$ **P9** +14 / **R9**-14	252.26791	252.26913	0.00122	14.01561
$C_{18}H_{36}N^+$ **R9**	266.28351	266.28478	0.00127	14.01560
$C_{19}H_{38}N^+$ **R9** +14	280.29916	280.30043	0.00127	14.01565

Appendix IV

MS characterization for all charged tags

R5

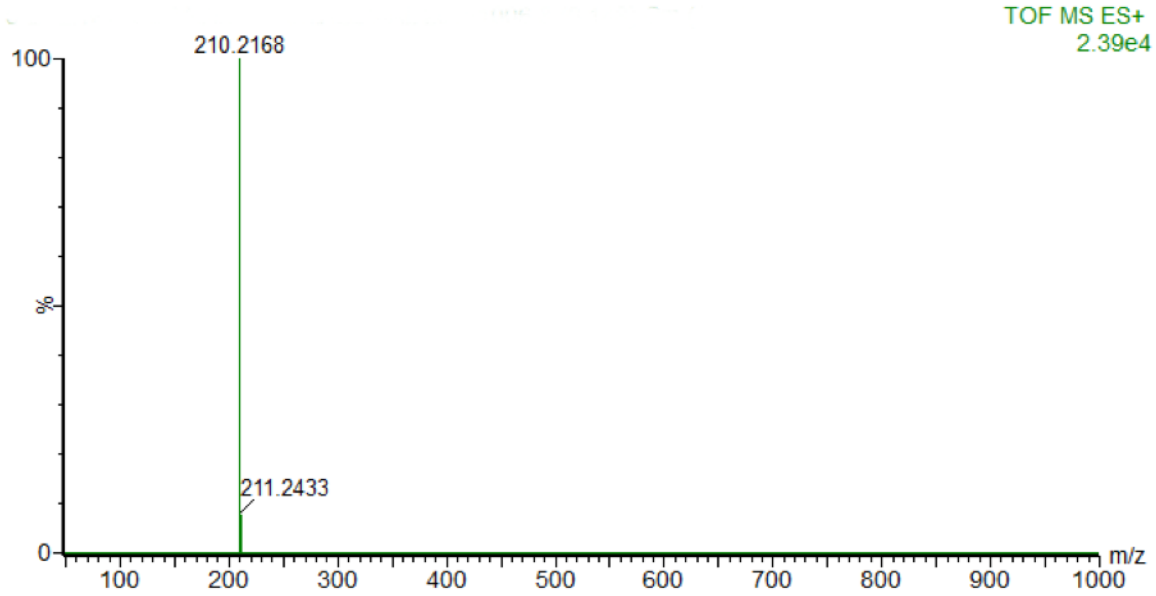

R6

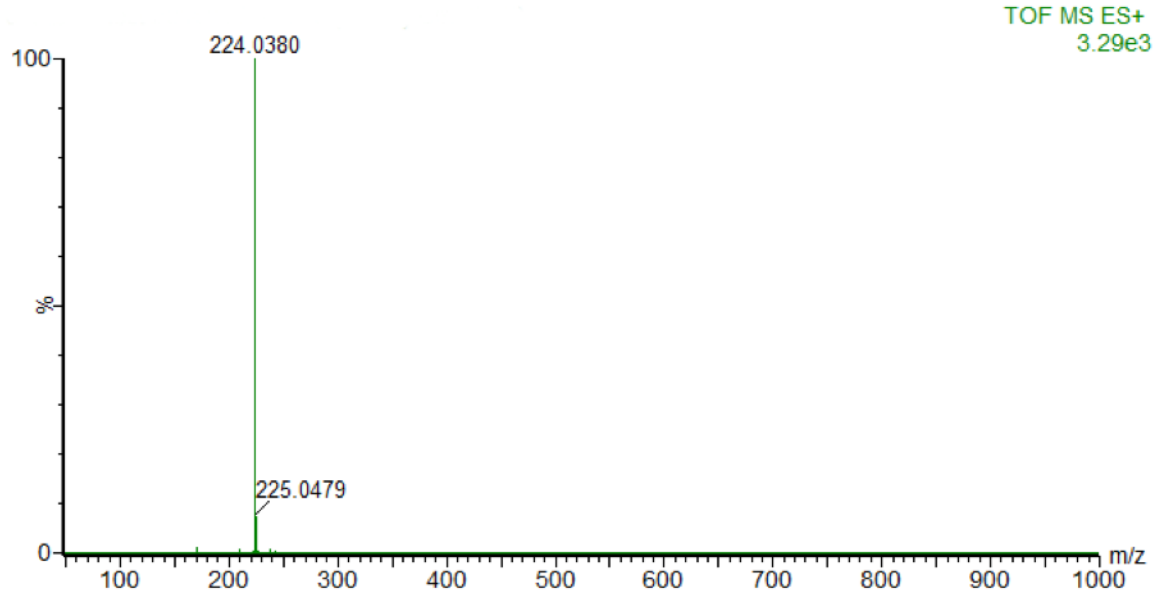

R7

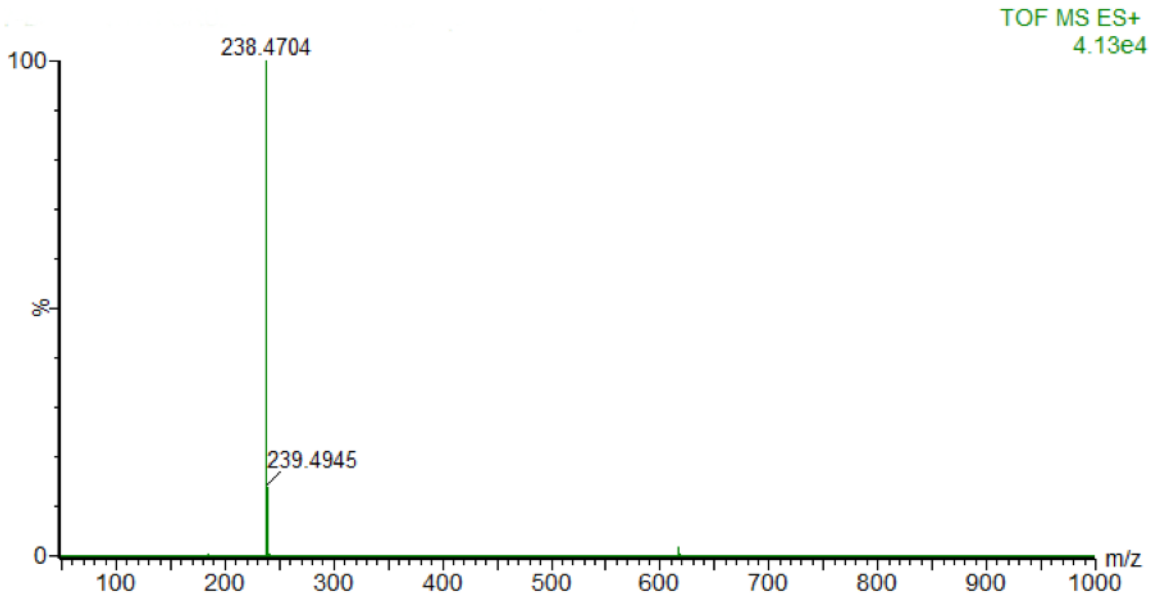
TOF MS ES+
4.13e4
238.4704
239.4945
100
%
0
100
200
300
400
500
600
700
800
900
1000
m/z

R8

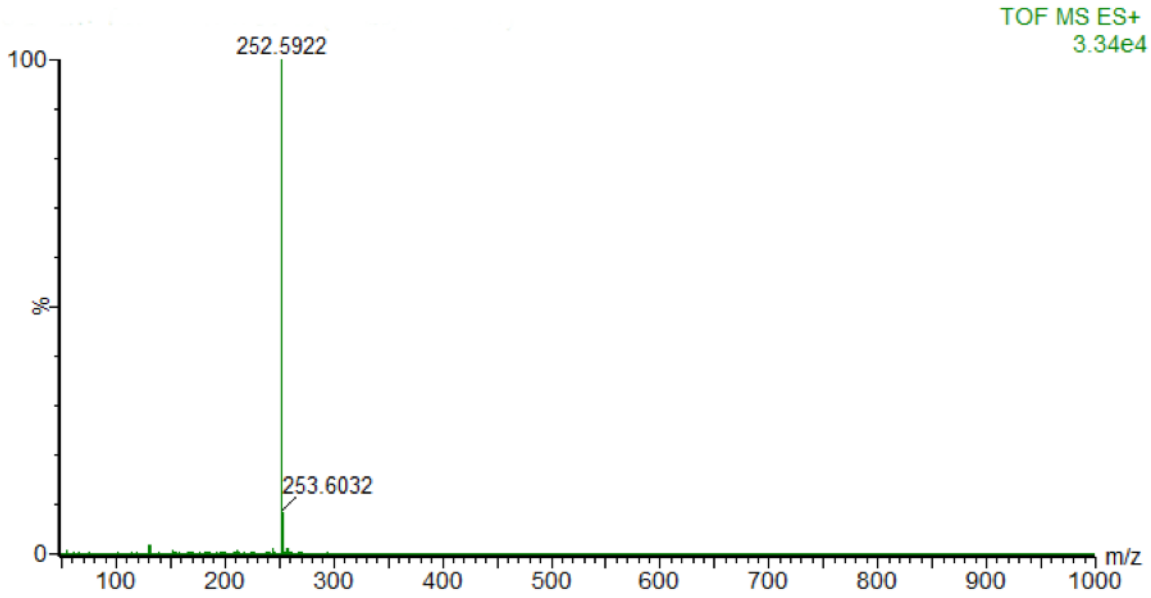
TOF MS ES+
3.34e4
252.5922
253.6032
100
%
0
100
200
300
400
500
600
700
800
900
1000
m/z

R9

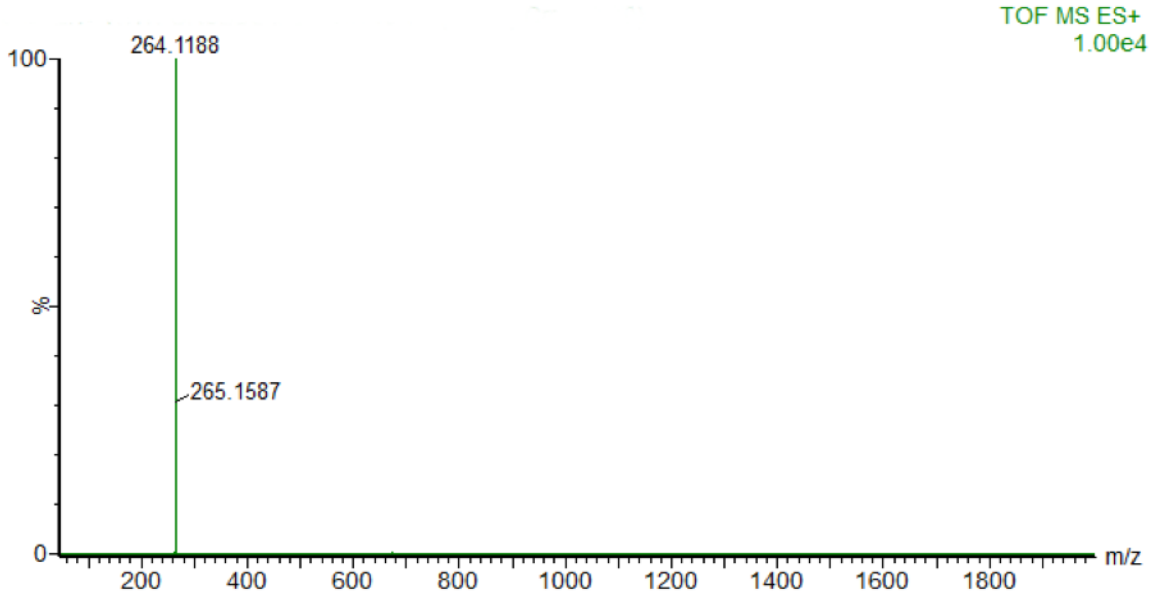
TOF MS ES+
1.00e4
264.1188
265.1587
100
%
0
200
400
600
800
1000
1200
1400
1600
1800
m/z

R11

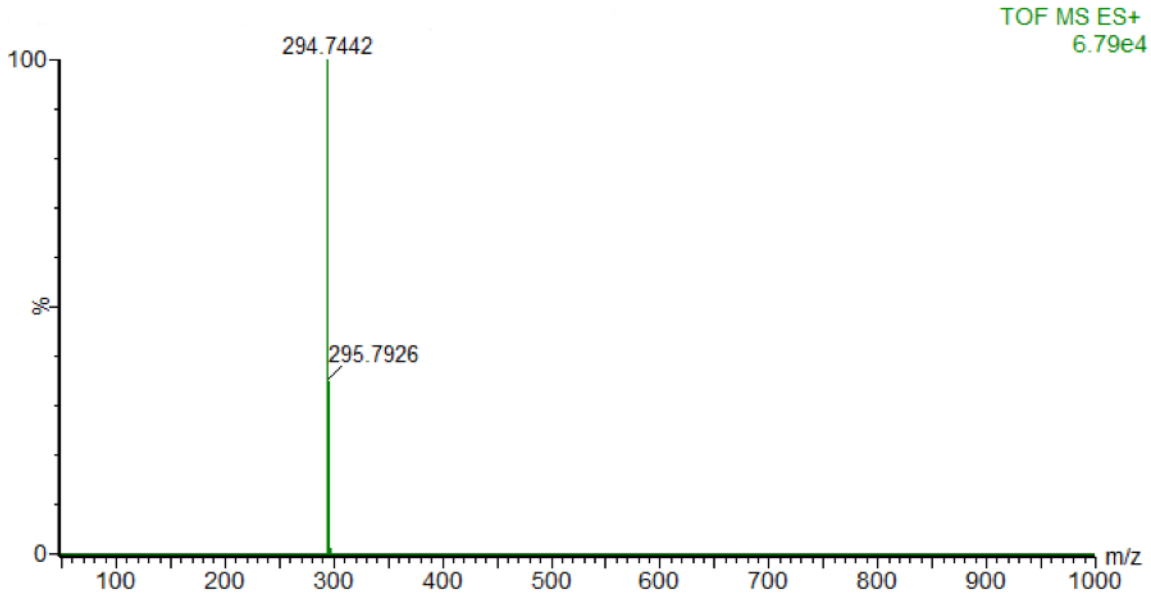
TOF MS ES+
6.79e4
294.7442
295.7926
100
%
0
100
200
300
400
500
600
700
800
900
1000
m/z

R13

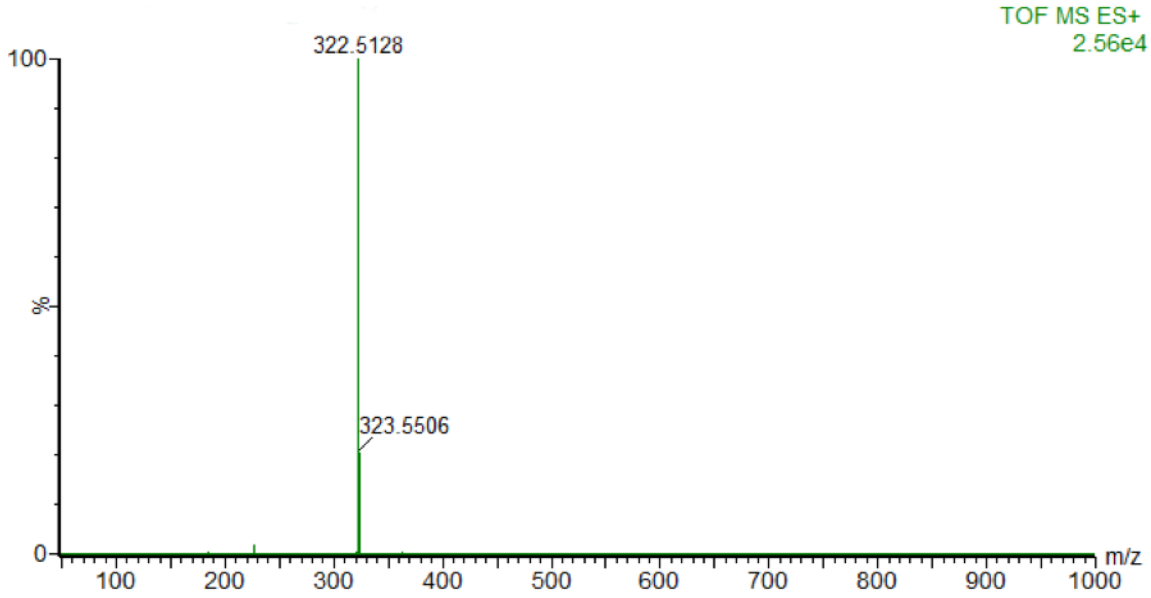
TOF MS ES+
2.56e4
322.5128
323.5506
100
%
0
100
200
300
400
500
600
700
800
900
1000
m/z

R15

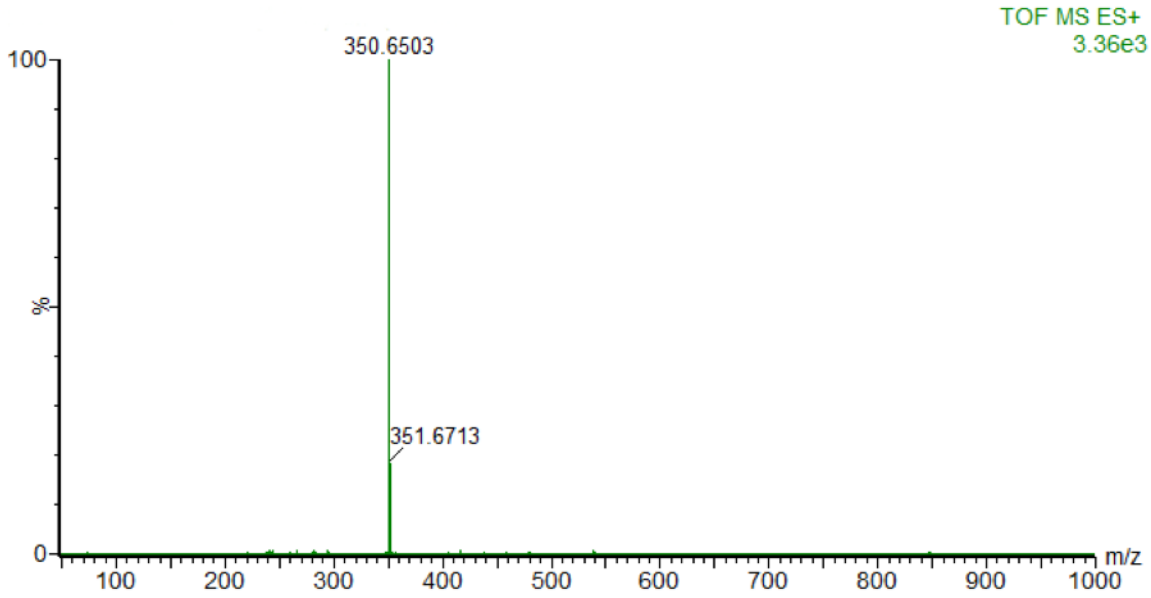
TOF MS ES+
3.36e3
350.6503
351.6713
100
%
0
100
200
300
400
500
600
700
800
900
1000
m/z

Bibliography

[1] Yarwood, J.; Douthwaite, R.; Duckett, S. B., *Spectroscopic Properties of Inorganic and Organimetallic Compounds: Techniques, Materials and Applications*. Royal Society of chemistry: Cambridge, UK., **2010**; Vol 41, P 324.

[2] Ashcroft, A. E., *Ionization Methods in Organic Mass Spectrometry*. Royal Society of chemistry: Cambridge, UK., **1997**, P 176.

[3] Plattner, D. A. *Int. J. Mass Spectrom*., **2001**, 207, 125-144.

[4] Dole, M., Mack, L. L., Hines, R.L., Mocley, R.C., Ferguson, L. D. and Alica, M.B., *J. Chem. Phys*., 1968, 49 2240.

[5] Fenn, J. B., Mann, M., Meng, C. K. and Wong, S. F., *Mass spectrum Rev.,* 1990, 9 37.

[666] Fenn, J. B., Mann, M., Meng, C. K., Wong, S. F. and Whitehouse, C.M., *Science*, 1989, 246 64.

[7] Fenn, J. B., *Angew. Chem., Int. Ed.,* 2003, 42 3871.

[8] Brik, A. *Adv. Synth. Catal*. **2008**, 350, 1661-1675.

[99] Adlhart, C.; Hinderling, C.; Baumann, H.; Chen, P. *J. Am. Chem. Soc.* 2000, 122, 8204–8214.

[10] W. Henderson, J. S. McIndoe, *Mass Spectrometry of Inorganic and Organometallic Compounds: Tools-Techniques-Tips.* John Wiley & Sons, **2005**, P 90-91.

[11] Iribarne, J. V.; Thomson, B. A. *The Journal of Chemical Physics* **1976**, *64*, 2287-2294

[12] Paul, W. And Steinwedel, H., Z. *Naturforsch*., 1953, 8a 448.

[13] Stephens, W., *Phys. Rev.*, 69, 691 (1946).

[14] Cameron, A. E. and Eggers, D. F. , *Rev. Sci. Instrum.*, 16, 1150 (1957).

[15] Ionov, N. I. and Mamyrin, B. A., *Zh. Tekh. Fiz.*, 23 2101 (1953).

[16] Wiley, W. L. and McLaren, I. H., *Rev. Sci. Instrum*., 16 1150 (1957).

[17] Mamyrin, B. A., Karataev, V. I., Shmikk, D. V. and Zagulin, V. A., *Sov. Phys. JETP*, **37**, 45 (1973).

[18] Scherer, S., Altwegg, K., Fischer, J. *et al., Int. J. Mass Spectrum.*, **251**, 73, 45 (1973).

[19] Edmond de Hoffmann and Vincent Stroobant, *Mass Spectrometry Principles and Applications* 2nd edn., John Wiley & Sons, Chichester West Sussex, England. **2002**, P 212.

[20] Goodrich, G. W. and Wiley, C. W., *Rev, Sci. Instrum*., **33**, 761 (1962).

[21] Allen, J. S. *Physical Review* **1939**, *55*, 966-971.

[22] Allen, J. S. *Review of Scientific Instruments* **1947**, *18*, 739-749.

[23] Duckworth, H. E., Barber, R. C. and Venkatasubramanian, V. S., *Mass spectroscopy* 2nd edn., Cambridge University Press, Cambridge, London, New York, New Rochelle, Melbourne, Sydney (1986).

[24] Q. Hu, R. J. Noll, H. Li., A. Makarov, W. Balschun, and R. G. Cooks, *J. Mass Spectrum*. 40, 430-443 (2005).

[25] A. Makarov, E. Denisov, A. Kholomeev, W. Balschun, O. Lange, K. Strupat, and S. Horning, *Anal. Chem*. **78**, 2113-2120 (2006).

[26] K. L. Vikse, M. P. Woods, and J. S. McIndoe. *Organometallics*, 2010, 29, 6615-6618.

[27] K. L. Vikse, Z. Ahmadi, J. Luo, N. van der Wal, K. Daze, N. Taylor and J. S. McIndoe. *International Journal of Mass Spectrometry.* **2012**, 8-13, 323-324.

[28] KL. Vikse, Z. Ahmad, J. Luo, N. van der Wal, K. Daze, N. Taylor and J. S. McIndoe. *International Journal of Mass Spectrometry*, **2012**, 323-324, 8-13.

[29] Schroder, D. *Acc. Chem. Res*. **2012**, 45, 1521−1532.

[30] O'Hair, R. A. J. *Int. J. Mass Spectrom*. **2015**, 377, 121−129.

[31] Vatamanu, M. *J. Catal.* **2015**, 323, 112−120.

[32] Santos, L. S.; Rosso, G. B.; Pilli, R. A.; Eberlin, M. N. *J. Org. Chem.* **2007**, 72, 5809−5812.

[33] Silva, M.; Mello, R. S.; Farrukh, M. A.; Venturini, J.; Bunton, C. A.; Milagre, H. M. S.; Eberlin, M. N.; Fiedler, H. D.; Nome, F. *J. Org. Chem.* **2009**, 74, 8254−8260.

[34] Torborg, C.; Beller, M. *Advanced Synthesis & Catalysis.* **2009**, *351*, 3027-3043.

[35] Neely, J. M.; Bezdek, M. J.; Chirik, P. J. *ACS Central Science* **2016**, *2*, 935-942.

[36] K. Kikukawa, T. Matsuda, *Chem. Lett*. **1977**, 159 – 162.

[37] K. Morta, Z. Suzuki and H. Hirose, *Bull. Chem. Soc. Jpn.*, **1968**, 41, 2815.

[38] R. Galaverna, N. S. Camilo, M. N. Godoi, F. Coelho, and M. N. Eberlin. *J. Org. Chem*. **2016**, 81, 1089-1098.

[39] Hoffmann, H. M. R.; Rabe, *J. Angew. Chem., Int. Ed. Engl*. **1983**, 22, 795−796.

[40] Robiette, R.; Aggarwal, V. K.; Harvey, *J. N. J. Am. Chem. Soc*. **2007**, 129, 15513−15525.

[41] Price, K. E.; Broadwater, S. J.; Jung, H. M.; McQuade, *D. T. Org. Lett*. **2005**, 7, 147−150.

[42] G. O. Spessard, G. L. Miessler. *Organometallic Chemistry* 3rd Ed., Oxford University Press, **2016**. Print. P 512.

[43] E. F. Peters and B. L. Evering, U.S. Patenet 2,963,447, assigned to Standard Oil of Indiana, 1960.

[44] R. L. Banks and G. C. Bailey, *Ind. Eng. Chem. Prod. Res*., **1964**, 3, 170 (Phillips Petroleum).

[45] A. J. Berger, U.S. Patent 3,726,938, 1973.

[46] P. A. Verbrugge and G. J. Heiszwolf, U. S. Patent, 3,776,975. 1973.

[47] E. R. Freitas and C. R. Gum, *Chem, Eng, Progr.*, **1979**, 75,73.

[48] W. Keim, F. H. Kowaldt, R. Goddard, and C. Kruger, *Angew, Chem. Int. Ed. Eng.,* **1978**, 17, 466.

[49] B. Reuben and H. Wittcoff, *J. Chem. Ed*., **1988**, *65*, 605.

[50] Didier Villemin, *Tetrahedron Letters*. **1980**, Vol. 21, pp 1715-1718.

[51] McReynolds, M. D.; Dougherty, J. M.; Hanson, P. R. *Chem. ReV.* **2004**, 104, 2239–2258.

[52] Deiters, A.; Martin, S. F. Chem. ReV. 2004, 104, 2199–2238.

[53] Collins, S. K. J. Organomet. Chem. 2006, 691, 5122–5128.

[54] Donohoe, T. J.; Fishlock, L. P.; Procopiou, P. A. *Chem.Eur. J*. **2008**, 14, 5716–5726.

[55] Kotha, S.; Lahiri, K. *Synlett* **2007**, 2767–2784.

[56] Brik, A. AdV. *Synth. Catal*. **2008**, 350, 1661–1675.

[57] Martin, W. H. C.; Blechert, S. Curr. Top. *Med. Chem*. **2005**, 5, 1521–1540.

[58] Plumet, J.; Gomez, A. M.; Lopez, J. C. Mini-ReV. *Org. Chem*. **2007**,4, 201–216.

[59] Madsen, R. Eur. J. Org. Chem. 2007, 399–415.

[60] Arisawa, M.; Nishida, A.; Nakagawa, M. J. Organomet. Chem. 2006,
691, 5109–5121.

[61] Gaich, T.; Mulzer, J. Curr. *Top. Med. Chem.* **2005**, 5, 1473–1494.

[62] Van de Weghe, P.; Eustache, *J. Curr. Top. Med. Chem.* 2005, 5,
1495–1519.

[63] Schall, A.; Reiser, O. *Eur. J. Org. Chem.* **2008**, 2353–2364.

[64] Jianing W., Ravindra K. R. and Chung K. C., "recent advances in carbocyclic nucleosides: synthesis and biological activity", *Medicinal Chemistry of Nucleic Acids.* **2012**.

[65] Masayuki Y., Yoshihiko O., Bae C. and Isao K., *Tetrahedrom* Vol.46, No. 21, pp. 7459-7470, 1990.

[66] R. Grubbs and T. K. Brunck, *J. Am. Chem. Soc*., **1972**, 94, 2538.

[67] C. G. Biefield, H. A. Eick, and R. H. Grubbs, *Inorg. Chem.*, **1973** , 12, 2166.

[68] C. P. Casey and T. J. Burkhardt, *J. Am. Chem. Soc*., 1974, 96, 7808.

[69] T.J. Katz, S. J. Lee and N. Acton, 47. *Tetrahedrom Lett.,* **1976,** 4247.

[70] T.J. Katz, and N. Acton, *Tetrahedrom Lett.,* **1976,** 4251.

[71] T.J. Katz, S. J. Lee and M. A. Shippey, *J. Mol. Catal.*, **1980**, 8, 219.

[72] G. S. Weatherhead, J. G. Ford, E. J. Alexanian, R. R. Schrock and A. H. Hoveyda, *J. Am. Chem. Soc*., **2000**, *122*, 1828.

[73] R. H. Grubbs, *Tetrahedrom,* **2004**, *60*, 7117.

[74] L. R. Gilliom and R. H. Grubbs, *J. Am. Chem. Soc*., **1986**, 108, 733

[75] S. T. Nguyen, L. K. Johnson, R. H. Grubbs and J. W. Ziller, *J. Am. Chem. Soc*., 1992, 114, 3974.

[76] M Scholl, T. M. Trnka, J. P. Morgan and R. H. Grubbs, *Tetrahedrom Lett.,* 1999, 40, 2247.

[77] S. B. Garber, J. S. Kingsbury, B. L. Gray and A. H. Hoveyda, *J. Am. Chem. Soc*., 2000, 144, 8168.

[78] Love, J. A.; Morgan, J. P.; Trnka, T. M.; Grubbs, R. H. (2002). *AngewChem. Int. Engl.* 41 (21), 4036-4037.

[79] Romero, P. E., Piers, W. E., *J. Am. Chem. Soc*., **2005**, 127, 5032.

[80] He´risson, J. L.; Chauvin, Y. *Makromol. Chem*. 1971, 141, 161–176

[81] Ivin, K. J.; Mol, J. C. *Olefin Metathesis and Metathesis Polymerization*;Academic Press: New York, 1997.

[82] S. Monfette, D. E. Fogg, *Chem. Rev.*, **2009**, 109, 3783-3816.

[83] S. H. Hong, M. W. Day and R. H. Grubbs, *J. Am. Chem. Soc.*, **2004**, 126, 7414–7415.

[84] S. H. Hong, A. G. Wenzel, T. T. Salguero, M. W. Day and R. H. Grubbs, *J. Am. Chem. Soc.*, **2007**, 129, 7961–7968.

[85] D. J. Nelson, S. Manzino, C. A. Urbina-Blanco and S. P. Nolan. *Chem. Commun*., **2014**, 50, 10355-10375.

[86] C. S. Higman, L. Plais and D. E. Fogg, *ChemCatChem*, **2013**, 5,3548–3551.

[87] C.S. Higman, A.E. Lanterna, M.L. Marin, J.C. Scaiano*, D.E. Fogg.* *ChemCatChem*. **2016**, 8, 2446-2449

[88] W.L. McClennan, S.A. Rufh, J.A. M. Lummiss, D.E. Fogg.* *J. Am. Chem. Soc*. **2016**, 138, 14668-14677.

[89] E. Larionov, H. Li, C. Mazet, *Chem. Commun*. **2014**, 50, 9816–9826;

[90] H. Mutlu, A. N. Parvulescu, P. C. A. Bruijnincx, B. M. Weckhuysen, M. A. R. Meier, *Macromolecules*, **2012**, 45, 1866–1878.

[91] B. J. van Lierop, J. A. M. Lummiss, D. E. Fogg. *Olefin Metathesis-Theory and Practice*, Wiley-VCH, Weinheim, 2014, pp. 85–152.

[92] V. Farina, A. Horv.th *Handbook of Metathesis*, Vol. 2, Wiley-VCH, Weinheim, 2015, pp. 633–658;

[93] J. R. Clark, J. R. Griffiths, and S. T. Diver. *J. Am. Chem. Soc*., **2013**, 135, 3327-3330.

[94] D. Bourgeois, A. Pancrazi, L. Ricard, J. Prunet, *Angew. Chem.* **2000**, 112, 742-744.

[95] A. Fürstner, O. R. Thiel, L. Ackermann, H.-J. Schanz, S. P. Nolan, *J. Org. Chem.* **2000**, 65, 2204_2207.

[96] Bernd Schmidt. *Eur. J. Org. Chem*. **2004**, 1865-1880.

[97] J. C. Conrad, M. D. Eelman, J. A. Duarte Silva, S. Monfette, H. H. Parnas, J. L. Snelgrove, and D. E. Fogg. *J. Am. Chem. Soc*., **2007**, 129, 1024-1025.

[98] J. C. Conard and D. E. Fogg. *Current Organic Chemistry*, **2006**, 10, 185-202.

[99] Schleyer PVR, Williams JE, Blanchard KR. *J. Am. Chem. Soc.,* **1970**, 92, 2378–2386.

[100] J. Bures, *Angew. Chem. Int. Ed*. **2016**, 55, 2028-2031.

[101] R. Theron, Y. Wu, L. Yunker, A. V. Hesketh, I. Pernik, A. S. Weller, and J. S. McIndoe. *A. C. S. Catal.* **2016**, 6, 6911-6917.

[102] E. Larionov, H. Li and C. Mazet. *Chem. Commin.*, **2014**, 50, 9816.

[103] J. Jiang, D. Zhao, H. Zhang, J. He and N. Li. *Anal. Methods*, **2017**, 9, 4201-4206.

[104] S. Ohno, K. Takamoto, H. Fujioka, and M. Arisawa, *Org. Lett.,* **2017**, 19(9), pp 2422-2425.